

Technical Report Documentation Page

1. REPORT No.

2. GOVERNMENT ACCESSION No.

3. RECIPIENT'S CATALOG No.

4. TITLE AND SUBTITLE

Undrained Lateral Pile and Pile Group Response in Saturated Sand

5. REPORT DATE

January 2000

6. PERFORMING ORGANIZATION

7. AUTHOR(S)

Ashour, Mohamed and Gary Norris

8. PERFORMING ORGANIZATION REPORT No.

9. PERFORMING ORGANIZATION NAME AND ADDRESS

University of Nevada, Reno
Department of Civil Engineering

10. WORK UNIT No.

11. CONTRACT OR GRANT No.

59A0071

12. SPONSORING AGENCY NAME AND ADDRESS

State of California
Department of Transportation

13. TYPE OF REPORT & PERIOD COVERED

14. SPONSORING AGENCY CODE

15. SUPPLEMENTARY NOTES

16. ABSTRACT

Strain wedge (SW) model formulation has been used, in previous work, to evaluate the response of a single pile or a group of piles (including its pile cap) in layered soils to lateral loading. The SW model approach provides appropriate prediction for the behavior of an isolated pile and pile group under lateral static loading in layered soil (sand and/or clay). The SW model analysis covers a wide range over the entire strain or deflection range that may be encountered in practice. The method allows development of p-y curves for the single pile based on soil-pile interaction by considering the effect of both soil and pile properties (i.e. pile size, shape, bending stiffness, and pile head fixity condition) on the nature of the p-y curve. In the SW model analysis, clay is assumed to respond under undrained conditions considering the effect of porewater pressure, and sand is subjected to drained conditions (no excess porewater pressure).

This study has extended the capability of the SW model in order to predict the response of a laterally loaded isolated pile and pile group in liquefiable soil by accounting for the developing excess porewater pressure in sand (undrained conditions) either in the near or free field. In order to accomplish such a goal, a series of formulations has been developed to assess the undrained behavior of saturated sand from its drained response, and to predict the potential of sand to liquefy under different circumstances. The SW model has shown the capability to evaluate such soil response due to both the near field porewater pressure around the loaded pile and the free-field excess porewater pressure due to level ground earthquake shaking after Seed.

17. KEYWORDS

CCEER 00-01
Federal Study No. F98SD01

18. No. OF PAGES:

159

19. DRI WEBSITE LINK

http://www.dot.ca.gov/hq/research/researchreports/1997-2001/undrained_pile.pdf

20. FILE NAME

undrained_pile.pdf

ACKNOWLEDGMENTS

The authors would like to thank Caltrans for its financial support of this project. The authors would also like to acknowledge Dr. Abbas Abghari, Mr. Angel Preze-Copo, Dr. Mahmoud Khojasteh, and Dr. Mohammed Islam for their support and guidance as the Caltrans monitors for this project. The authors would also like to express their gratitude for Tim Leahy and Chris Campbell for their encouragement and support.

DISCLAIMER

The contents of this report reflect the views of the authors who are responsible for the facts and accuracy of the data presented herein. The contents do not necessarily reflect the official views or policies of the State of California or the Federal Highway Administration. This report does not constitute standard specifications, or regulations.

ABSTRACT

Strain wedge(SW) model formulation has been used, in previous work, to evaluate the response of a single pile or a group of piles (including its pile cap) in layered soils to lateral loading. The SW model approach provides appropriate prediction for the behavior of an isolated pile and pile group under lateral static loading in layered soil (sand and/or clay). The SW model analysis covers a wide range over the entire strain or deflection range that may be encountered in practice. The method allows development of p-y curves for the single pile based on soil-pile interaction by considering the effect of both soil and pile properties (i.e. pile size, shape, bending stiffness, and pile head fixity condition) on the nature of the p-y curve. In the SW model analysis, clay is assumed to respond under undrained conditions considering the effect of porewater pressure, and sand is subjected to drained conditions (no excess porewater pressure).

This study has extended the capability of the SW model in order to predict the response of a laterally loaded isolated pile and pile group in liquefiable soil by accounting for the developing excess porewater pressure in sand (undrained conditions) either in the near- or free-field. In order to accomplish such a goal, a series of formulations has been developed to assess the undrained behavior of saturated sand from its drained response, and to predict the potential of sand to liquefy under different circumstances. The SW model has shown the capability to evaluate such soil response due to both the near field porewater pressure around the loaded pile and the free-field excess porewater pressure due to level ground earthquake shaking after Seed.

The undrained results obtained using the SW model are significantly different than the drained results for a pile or pile group driven into a site with liquefiable soil.. The assessed results foretell that the behavior of laterally loaded piles is function of both soil and pile properties and is influenced by the level of porewater pressure build-up in the soil surrounding the pile. The capacity of a loaded pile or pile group might significantly drop under such conditions.

**UNDRAINED LATERAL PILE AND PILE
GROUP RESPONSE IN SATURATED SAND**

CCEER 00-01

Prepared by:

Mohamed Ashour
Research Assistant Professor

and

Gary Norris
Professor of Civil Engineering

University of Nevada, Reno
Department of Civil Engineering

Prepared for:

State of California
Department of Transportation

Federal Study No. F98SD01
Contract No. 59A0071

with

Funds from Caltrans

January 2000

CHAPTER 1

INTRODUCTION

This report provides a summary of strain wedge model assessment of the behavior of piles and pile groups subjected to lateral loading in liquefied soil. The computer program attached to this report is capable of assessing the response of a single pile and pile group in liquefiable soils and generating the p-y curves for various soil and pile conditions for use in other programs.

The strain wedge model as proposed by Norris (Abdollahiaee, 1985; Gowda, 1991; Ashour, 1996) relates one-dimensional beam on elastic foundation analysis to the three-dimensional soil pile interaction response. It relates the deflection of a pile versus depth (or its rotation) to the relative soil strain that exists in the growing passive wedge which develops in front of a pile under horizontal load. The strain wedge model assumes that the deflection of a pile under increasing horizontal load is due solely to the deformation of the soil within the mobilized passive wedge, that plane stress change conditions exist within the wedge, and that soil strain is constant with depth in the current wedge.

The passive wedge will exhibit a height that corresponds to the pivot point as determined by a linear approximation of the pile deflection. If the soil strain is known, an equivalent linear Young's modulus value, associated with the soil within the wedge at any depth, can be determined. Assuming plane stress change conditions exist, the increase in horizontal stress can then be determined. In addition, the beam-on-elastic-foundation line load reaction at any depth along the pile face is equivalent to the increase in horizontal stress times the wedge width at that depth plus the mobilized side shear resistance that develops at that depth along the pile faces parallel to the direction of movement. Since the geometry of the developing wedge is based on known soil properties and the current value of soil strain, the wedge width can be determined at any depth within the wedge. An equivalent face stress from beam on elastic foundation (BEF) analyses can therefore be related to the horizontal stress change in the soil.

The strain wedge model relates one-dimensional BEF analysis (p-y response) to a three-dimensional

The undrained behavior of isotropically consolidated saturated sand under monotonic loading is characterized by a change in the excess porewater pressure which, in turn, leads to different forms of undrained response. Such behavior featuring a positive build up in excess porewater pressure, yields a contractive response. The growth of the excess porewater pressure continues until reaching a stable value corresponding to the lowest value of undrained resistance of the sand, known as its steady state strength. Moreover, the sand shows continuous large deformation under constant effective confining pressure, constant shear stress, and constant rate of shear strain. Such behavior of sand is known as complete liquefaction. However, saturated sands may exhibit a large increase followed by a decrease in the excess porewater pressure which results in dilative response. Such behavior is a consequence of the higher relative density of the sand.

Only soils that tend to decrease in volume during shear, i.e. contractive soils, suffer the loss of shear resistance that results in liquefaction. However, even contractive soils are not susceptible to liquefaction unless the driving shear stresses are large enough. Soils that tend to exhibit a net increase in volume due to the imposed shear stresses, i.e. dilative soils, are not susceptible to liquefaction because their undrained strength is equal to or greater than their drained strength. It is known that liquefaction may occur in silts, and quick clays as well as sands and silty sands.

Until recently, no one study provided a clear picture of the mobilized undrained behavior and the associated effective stress path under the undrained monotonic loading. The available studies indicated the potential for sand to liquefy and characterized it as liquefiable or non-liquefiable material. The only way to assess the mobilized undrained behavior of a saturated sand (stress-strain and stress path) under the monotonic loading was via laboratory testing. Consolidating the saturated sand to different values of confining pressure or void ratio, a series of isotropically consolidated undrained tests (ICU) allowed one to assess the variation in the peak undrained resistance, the residual stress of the saturated sand and the associated levels of strain.

This work was developed to deal with uniform sands with different particles (well rounded, subrounded, subangular, or angular) under different levels of confining pressure. The validity of the work presented and the equations formulated are verified by several comparisons with observed results of Nevada, Ione, Ottawa, and Banding sands. The proposed evaluation of the deviatoric

CHAPTER 2

LATERAL LOADING OF A PILE IN LAYERED SOIL USING THE STRAIN WEDGE MODEL

2.1 INTRODUCTION

The strain wedge (SW) model is an approach that has been developed to predict the response of a flexible pile under lateral loading (Norris 1986, Ashour et al. 1996 and Ashour et al. 1998). The main concept associated with the SW model is that traditional one-dimensional Beam on Elastic Foundation (BEF) pile response parameters can be characterized in terms of three-dimensional soil-pile interaction behavior. The strain wedge model was initially established to analyze a free-head pile embedded in one type of uniform soil (sand or clay). However, the SW model has been improved and modified through additional research to accommodate a laterally loaded pile embedded in multiple soil layers (sand and clay). The strain wedge model has been further modified to include the effect of pile head conditions on soil-pile behavior. The main objective behind the development of the SW model is to solve the BEF problem of a laterally loaded pile based on the envisioned soil-pile interaction and its dependence on both soil and pile properties.

The problem of a laterally loaded pile in layered soil has been solved by Reese (1977) as a BEF based on modeling the soil response by p-y curves. However, as mentioned by Reese (1983), the p-y curve employed does not account for soil continuity and pile properties such as pile stiffness, pile cross-section shape and pile head conditions.

2.2 THE THEORETICAL BASIS OF STRAIN WEDGE MODEL CHARACTERIZATION

The SW model parameters are related to an envisioned three-dimensional passive wedge of soil developing in front of the pile. The basic purpose of the SW model is to relate stress-strain-strength behavior of the soil in the wedge to one-dimensional BEF parameters. The SW model is, therefore, able to provide a theoretical link between the more complex three-dimensional soil-pile interaction

(1986). This assumption allows uniform horizontal and vertical soil strains to be assessed (as seen later in a Fig. 2.6). Changes in the shape and depth of the passive wedge, along with changes in the state of loading and pile deflection, occur with change in the uniform strain in the developing passive wedge. The configuration of the wedge at any instant of load and, therefore, mobilized friction angle, φ_m , and wedge depth, h , is given by the following equation:

$$\Theta_m = 45 - \frac{\varphi_m}{2} \quad (2.2)$$

or its complement

$$\beta_m = 45 + \frac{\varphi_m}{2} \quad (2.3)$$

The width, \overline{BC} , of the wedge face at any depth is

$$\overline{BC} = D + (h - x) 2 \tan \beta_m \tan \varphi_m \quad (2.4)$$

where x denotes the depth below the top of the studied passive wedge, and D symbolizes the width of the pile cross-section (see Fig. 2.1). It should be noted that the SW model is based upon an effective stress analysis of both sand and clay soils. As a result, the mobilized fanning angle, φ_m , is not zero in clay soil as assumed by Reese (1958, 1983).

2.4 STRAIN WEDGE MODEL IN LAYERED SOIL

The SW model can handle the problem of multiple soil layers of different types. The approach employed, which is called the multi-sublayer technique, is based upon dividing the soil profile and the loaded pile into sublayers and segments of constant thickness, respectively, as shown in Fig. 2.3. Each sublayer of soil is considered to behave as a uniform soil and have its own properties according to the sublayer location and soil type. In addition, the multi-sublayer technique depends on the deflection pattern of the embedded pile being continuous regardless of the variation of soil types. However, the depth, h , of the deflected portion of the pile is controlled by the stability analysis of the pile under the conditions of soil-pile interaction. The effects of the soil and pile properties are associated with the soil reaction along the pile by the Young's modulus of the soil, the stress level

response of a given soil layer is not unique. The governing equations of the mobilized passive wedge shape are applied within each one- or two-foot sublayer i (of a given soil layer I) and can be written as follows:

$$(\Theta_m)_i = 45 - \frac{(\varphi_m)_i}{2} \quad (2.5)$$

$$(\beta_m)_i = 45 + \frac{(\varphi_m)_i}{2} \quad (2.6)$$

$$(\overline{BC})_i = D + (h - x_i) 2(\tan \beta_m)_i (\tan \varphi_m)_i \quad (2.7)$$

where h symbolizes the entire depth of the compound passive wedge in front of the pile and x_i represents the depth from the top of the pile or compound passive wedge to the middle of the sublayer under consideration. The equations above are applied at the middle of each sublayer.

2.5 SOIL STRESS-STRAIN RELATIONSHIP

The horizontal strain (ϵ) in the soil in the passive wedge in front of the pile is the predominant parameter in the SW model; hence, the name “strain wedge”. Consequently, the horizontal stress change ($\Delta\sigma_h$) is constant across the width of the rectangle BCLM (of face width \overline{BC} of the passive wedge), as shown in Fig. 2.1. The stress-strain relationship is defined based on the results of the isotropically consolidated drained (sand) or undrained (clay) triaxial test. These properties are summarized as follows:

- The major principle stress change ($\Delta\sigma_h$) in the wedge is in the direction of pile movement, and it is equivalent to the deviatoric stress change in the triaxial test as shown in Fig. 2.2 (assuming that the horizontal direction in the field is taken as the axial direction in the triaxial test).
- The vertical stress change ($\Delta\sigma_v$) and the perpendicular horizontal stress change ($\Delta\sigma_{ph}$) equal zero, corresponding to the standard triaxial compression test where deviatoric stress is increased while confining pressure remains constant.
- The initial horizontal effective stress is taken as

soil pile interaction response. Because of this relation, the strain wedge model is also capable of determining the maximum moment and developing p-y curves for a pile under consideration since the pile load and deflection at any depth along the pile can be determined. A detailed summary of the theory incorporated into the strain wedge model is presented in Chapter 2.

The problem associated with analyzing a pile group is that loading one pile in the group can dramatically affect the response of other piles in the group. Since the strain wedge model determines the geometry of the developing passive wedge, it allows any overlap between passive wedges within the group to be quantified. By knowing the amount of passive wedge overlap, the effective strain associated with the pile under consideration can be determined which ultimately reduces the lateral load capacity of the pile for a given level of deflection.

This report illustrates the links between the single pile and the pile group analysis. This is different from the current procedure in common use which employs a p-y multiplier technique. Such multiplier technique is based on reducing the stiffness of the traditional (Matlock-Reese) p-y curve using a multiplier that reduces the stiffness of the p-y curve of the single pile to yield a softer response for an individual pile in the group. A detailed summary of the theory in which the strain wedge analyzes pile group behavior is presented in Chapter 3.

The undrained behavior of saturated sands under monotonic, cyclic or dynamic loads is a research area which commands the interest of many investigators in the geotechnical field. Several studies have been conducted to provide a better understanding of the undrained behavior of saturated sand under different types of loading. An approach for assessing the undrained axial compression behavior of a saturated sand based on its drained behavior or effective stress response is given in this report. The formulation presented is based on extensive experimental work performed for the Army Corps of Engineers. One of the main points of interest in this study was to relate the undrained strength of a sand to its initial state, and thereby allow the designer to predict the potential for a saturated sand to liquefy. In other words, most of these investigations focused on the influence of the consolidation pressure and the associated void ratio of the sand on the undrained behavior of the saturated sand under monotonic and cyclic loading.

stress-axial strain response of sand under undrained conditions allows the strain wedge model to predict the response of a laterally loaded pile in saturated sand under undrained conditions. This approach is presented in detail in Chapter 4.

A methodology to assess the response of an isolated pile and pile group in sand under undrained conditions in the sand is presented in this report. The degradation in soil strength due to the free-field excess porewater, generated by the earthquake, is considered along with the near-field excess porewater pressure generated by lateral loading from the superstructure. The strain wedge (SW) model has been extended to incorporate such undrained response characterization of a laterally loaded pile in sand. Chapter 5 characterizes the reduction in pile response due to a drop in sand strength and Young's modulus as a result of developing liquefaction in the sand.

and the simpler one-dimensional BEF characterization. The previously noted correlation between the SW model response and BEF characterization reflects the following interdependence:

- the horizontal soil strain (ϵ) in the developing passive wedge in front of the pile to the deflection pattern (y versus depth, x) of the pile;
- the horizontal soil stress change ($\Delta\sigma_h$) in the developing passive wedge to the soil-pile reaction (p) associated with BEF; and
- the nonlinear variation in the Young's modulus ($E = \Delta\sigma_h/\epsilon$) of the soil to the nonlinear variation in the modulus of soil subgrade reaction ($E_s = p/y$) associated with BEF characterization.

The analytical relations presented above reflect soil-pile interaction response characterized by the SW model that will be illustrated later. The reason for linking the SW model to BEF analysis is to allow the appropriate selection of BEF parameters to solve the following fourth-order ordinary differential equation to proceed.

$$EI \left(\frac{d^4 y}{d^4 x} \right) + E_s(x)y + P_x \left(\frac{d^2 y}{d^2 x} \right) = 0 \quad (2.1)$$

The closed form solution of the above equation has been obtained by Matlock and Reese (1961) for the case of uniform soil. In order to appreciate the SW model's enhancement of BEF analysis, one should first consider the governing analytical formulations related to the passive wedge in front of the pile, the soil's stress-strain relationship, and the related soil-pile interaction.

2.3 SOIL PASSIVE WEDGE CONFIGURATION IN UNIFORM SOIL

The SW model represents the mobilized passive wedge in front of the pile which is characterized by base angles, Θ_m and β_m , the current passive wedge depth h , and the spread of the wedge fan angle, φ_m (the mobilized friction angle). The horizontal stress change at the passive wedge face, $\Delta\sigma_h$, and side shear, τ , act as shown in Fig. 2.1. One of the main assumptions associated with the SW model is that the deflection pattern of the pile is taken to be linear over the controlling depth of the soil near the pile top resulting in a linearized deflection angle, δ , as seen in Fig. 2.2. The relationship between the actual (closed form solution) and linearized deflection patterns has been established by Norris

in the soil, the pile deflection, and the modulus of subgrade reaction between the pile segment and each soil sublayer. To account for the interaction between the soil and the pile, the deflected part of the pile is considered to respond as a continuous beam loaded with different short segments of uniform load and supported by nonlinear elastic supports along soil sublayers, as shown in Fig. 2.4. At the same time, the point of zero deflection (X_0 in Fig. 2.4a) for a pile in a particular layered soil varies according to the applied load and the soil strain level.

The SW model in layered soil provides a means for distinguishing layers of different soil types as well as sublayers within each layer where conditions (ϵ_{50} , SL, ϕ_m) vary even though the soil and its properties ($\bar{\gamma}$, e or D_r , ϕ , etc.) remain the same. As shown in Fig. 2.5, there may be different soil layers and a transition in wedge shape from one layer to the next, with all components of the compound wedge having in common the same depth h . In fact, there may be a continuous change over a given sublayer; but the values of stress level (SL) and mobilized friction angle (ϕ_m) at the middle of each sublayer of height, H_i , are treated as the values for the entire sublayer.

As shown in Fig. 2.5, the geometry of the compound passive wedge depends on the properties and the number of soil types in the soil profile, and the global equilibrium between the soil layers and the loaded pile. An iterative process is performed to satisfy the equilibrium between the mobilized geometry of the passive wedge of the layered soil and the deflected pattern of the pile for any level of loading.

While the shape of the wedge in any soil layer depends upon the properties of that layer and, therefore, satisfies the nature of a Winkler foundation of independent “soil” springs in BEF analysis, realize that there is forced interdependence given that all components of the compound wedge have the same depth (h) in common. Therefore, the mobilized depth (h) of the compound wedge at any time is a function of the various soils (and their stress levels), the bending stiffness (EI), and head fixity conditions (fixed, free, or other) of the pile. In fact, the developing depth of the compound wedge can be thought of as a retaining wall of changing height, h . Therefore, the resultant “soil” reaction, p , from any soil layer is really a “soil-pile” reaction that depends upon the neighboring soil layers and the pile properties as they, in turn, influence the current depth, h . In other words, the p - y

$$\bar{\sigma}_{ho} = K \bar{\sigma}_{vo} = \bar{\sigma}_{vo}$$

where $K=1$ due to pile installation effects. Therefore, the isotropic confining pressure in the triaxial test is taken as the vertical effective stress ($\bar{\sigma}_{vo}$) at the associated depth.

- The horizontal stress change in the direction of pile movement is related to the current level of horizontal strain (ϵ) and the associated Young's modulus in the soil as are the deviatoric stress and the axial strain to the secant Young's modulus ($E = \Delta\sigma_h/\epsilon$) in the triaxial test.
- Both the vertical strain (ϵ_v) and the horizontal strain perpendicular to pile movement (ϵ_{ph}) are equal and are given as

$$\epsilon_v = \epsilon_{ph} = -\nu \epsilon$$

where ν is the Poisson's ratio of the soil.

It can be demonstrated from a Mohr's circle of soil strain, as shown in Fig. 2.6, that shear strain, γ , is defined as

$$\frac{\gamma}{2} = \frac{1}{2}(\epsilon - \epsilon_v) \sin 2\Theta_m = \frac{1}{2}\epsilon (1 + \nu) \sin 2\Theta_m \quad (2.8)$$

The corresponding stress level (SL) in sand (see Fig. 2.7) is

$$SL = \frac{\Delta\sigma_h}{\Delta\sigma_{hf}} = \frac{\tan^2(45 + \varphi_m) - 1}{\tan^2(45 + \varphi) - 1} \quad (2.9)$$

where the horizontal stress change at failure (or the deviatoric stress at failure in the triaxial test) is

$$\Delta\sigma_{hf} = \bar{\sigma}_{vo} \left[\tan^2 \left(45 + \frac{\varphi}{2} \right) - 1 \right] \quad (2.10)$$

In clay,

$$SL = \frac{\Delta\sigma_h}{\Delta\sigma_{hf}} ; \quad \Delta\sigma_{hf} = 2 S_u \quad (2.11)$$

where S_u represents the undrained shear strength which may vary with depth. Determination of the values of SL and φ_m in clay requires the involvement of an effective stress analysis which is

presented later in this chapter.

The relationships above show clearly that the passive wedge response and configuration change with the change of the mobilized friction angle (φ_m) or stress level (SL) in the soil. Such behavior provides the flexibility and the accuracy for the strain wedge model to accommodate both small and large strain cases.

A power function stress-strain relationship is employed in SW model analysis for both sand and clay soils. It reflects the nonlinear variation in stress level (SL) with axial strain (ϵ) for the condition of constant confining pressure. To be applicable over the entire range of soil strain, it takes on a form that varies in stages as shown in Fig. 2.8. The advantage of this technique is that it allows the three stages of horizontal stress, described in the next section, to occur simultaneously in different sublayers within the passive wedge.

2.5.1 Horizontal Stress Level (SL)

Stage I ($\epsilon \leq \epsilon_{50\%}$)

The relationship between stress level and strain at each sublayer (i) in the first stage is assessed using the following equation,

$$SL_i = \frac{\lambda_i \epsilon}{(\epsilon_{50})_i} \exp(-3.707 SL_i) \quad (2.12)$$

where 3.707 and λ ($\lambda = 3.19$) represent the fitting parameters of the modified hyperbolic relationship, and ϵ_{50} symbolizes the soil strain at 50 percent stress level.

Stage II ($\epsilon_{50\%} \leq \epsilon \leq \epsilon_{80\%}$)

In the second stage of the stress-strain relationship, Eqn. 2.12 is still applicable. However, the value of the fitting parameter λ is taken to vary in a linear manner from 3.19 at the 50 percent stress level to 2.14 at the 80 percent stress level as shown in Fig. 2.8.

Stage III ($\epsilon \geq \epsilon_{80\%}$)

This stage represents the final loading zone which extends from 80 percent to 100 percent stress level. The following Equation is used to assess the stress-strain relationship in this range,

$$SL_i = \exp \left[\ln 0.2 + \frac{100 \epsilon}{(m \epsilon + q_i)} \right] \quad SL_i \geq 0.80 \quad (2.13)$$

where $m=59.0$ and $q=95.4 \epsilon_{50}$ are the required values of the fitting parameters.

The three stages mentioned above are developed based on unpublished experimental results (Norris 1977). In addition, the continuity of the stress-strain relationship is maintained along the SL- ϵ curve at the merging points between the mentioned stages.

As shown in Fig. 2.9, if ϵ_{50} of the soil is constant with depth (x), then, for a given horizontal strain (ϵ), SL from Eqns. 2.12 or 2.13 will be constant with x . On the other hand, since strength, $\Delta\sigma_{hf}$, varies with depth (e.g., see Eqns. 2.10 and 2.11), $\Delta\sigma_h (= SL \Delta\sigma_{hf})$ will vary in a like fashion. However, ϵ_{50} is affected by confining pressure ($\bar{\sigma}_{v0}$) in sand, as is S_u in clay. Therefore, SL for a given ϵ will vary somewhat with depth.

The Young's modulus of the soil from both the shear loading phase of the triaxial test and the strain wedge model is

$$E_i = \frac{(\Delta\sigma_h)_i}{\epsilon} = \frac{SL_i (\Delta\sigma_{hf})_i}{\epsilon} \quad (2.14)$$

It can be seen from the previous equations that stress level, strain and Young's modulus at each sublayer (i) depend on each other, which results in the need for an iterative solution technique to satisfy the equilibrium between the three variables.

2.6 SHEAR STRESS ALONG THE PILE SIDES (SL_i)

Shear stress (τ) along the pile sides in the SW model (see Fig. 2.1) is defined according to the soil type (sand or clay).

2.6.1 Pile Side Shear in Sand

In the case of sand, the shear stress along the pile sides depends on the effective stress ($\bar{\sigma}_{vo}$) at the depth in question and the mobilized angle of friction between the sand and the pile (φ_s). The mobilized side shear depends on the stress level and is given by the following equation,

$$\tau_i = (\bar{\sigma}_{vo})_i \tan(\varphi_s)_i; \quad \text{where} \quad \tan(\varphi_s)_i = 2 \tan(\varphi_m)_i \quad (2.15)$$

In Eqn. 2.15, note that mobilized side shear angle, $\tan\varphi_s$, is taken to develop at twice the rate of the mobilized friction angle ($\tan\varphi_m$) in the mobilized wedge. Of course, φ_s is limited to the fully developed friction angle (φ) of the soil.

2.6.2 Pile Side Shear Stress in Clay

The shear stress along the pile sides in clay depends on the clay's undrained shear strength. The stress level of shear along the pile sides (SL_i) differs from that in the wedge in front of the pile. The side shear stress level is function of the shear movement, equal to the pile deflection (y) at depth x from the ground surface. This implies a connection between the stress level (SL) in the wedge and the pile side shear stress level (SL_i). Using the Coyle-Reese (1966) "t-z" shear stress transfer curves (Fig. 2.10), values for SL_i can be determined. The shear stress transfer curves represent the relationship between the shear stress level experienced by a one-foot diameter pile embedded in clay with a peak undrained strength, S_u , and side resistance, τ_{ult} (equal to ζ times the adhesional strength αS_u), for shear movement, y . The shear stress load transfer curves of Coyle-Reese can be normalized by dividing curve A ($0 < x < 3$ m) by $\zeta = 0.53$, curve B ($3 < x < 6$ m) by $\zeta = 0.85$, and curve C ($x > 6$ m) by $\zeta = 1.0$. These three values of normalization (0.53, 0.85, 1.0) represent the peaks of the curves A, B, and C, respectively, in Fig. 2.10a. Figure 2.10b shows the resultant normalized curves. Knowing pile deflection (y), one can assess the value of the mobilized pile side shear stress (τ) as

$$\tau_i = (SL_i)_i (\tau_{ult})_i \quad (2.16)$$

where

$$(\tau_{ult})_i = \zeta \alpha (S_u)_i \quad (2.17)$$

and α indicates the adhesion value after Tomlinson (1957).

The normalized shear stress load transfer curves can be represented by the following equations.

For the normalized curves A ($x < 3$ m) and B ($3 < x < 6$ m),

$$SL_t = 12.9 y D - 40.5 y^2 D^2 \quad (2.18)$$

For the normalized curve C ($x > 6$ m)

$$SL_t = 32.3 y D - 255 y^2 D^2 \quad (2.19)$$

where y in cm and D in m.

From the discussion above, it is obvious that SL_t varies nonlinearly with the pile deflection, y , at a given soil depth, x . Also, SL_t changes nonlinearly with soil depth for a given value of soil strain (see Fig. 2.11). These concepts are employed in each sublayer of clay.

2.7 SOIL PROPERTY CHARACTERIZATION IN THE STRAIN WEDGE MODEL

One of the main advantages of the SW model approach is the simplicity of the required soil properties necessary to analyze the problem of a laterally loaded pile. The properties required represent the basic and the most common properties of soil, such as the effective unit weight and the angle of internal friction or undrained strength..

The soil profile is divided into one or two foot sublayers, and each sublayer is treated as an independent entity with its own properties. In this fashion, the variation in soil properties or response (such as ϵ_{50} and φ_m in the case of sand, or S_u and $\bar{\varphi}_m$ in the case of clay) at each sublayer of soil can be explored. It is obvious that soil properties should not be averaged at the midheight of the passive wedge in front of the pile for a uniform soil profile (as in the earlier work of Norris 1986), or averaged for all sublayers of a single uniform soil layer of a multiple layer soil profile.

2.7.1 Properties Employed for Sand Soil

- Effective unit weight (total above water table, buoyant below), $\bar{\gamma}$
- Void ratio, e , or relative density, D_r
- Angle of internal friction, φ
- Soil strain at 50% stress level, ϵ_{50}

While standard subsurface exploration techniques and available correlations may be used to evaluate or estimate $\bar{\gamma}$, e or D_r , and $\bar{\phi}$, some guidance may be required to assess ϵ_{50} .

The ϵ_{50} represents the axial strain (ϵ_1) at a stress level equal to 50 percent in the ϵ_1 -SL relationship that would result from a standard drained (CD) triaxial test. The confining (consolidation) pressure for such tests should reflect the effective overburden pressure ($\bar{\sigma}_{vo}$) at the depth (x) of interest. The ϵ_{50} changes from one sand to another and also changes with density state. In order to obtain ϵ_{50} for a particular sand, one can use the group of curves shown in Fig. 2.12 (Norris 1986) which show a variation based upon the uniformity coefficient, C_u , and void ratio, e . These curves have been assessed from sand samples tested with “frictionless” ends in CD tests at a confining pressure equal to 42.5 kPa (Norris 1977). Since the confining pressure changes with soil depth, ϵ_{50} , as obtained from Fig. 2.12, should be modified to match the existing pressure as follows:

$$(\epsilon_{50})_i = (\epsilon_{50})_{42.5} \left(\frac{(\bar{\sigma}_{vo})_i}{42.5} \right)^{0.2} \quad (2.20)$$

$$(\Delta\sigma_{hf})_i = (\bar{\sigma}_{vo})_i \left[\tan^2 \left(45 + \frac{\bar{\phi}_i}{2} \right) - 1 \right] \quad (2.21)$$

where $\bar{\sigma}_{vo}$ should be in kPa.

2.7.2 The Properties Employed for Normally Consolidated Clay

- Effective unit weight $\bar{\gamma}$
- Plasticity index, PI
- Effective angle of friction, $\bar{\phi}$
- Undrained shear strength, S_u
- Soil strain at 50% stress level, ϵ_{50}

Plasticity index, PI, and undrained shear strength, S_u , are considered the governing properties because the effective angle of internal friction, $\bar{\phi}$, can be estimated from the PI based on Fig. 2.13. The ϵ_{50} from an undrained triaxial test (UU at depth x or CU with $\sigma_3 = \bar{\sigma}_{vo}$) can be estimated based

on S_u as indicated in Fig. 2.14.

An effective stress (ES) analysis is employed with clay soil as well as with sand soil. The reason behind using the ES analysis with clay, which includes the development of excess porewater pressure with undrained loading, is to define the three-dimensional strain wedge geometry based upon the more appropriate effective stress friction angle, $\bar{\varphi}$. The relationship between the normally consolidated clay undrained shear strength, S_u , and $\bar{\sigma}_{vo}$ is taken as

$$S_u = 0.33 \bar{\sigma}_{vo} \quad (2.22)$$

assumi

ng that S_u is the equivalent standard triaxial test strength. The effective stress analysis relies upon the evaluation of the developing excess porewater pressure based upon Skempton's equation (1954), i.e.

$$\Delta u = B [\Delta\sigma_3 + A_u(\Delta\sigma_1 - \Delta\sigma_3)] \quad (2.23)$$

where B equals 1 for saturated soil. Accordingly,

$$\Delta u = \Delta\sigma_3 + A_u(\Delta\sigma_1 - \Delta\sigma_3) \quad (2.24)$$

Note that $\Delta\sigma_3 = 0$ both in the shear phase of the triaxial test and in the strain wedge. Therefore, the mobilized excess porewater pressure is

$$\Delta u = A_u \Delta\sigma_1 \quad (2.25)$$

where $\Delta\sigma_1$ represents the deviatoric stress change in the triaxial test and $\Delta\sigma_h$ in the field, i.e.

$$\Delta u = A_u \Delta\sigma_h \quad (2.26)$$

Therefore, using the previous relationships, the Skempton equation can be rewritten for any sublayer (i) as follows:

$$(\Delta u)_i = (A_u)_i SL_i \quad (\Delta\sigma_{hf})_i = (A_u)_i SL_i \quad 2(S_u)_i \quad (2.27)$$

The initial value of parameter A_u is 0.333 and occurs at very small strain for elastic soil response. In addition, the value of parameter A_{uf} that occurs at failure at any sublayer (i) is given by the following relationship.

$$(A_{uf})_i = \frac{1}{2} \left(1 + \frac{1}{\frac{(S_u)_i}{(\bar{\sigma}_{vo})_i}} - \frac{1}{\sin \bar{\varphi}_i} \right) \quad (2.28)$$

after Wu (1966) as indicated in Fig. 2.15.

In Eqn. 2.28, $\bar{\varphi}$ symbolizes the effective stress angle of internal friction; and, based on Eqn. 2.22, $S_u/\bar{\sigma}_{v_o}$ equals 0.33. However, A_u is taken to change with stress level in a linear fashion as

$$(A_u)_i = 0.333 + SL_i [(A_{uf})_i - 0.333] \quad (2.29)$$

By evaluating the value of A_u , one can effectively calculate the excess porewater pressure, and then can determine the value of the effective horizontal stress, $(\bar{\sigma}_{v_o} + \Delta\sigma_h - \Delta u)$, and the effective confining pressure, $(\bar{\sigma}_{v_o} - \Delta u)$ at each sublayer, as shown in Fig. 2.15. Note that the mobilized effective stress friction angle, $\bar{\varphi}_m$, can be obtained from the following relationship.

$$\tan^2\left(45 + \frac{(\bar{\varphi}_m)_i}{2}\right) = \frac{(\bar{\sigma}_{v_o} + \Delta\sigma_h - \Delta u)_i}{(\bar{\sigma}_{v_o} - \Delta u)_i} \quad (2.30)$$

The targeted values of $(\bar{\varphi}_m)_i$ and SL_i in a clay sublayer and at a particular level of strain (ϵ) can be obtained by using an iterative solution that includes Eqns 2.11 through 2.13, and 2.27 through 2.30.

2.8 SOIL-PILE INTERACTION IN THE STRAIN WEDGE MODEL

The strain wedge model relies on calculating the modulus of subgrade reaction, E_s , which reflects the soil-pile interaction at any level during pile loading or soil strain. E_s also represents the secant slope at any point on the p-y curve, i.e.

$$E_s = \frac{p}{y} \quad (2.31)$$

Note that p represents the force per unit length of the pile or the BEF soil-pile reaction, and y symbolizes the pile deflection at that soil depth. In the SW model, E_s is related to the soil's Young's modulus, E, by two linking parameters, A and Ψ_s . It should be mentioned here that the SW model establishes its own E_s from the Young's modulus of the strained soil, and therefore, one can assess the p-y curve using the strain wedge model analysis. Therefore, E_s should first be calculated using the strain wedge model analysis to identify the p and y values.

Corresponding to the horizontal slice (a soil sublayer) of the passive wedge at depth x (see Fig. 2.1),

the horizontal equilibrium of horizontal and shear stresses is expressed as

$$p_i = (\Delta\sigma_h)_i \overline{BC}_i S_1 + 2\tau_i D S_2 \quad (2.32)$$

where S_1 and S_2 equal to 0.75 and 0.5, respectively, for a circular pile cross section, and equal to 1.0 for a square pile (Briaud et al. 1984). Alternatively, one can write the above equation as follows:

$$A_i = \frac{p_i/D}{(\Delta\sigma_h)_i} = \frac{\overline{BC}_i S_1}{D} + \frac{2\tau_i S_2}{(\Delta\sigma_h)_i} \quad (2.33)$$

where A symbolizes the ratio between the equivalent pile face stress, p/D , and the horizontal stress change, $\Delta\sigma_h$, in the soil. (In essence, it is the multiplier that, when taken times the horizontal stress change, gives the equivalent face stress.) From a different perspective, it represents a normalized width (that includes side shear and shape effects) that, when multiplied by $\Delta\sigma_h$ yields P/D . By combining the equations of the passive wedge geometry and the stress level with the above relationship, one finds that

$$A_i = S_1 \left(1 + \frac{(h - x_i) 2(\tan\beta_m \tan\varphi_m)_i}{D} \right) + \frac{2S_2 (\overline{\sigma}_{vo})_i (\tan\varphi_s)_i}{(\Delta\sigma_h)_i} \quad \text{in sand} \quad (2.34)$$

$$A_i = S_1 \left(1 + \frac{(h - x_i) 2(\tan\beta_m \tan\overline{\varphi}_m)_i}{D} \right) + \frac{S_2 (SL_i)_i}{SL_i} \quad \text{in clay} \quad (2.35)$$

Here the parameter A is a function of pile and wedge dimensions, applied stresses, and soil properties. However, given that $\Delta\sigma_h = E\varepsilon$ in Eqn. 2.33,

$$p_i = A_i D (\Delta\sigma_h)_i = A_i D E_i \varepsilon \quad (2.36)$$

The second linking parameter, Ψ_s , relates the soil strain in the SW model to the linearized pile deflection angle, δ . Referring to the normalized pile deflection shape shown in Figs. 2.2 and 2.6

$$\delta = \frac{\Upsilon}{2} \quad (2.37)$$

$$\frac{\Upsilon}{2} = \frac{\Upsilon_{\max}}{2} \sin 2\Theta_m \quad (2.38)$$

and

$$\frac{\gamma_{\max}}{2} = \frac{\varepsilon - \varepsilon_v}{2} = \frac{(1 + \nu)\varepsilon}{2} \quad (2.39)$$

where γ denotes the shear strain in the developing passive wedge. Using Eqns. 2.38 and 2.39, Eqn. 2.37 can be rewritten as

$$\delta = \frac{\varepsilon (1 + \nu) \sin 2\Theta_m}{2} \quad (2.40)$$

Based on Eqn. 2.40, the relationship between ε and δ can be expressed as

$$\text{or } \Psi = \frac{\varepsilon}{\delta} \quad (2.41)$$

$$\Psi = \frac{2}{(1 + \nu) \sin 2\Theta_m} \quad (2.42)$$

The parameter Ψ varies with the Poisson's ratio of the soil and the soil's mobilized angle of internal friction (φ_m) and the mobilized passive wedge angle (Θ_m).

Poisson's ratio for sand can vary from 0.1 at a very small strain to 0.5 or larger (due to dilatancy) at failure, while the base angle, Θ_m , can vary between 45° (for $\varphi_m = 0$ at $\varepsilon = 0$) and 25° (for, say, $\varphi_m = 40^\circ$ at failure), respectively. For this range in variation for ν and φ_m , the parameter Ψ for sand varies between 1.81 and 1.74 with an average value of 1.77. In clay soil, Poisson's ratio is assumed to be 0.5 (undrained behavior) and the value of the passive wedge base angle, Θ_m , can vary between 45° (for $\bar{\varphi}_m = 0$ at $\varepsilon = 0$) and 32.5° (for, say, $\bar{\varphi}_m = 25^\circ$ at failure). Therefore, the value of the parameter Ψ will vary from 1.47 to 1.33, with an average value of 1.4.

It is clear from the equations above that employing the multi-sublayer technique greatly influences the values of soil-pile interaction as characterized by the parameter, A_i , which is affected by the changing effective stress and soil strength from one sublayer to another. The final form of the modulus of subgrade reaction can be expressed as

$$(E_s)_i = \frac{p_i}{y_i} = \frac{A_i D \varepsilon E_t}{\delta (h - x_i)} = \frac{A_i}{(h - x_i)} D \Psi E_t \quad (2.43)$$

It should be mentioned that the SW model develops its own set of non-unique p-y curves which are function of both soil and pile properties, and are affected by soil continuity (layering) as presented

by Ashour et al. (1996).

2.9 PILE HEAD DEFLECTION

As mentioned previously, the deflection pattern of the pile in the SW model is continuous and linear. Based on this concept, pile deflection can be assessed using a simplified technique which provides an estimation for the linearized pile deflection, especially y_o at the pile head. By using the multi-sublayer technique, the deflection of the pile can be calculated starting with the base of the mobilized passive wedge and moving upward along the pile, accumulating the deflection values at each sublayer as shown in the following relationships and Fig. 2.16.

$$y_i = H_i \delta_i = H_i \frac{\varepsilon}{\Psi} \quad (2.44)$$

where the Ψ_s value changes according to the soil type (sand or clay), and

$$y_o = \sum y_i \quad i = 1 \text{ to } n \quad (2.45)$$

H_i indicates the thickness of sublayer i and n symbolizes the current number of sublayers in the mobilized passive wedge.

The main point of interest is the pile head deflection which is a function of not only the soil strain but also of the depth of the compound passive wedge that varies with soil and pile properties and the level of soil strain.

2.10 ULTIMATE RESISTANCE CRITERIA IN STRAIN WEDGE MODEL

The mobilized passive wedge in front of a laterally loaded pile is limited by certain constraint criteria in the SW model analysis. Those criteria differ from one soil to another and are applied to each sublayer. Ultimate resistance criteria govern the shape and the loading capacity of the wedge in any sublayer in SW model analysis. The progressive development of the ultimate resistance with depth is difficult to implement without employing the multi-sublayer technique.

2.10.1 Ultimate Resistance Criterion of Sand Soil

The mobilization of the passive wedge in sand soil depends on the horizontal stress level, SL , and the pile side shear resistance, τ . The side shear stress is a function of the mobilized side shear

friction angle, φ_s , as mentioned previously, and reaches its ultimate value ($\varphi_s = \varphi$) earlier than the mobilized friction angle, φ_m , in the wedge (i.e. $SL_i \geq SL$). This causes a decrease in the rate of growth of sand resistance and the fanning of the passive wedge as characterized by the second term in Eqns 2.32 and 2.34, respectively.

Once the stress level in a sublayer of the wedge reaches unity ($SL_i = 1$), the stress change and wedge fan angle in that sublayer cease to grow. However, the width \overline{BC} of the face of the wedge can continue to increase as long as ε (and, therefore, h in Eqn. 2.7) increases. Consequently, “soil” resistance, p , will continue to grow more slowly until a condition of initial soil failure ($SL_i = 1$) develops in that sublayer. At this instance, $p = p_{ult}$ where p_{ult} in sand, given as

$$(p_{ult})_i = (\Delta\sigma_{hf})_i \overline{BC}_i S_1 + 2(\tau_f)_i D S_2 \quad (2.46)$$

p_{ult} is a temporary ultimate condition, i.e. the fanning angle of the sublayer is fixed and equal to φ_i , but the depth of the passive wedge and, hence, \overline{BC} will continue to grow. The formulation above reflects that the near-surface “failure” wedge does not stop growing when all such sublayers reach their ultimate resistance at $SL = 1$ because the value of h at this time is not limited. Additional load applied at the pile head will merely cause the point at zero deflection and, therefore, h to move down the pile. More soil at full strength ($SL = 1$) will be mobilized to the deepening wedge as \overline{BC} and, therefore, p_{ult} increase until either flow around failure or a plastic hinge occurs.

Recognize that flow around failure occurs in any sublayer when it is easier for the sand at that depth to flow around the pile in a local bearing capacity failure than for additional sand to be brought to failure and added to the already developed wedge. However, the value at which flow failure occurs [$A_i = (A_{ult})_i$, $(p_{ult})_i = (\Delta\sigma_{hf})_i (A_{ult})_i D$] in sand is so large that it is not discussed here. Alternatively, a plastic hinge can develop in the pile when the pile material reaches its ultimate resistance at a time when $SL_i \leq 1$ and $A_i < (A_{ult})_i$. In this case, h becomes fixed, and \overline{BC}_i and p_i will be limited when SL_i becomes equal to 1.

2.10.2 Ultimate Resistance Criterion of Clay Soil

The situation in clay soil differs from that in sand and is given by Gowda (1991) as a function of the

undrained strength $(S_u)_i$ of the clay sublayer.

$$(p_{ult})_i = 10(S_u)_i D S_1 + 2(S_u)_i D S_2 \quad (2.47)$$

Consequently,

$$(A_{ult})_i = \frac{(p_{ult})_i}{(\Delta\sigma_{hf})_i} = \frac{(p_{ult})_i}{D 2(S_u)_i} = 5S_1 + S_2 \quad (2.48)$$

A_{ult} indicates the limited development of the sublayer wedge geometry for eventual development of flow around failure ($SL_i = 1$) and, consequently, the maximum fanning angle in that sublayer becomes fixed, possibly at a value $\bar{\varphi}_m \leq \bar{\varphi}$. If a plastic hinge develops in the pile at SL_i less than 1, then h will be limited, but \overline{BC}_i , and p_i will continue to grow until A_i is equal to A_{ult} or p_i is equal to $(p_{ult})_i$.

2.11 STABILITY ANALYSIS IN THE STRAIN WEDGE MODEL

The objective of the SW model is to establish the soil response as well as model the soil-pile interaction through the modulus of subgrade reaction, E_s . The shape and the dimensions of the passive wedge in front of the pile basically depend on two types of stability which are the local stability of the soil sublayer and the global stability of the pile and the passive wedge. However, the global stability of the passive wedge depends, in turn, on the local stability of the soil sublayers.

2.11.1 Local Stability of a Soil Sublayer in the Strain Wedge Model

The local stability analysis in the strain wedge model satisfies equilibrium and compatibility among the pile segment deflection, soil strain, and soil resistance for the soil sublayer under consideration. Such analysis allows the correct development of the actual horizontal stress change, $\Delta\sigma_h$, pile side shear stress, τ , and soil-pile reaction, p , associated with that soil sublayer (see Fig. 2.1). It is obvious that the key parameters of local stability analysis are soil strain, soil properties, and pile properties.

2.11.2 Global Stability in the Strain Wedge Model

The global stability, as analyzed by the strain wedge model, satisfies the general compatibility

among soil reaction, pile deformations, and pile stiffness along the entire depth of the developing passive wedge in front of the pile. Therefore, the depth of the passive wedge depends on the global equilibrium between the loaded pile and the developed passive wedge. This requires a solution for Eqn. 2.1.

The global stability is an iterative beam on elastic foundation (BEF) problem that determines the correct dimensions of the passive wedge, the corresponding straining actions (deflection, slope, moment, and shear) in the pile, and the external loads on the pile. Satisfying global stability conditions is the purpose of linking the three-dimensional strain wedge model to the BEF approach. The major parameters in the pile global stability problem are pile stiffness, EI , and the modulus of subgrade reaction profile, E_s , as determined from local stability in the strain wedge analysis. Since these parameters are determined for the applied soil strain, the stability problem is no longer a soil interaction problem but a one-dimensional BEF problem. Any available numerical technique, such as the finite element or the finite difference method, can be employed to solve the global stability problem. The modeled problem, shown in Fig. 2.4c, is a BEF and can be solved to identify the depth, X_0 , of zero pile deflection.

2.12 APPROACH VERIFICATION

Based on the SW model concepts presented in this chapter and Ashour et al. (1996), a computer program (SWSG) has been developed to solve the problem of a laterally loaded isolated pile and a pile group in layered soil (Ashour et al. 1996). Any verification of the methodology and algorithms employed should incorporate comparisons to field and laboratory tests for single piles and pile groups. The results presented below demonstrate the capability of the SW model approach and SWSG program in solving problems of laterally loaded piles relative to different soil and pile properties. It should be noted that pile and soil properties employed with the SW model analyses for the following field tests are the same properties mentioned in the references below.

2.12.1 Mustang Island Full-Scale Load Test on a Pile in Submerged Dense Sand (Reese et al. 1974 and Cox et al. 1974)

Figure 2.17 presents a comparison of field results versus SW model results and results obtained

using the computer program COM624 (Reese 1977). Note that it is from this specific field test that the COM624 p-y curves for sand were derived and, therefore, a good correspondence between COM624 and measured results is to be expected. The SW model results in Fig. 2.17a are in excellent agreement at lower pile-head deflections (lower strain levels) and within 5 percent at higher levels of deflection (higher strain levels). The SW model predicted maximum moment of Fig. 2.17b is in excellent agreement with measured results throughout.

2.12.2 Pyramid Building at Memphis, Tennessee, Full-Scale Load Test on a Pile in Layered Clay Soil (Reuss et al. 1992)

A lateral load test was performed on a full-scale pile in downtown Memphis. In order to improve the lateral capacity of the piles associated with this building, 1.8 meters of soft soil around the piles was removed and replaced with stiff compacted clay. Since the improved soil profile consisted of different types of soil, the corresponding test represents a layered field case study. The soil properties of the fill soils and the second stratum (the natural clay soil) were modified by Reuss et al. (1992) to force good agreement between the results assessed with COM624 (Reese 1977) and the field results (see Fig. 2.18a). The measured values of the undrained shear strength of the first and second strata were increased by 40 percent and 20 percent, respectively, to achieve such agreement. The measured soil properties were employed with the SW model to analyze the response of the pile in the improved soil profile. Figure 2.18a shows good agreement between the measured values and SW model predicted pile-head response in the improved soil profile. Figure 2.18b shows the pile-head response predicted by COM624 and SW model analysis for the same pile in the original soil profile (natural clay at its measured undrained strength).

2.12.3 Sabine River Full-Scale Load Tests on a Pile in Soft Clay (Matlock 1970)

The benefit of the Sabine River tests derives from having load tests on piles of both free- and fixed-head conditions. Note that the results of the free-head test were performed to establish the p-y curve criteria for piles in soft clay (Matlock 1970). As seen in Fig. 2.19a, the predicted free-head SW model results are in good agreement with the observed results at the Sabine River site. At higher levels of deflection, the results calculated using the SW model fall approximately 5 to 10 percent below those measured in the field. By comparison, the SW model predicted and the observed

fixed-head pile response at Sabine River are in excellent agreement as shown in Fig. 2.19b. SW model results were established for two cases, i.e. the clay with a single average S_u and, separately, for a varying S_u .

2.13 SUMMARY

The SW model approach presented here provides an effective method for solving the problem of a laterally loaded pile in layered soil. This approach assesses its own nonlinear variation in modulus of subgrade reaction or p-y curves. The strain wedge model allows the assessment of the nonlinear p-y curve response of a laterally loaded pile based on the envisioned relationship between the three-dimensional response of a flexible pile in the soil to its one-dimensional beam on elastic foundation parameters. In addition, the strain wedge model employs stress-strain-strength behavior of the soil as established from the triaxial test and the effective stress condition to evaluate the mobilized soil behavior.

Compared to other approaches which have been developed empirically based upon a limited number of field tests, the SW approach depends on well known or accepted principles of soil mechanics (the stress-strain-strength relationship) and an effective stress soil analysis. Moreover, the required parameters to solve the problem of the laterally loaded pile are a function of the basic soil properties that are typically available to the designer.

CHAPTER 3

THE RESPONSE OF PILE GROUPS TO LATERAL LOADING USING THE STRAIN WEDGE MODEL

3.1 INTRODUCTION

As discussed previously in Chapter 2, the prediction of single pile response to lateral loading using the strain wedge model correlates traditional one-dimensional beam on an elastic foundation response to the three dimensional soil-pile interaction. In particular, the Young's modulus of a soil is related to a corresponding horizontal subgrade modulus; the deflection of the pile is related to the strain that exists in the developing passive wedge in front of the pile; and the beam on an elastic foundation line load for a given deflection is related to the horizontal stress change acting along the face of the developing passive wedge. The three-dimensional characterization of the laterally loaded pile in the SW model analysis provides an excellent chance to study the interference among the piles in a pile group in a realistic way. The influence of the neighboring piles on an individual pile in the group will be a function of soil and pile properties, pile spacing, and the level of loading. These parameters are employed together in the SW model analysis to reflect the soil-pile interaction on the pile group behavior.

The chapter presented will illustrate the links between the single pile and the pile group analysis. The current procedure, commonly used, employs the p-y multiplier technique (Brown and Reese 1988). Such procedure is based on reducing the stiffness of the traditional (Matlock-Reese) p-y curve by using a multiplier ($f < 1$), as seen in Fig. 3.1. The value of the p-y curve multiplier should be assumed by the designer and is based on the data collected from the full-scale field tests on pile groups which are very few (Brown and Reese 1988). Consequently, a full-scale field test (which is costly) is strongly recommended in order to determine the value of the multiplier (f) of the soil profile at that site. Moreover, the suggested value of the multiplier (f) will be constant in the same soil and under any level of loading. As seen in Fig. 3.2, the interference among the piles in the group varies with depth, even in the same uniform soil, and increases with level of loading as the

wedge grows deeper. Therefore, the use of the multiplier that is both constant with depth and constant over the full range of load/deflection would seem to involve significant compromise.

3.2 DEFINITIONS AND ASSUMPTIONS IN THE ANALYSIS OF PILE GROUPS

In expanding the strain wedge model to account for pile groups, a number of simplifying assumptions were required. Before identifying the assumptions used in developing the model, the following lists some definition of terms is provided below:

- The lead row of piles is defined as the row of piles perpendicular to the direction of loading and that row closest to the developing passive wedge in front of the pile group as shown on Fig. 3.3.
- A trailing row of piles is defined as a row of piles perpendicular to the direction of loading having a row of piles in front of it (Fig. 3.3).
- An interior pile is defined as a pile that has piles on both of its sides (Fig. 3.3).
- An exterior pile is defined as a pile that has a pile on only one of its sides (Fig. 3.3).
- A lateral pile is defined as a pile that exists to the side of a pile under consideration, perpendicular to the direction of loading.
- A leading pile is defined as a pile that exists in front of the pile under consideration, parallel to the direction of loading.

The following identifies the assumptions employed in the model analysis of pile groups.

- The pile group to be analyzed would consist of either a square or rectangular arrangement of piles.
- A pile in the group is not affected by the response of piles trailing it.
- A pile in the group is affected by the response of a leading pile directly in front of it, and in front and one to the side.
- An interior pile is affected by the two lateral piles on either sides.
- An exterior pile is affected by the first lateral pile to one of its sides.
- All trailing rows of piles will exhibit the same response.
- All piles within a group are connected at their tops by a common rigid cap structure that

provides either a free- or a fixed-pile head condition.

3.3 METHOD OF ANALYSIS

As seen in Fig. 3.4, the piles in the group interfere with adjacent piles horizontally of varying amount with depth. The multi-sublayer technique presented in Chapter 2 allows the SW model to determine the overlap of the neighboring piles in different sublayers over the depth of the interference. This provides a great deal of flexibility in the calculation of the growth stress (i.e. strain) in the overlap zones which increase with growth of the passive wedges of soil. The main objective in the calculation of the area of overlap among the piles is to determine the increase in soil strain in the passive wedge of the pile in question. Thereafter, the changes in the soil Young's modulus and the modulus of subgrade reaction in each sublayer will be assessed. Once the profile of the modulus of subgrade reaction along the individual pile is predicted, the pile will be analyzed as an equivalent single pile. The procedure of analyzing the piles in the group will be performed as presented in the next section.

3.3.1 Determination of Average Soil Strain in the Passive Wedge Due to Pile Interference

A value of soil strain (ϵ) (i.e. a load level) in the passive wedge is assumed for a given soil profile. The response of a single pile (similar to the piles in the group) in the same soil profile will be determined at this value of soil strain. As a result, the shape and the dimensions of the developed passive wedge will be assessed (CD , h , ϕ_m , and β_m), as seen in Fig. 2.1 and presented in Chapter 2. This will include the values of stress level in each soil sublayer i (SL_i), Young's modulus (E_i), and modulus of subgrade reaction, ($E_{s,i}$). The associated values of pile-head deflection, pile head load, and maximum bending moment will be (Y_o), (P_o), and (M). t represents the increment (i.e. level) of loading which affects the reduction in the modulus of subgrade reaction of an individual pile in the pile group.

Considering a group of single piles under the same previous conditions (SL_i , CD , h , ϕ_m , and β_m), the passive wedge of soil in front of the piles will interact and overlap the neighboring ones, as seen in Fig. 3.4a. Therefore, overlap zones of stress will exhibit larger values of soil strains and stresses. The increase in soil strain in the passive wedge depends on the number of the interfered passive

wedges over the same area as shown in Fig.3.4a. Such interference also depends on the location of the pile in the group (i.e. the pile type).

The average value of strain accumulated in a particular soil sublayer (i) in the passive wedge of an individual pile will be calculated, $(\epsilon_{ave})_i$.

$$(\epsilon_{ave})_i = \epsilon_i + \Delta\epsilon_i \quad (3.1)$$

where $\Delta\epsilon$ is the growth in soil strain in that soil sublayer due to the overlap of adjacent pile wedges. ϵ_{ave} will be assessed for each soil sublayer in each passive wedge of pile type P1 - P4 in order to determine the average value of soil strains.

3.3.2 Evaluation of the Average Young's Modulus in the Passive Wedge of a Pile in a Group, E_{ave}

Based on the information discussed in Chapter 2, the value of Young's modulus, $(E_{ave})_i$, of the soil in each sublayer i is expressed as

$$(E_{ave})_i = \frac{SL_i (\Delta\sigma_{hf})_i}{(\epsilon_{ave})_i} \quad (3.2)$$

where stress level (SL_i) is determined based on Eqns. 2.12 and 2.13 in Chapter 2.

The relationship between the corresponding stress level (SL) in sand and the associated mobilized effective stress friction angle (ϕ_m) in a sand sublayer i is

$$(SL_{ave})_i = \left(\frac{(\Delta\sigma_h)_{ave}}{\Delta\sigma_{hf}} \right)_i = \frac{\tan^2(45 + (\phi_m)_i) - 1}{\tan^2(45 + \phi_i) - 1} \quad (3.3)$$

where $(\Delta\sigma_h)_{ave}$ and $\Delta\sigma_{hf}$ are the horizontal average stress change and the deviatoric stress at failure, respectively, both at the same (current) effective confining pressure. The stress level calculated in Eqn. 3.3 reflects the stresses in the soil around the pile in question due to the pile head load and the stresses from the neighboring piles

It should be noted the Young's modulus (E_{ave}) calculated by Eqn. 3.2 results from the original strain in the passive wedge as a single pile, and the additional soil strain which develops in the overlap zones between the pile in question and the neighboring piles. Based on the amount of interference among the piles in the group, the value of E_{ave} should be less or equal to the associated one of the single pile.

3.3.3 Characterization of the Soil Passive Wedge of a Pile in a Group

As presented in Chapter 2, equations relating to the shape of the effective stress wedge are applied within each soil sublayer i and can be written as follows:

$$(\Theta_m)_i = 45 - \frac{(\varphi_m)_i}{2} \quad (3.4)$$

$$(\beta_m)_i = 45 + \frac{(\varphi_m)_i}{2} \quad (3.5)$$

$$(\overline{BC})_i = D + (h - x_i) 2(\tan \beta_m)_i (\tan \varphi_m)_i \quad (3.6)$$

where h symbolizes the entire depth of the compound passive wedge in front of the pile, and x_i represents the depth from the top of the pile or compound passive wedge to the middle of the sublayer under consideration. The equations above are applied at the middle of each sublayer, and characterize the new geometry of the passive wedge of an individual pile in a group including the effect of neighboring piles (i.e. ϵ_{ave} , SL_{ave} , and φ_m). As described by Eqn. 3.3, φ_m is a function of SL_{ave} . Therefore, all the parameters listed in the above equations are influenced by SL_{ave} .

3.3.4 Evaluation of the Modulus of Subgrade Reaction of a Pile in a Group, $(E_s)_{ave}$

Compared to the case of the single pile, the developing passive wedge of a pile in a group will be larger or equal to that one of the single pile (depending on the amount of pile interference). However, the criteria which governs the development of flow around failure, and variation of the soil-pile reaction (p_i) in the single pile analysis will continue be employed with the pile group analysis (see Chapter 2), i.e.

$$(E_s)_i = \frac{P_i}{y_i} \quad (3.7)$$

Corresponding to a horizontal slice of a soil sublayer in the passive wedge at depth x (see Fig. 2.1),

$$p_i = [(\Delta\sigma_h)_{ave}]_i \overline{BC}_i S_1 + 2\tau_i D S_2 \quad (3.8)$$

where S_1 and S_2 equal to 0.75 and 0.5, respectively, for a circular pile cross section, and equal to 1.0 for a square pile (Briaud et al. 1984).

It should be expected that the resulting modulus of subgrade reaction of a pile in a group $(E_s)_{ave}$ will equal to or softer than the E_s of the single pile. The value of E_s will vary with the level of loading and the growth of the soil stress in the developing passive wedge. Thus, there is no constant variation or specific pattern for changes in $(E_s)_{ave}$.

As seen in Fig. 3.5, the modulus of subgrade reaction of a pile in a group should reflect the mutual resistance between the soil and the pile. However, a portion of the pile deformation, $(\Delta y)_i$, results from the additional stresses in the soil (i.e. strains, $\Delta\epsilon$) which result from the effect of the neighboring piles. Therefore, under a particular lateral load the pile in the group will yield deflections more than these of the single pile. The additional deflection at any pile segment, $(\Delta y)_i$, due to $\Delta\epsilon_i$ does not contribute any additional resistance for the pile in question (Fig. 3.5). According to the procedure presented, the modulus of subgrade reaction in a sublayer will be a function of the level of loading. Compared to the p-y curve of a single pile, the resulting p-y curve for a pile in a group (at depth x) will exhibit an increasing reduction factor ($f \leq 1$) with growing level of loading

(Fig. 3.5).

Having the reduced values of E_s along the individual piles in the group, the piles in the group will be analyzed as equivalent single piles (Beam on Elastic Foundation). The pile head load and deflection of the piles in the group can be predicted and compared to the single pile response.

3.4 CASE STUDY

The following information provides an evaluation of the strain wedge model program for laterally loaded pile groups by comparing the results obtained from the program to measured results observed during lateral load tests on pile groups. When available, site-specific foundation conditions were used to develop the necessary input parameters for use in the program. Otherwise, material properties were assumed based on available laboratory test data and/or material descriptions.

3.4.1 University of Houston, Texas Full-Scale Load Test on a Pile Group in Sand

As documented by Morrison et al (1986), a full-scale lateral load test on a 3 x 3 pile group in sand overlying an overconsolidated clay was conducted at the University of Houston, Texas. The results obtained from this load test were used by Morrison et al (1986) to develop an approach to predict the response of laterally loaded pile groups in sand. The method proposed by Morrison et al (1986) is based on the same method proposed by Brown et al (1985).

- **Pile Group Configuration and Material Properties**

The pile group configuration tested and analyzed by Morrison et al (1986) consisted of a 3 x 3 pile group embedded in approximately 10 feet of a dense to very dense uniform sand overlying an overconsolidated clay (Fig. 3.6). The piles had been previously installed in 1979 for the purposes of an axial load test on a pile group as described by O'Neill et al (1982), and were then subsequently tested under lateral loading conditions as described by Brown et al (1985). The piles consisted of steel pipe, with an outside diameter of 10.75 inches and a wall thickness of 0.365 inches. As documented by O'Neill et al (1982), the piles exhibited an approximate stiffness, EI , of 6.64×10^9 pounds-inch². The piles were driven closed-ended, at a pile spacing of three pile diameters, to an approximate depth of 43 feet below existing grade (approximately 40 feet below finished grade).

To facilitate installation, the piles were driven into an 8-inch-diameter pilot shaft that had been advanced to a depth of approximately 10 feet below the existing ground surface. Minimal lateral drift of the piles was observed subsequent to installation. Prior to the beginning of Morrison's test and subsequent to Brown's test, the existing clay foundation soils around the pile group were overexcavated to a depth approximately 10 feet below the existing ground surface and backfilled with a uniform sand. The sand was flooded in an attempt to saturate the resulting subsurface sand soils at the site. A single isolated steel pipe pile, with the same material properties as the piles in the group, was also installed at the site to allow the comparison of single pile response to pile group response. The area of the isolated pile was also overexcavated and backfilled to match the subsurface conditions of the pile group.

- **Foundation Material Characterization**

Since the subsurface conditions at this site have been defined in the section above, only the sand backfill placed after overexcavation at this site will be characterized in this section. Medium-graded clean sand (SP) was placed in thin lifts and hand compacted to a relative density of approximately 50 percent. The coefficient of uniformity, C_u , of the sand ranged from 1.70 to 1.96, with an assumed average value of 1.83. A grain size distribution curve representative of the sand used by Morrison et al (1986) is shown on Figure 3.7.

The sand exhibited an average dry unit weight of approximately 98.5 pcf and an average moisture content of approximately 2.5 percent from the base of the excavated pit to a depth of approximately 5 feet. From 5 feet to a depth of approximately 10 feet, the sand exhibited a dry unit weight of approximately 94.7 pcf and an average moisture content of approximately 7 percent. Knowing that the sand was inundated with water prior to testing but not knowing if submerged soil conditions existed, an effective unit weight of 110 pcf was used for the first cycle of loading when analyzed by the strain wedge model as described below.

Using this information and assuming that the sand exhibited a specific gravity of 2.65, a void ratio of 0.68 was initially assigned to the sand within the upper 5 feet of the sand layer, while a void ratio of 0.75 was initially assigned to the sand in the lower 5 feet of the sand layer. Using these void ratio

values and an average coefficient of uniformity of 1.83, ϵ_{50} values of 0.004 and 0.0045 as proposed by Norris (1986) were initially assigned to the sand in the upper five feet and lower five feet, respectively, of the sand layer (See Fig 2.12).

The sand exhibits an angle of internal friction that ranges from a value of 34 degrees near the surface to a value of 45 degrees near the bottom of the sand layer (Fig 3.8). In addition O'Neill (1986) reported that the total unit weight of 120 pcf was appropriate for the sand layer after the first cyclic load had been applied to the group. Knowing the increase in the angle of internal friction and that densification of the sand resulted subsequent to the first load cycle to the pile group, an ϵ_{50} value of 0.0035 was assumed to be representative of the sand after the first cycle of loading.

- **Testing Program and Test Results**

As reported by Morrison et al (1986), the steel pipe piles were instrumented with strain gauges in order to record pile bending moments and pile stresses with depth, and to develop p-y curves for the piles. The loading frame used by Brown et al (1985), with moment-free connections to each pile, was used to allow for well controlled pile head conditions. Cyclic, two-directional loads were applied to the pile group using a constant deflection during loading. A total of 200 cycles for 6 different deflections were applied to the pile group in north-south directions. For the study, loading to the north was assumed to be in compression, while loading to the south was assumed to be in tension. Results were recorded using a data acquisition system. The same loading applied to the pile group was also applied to the single isolated pile.

- **Comparison of Results of Load Test with Results Predicted by the Strain Wedge Model**

The strain wedge model was run using the pile and soil input properties outlined above. In general, the strain wedge model provided a very good prediction of pile group response for the case analyzed. The following summarizes the results of the strain wedge model as compared to the results obtained from the full-scale pile group load test described above.

Before a comparison between pile group response can be made in this case, it is again important that

the strain wedge model accurately predicts the response of an isolated pile embedded in the same soil profile. Fortunately, the load test conducted by Morrison et al (1986) included the testing of an isolated pile as shown in Fig.3.9. The results of the strain wedge model associated with the isolated pile have also been shown on this figure. As can be seen from the results presented, the strain wedge model accurately predicts the response of the single pile in good agreement with the observed values (before cyclic motion of the piles, which densified the sand).

Knowing that the strain wedge model accurately predicts the response of an isolated pile embedded in the same soil profile, an accurate prediction of pile group response should be expected. Figure 3.9 also shows the average load per pile within the group for the applied levels of deflection. The results of the strain wedge model associated with the average load per pile within the group have also been shown on this figure.

Morrison et al (1986) also measured the maximum pile moment for the isolated pile and for piles within the group during the load test. The results presented in Fig. 3.10 indicate that for a given level of average pile head load, the maximum moment for an isolated pile will be less than that measured in the pile group as described previously. All the maximum moments predicted by the strain wedge model for given average pile head loads fall within the range of maximum moments within the group as measured by Morrison et al.

3.5 SUMMARY

As presented in this chapter, the strain wedge model has the capability to assess the response of laterally loaded pile group. The strain wedge model characterizes the interaction among the piles in the group based on three-dimensional analysis to calculate the associated modulus of subgrade reaction for each pile in the group. Thereafter, each individual pile in the group is analyzed as a Beam on Elastic Foundation. This procedure allows the calculation of the amount of interference among the piles in the group according to soil and pile properties, and the level of loading. No reduction factor or a multiplier are needed to be assumed in this procedure.

CHAPTER 4

LIQUEFACTION AND UNDRAINED RESPONSE EVALUATION OF SANDS FROM DRAINED FORMULATION

4.1 INTRODUCTION

Several studies have been conducted to provide a better understanding of the undrained behavior of saturated sand under different types of loading. Some of the pioneering work in this field has been performed by Seed and Lee (1967) Castro (1969), Ishihara et al. (1975), Casagrande (1976), Castro and Poulos (1977), Poulos (1981) and Castro et al. (1982). In addition, several recent studies (Mohamad and Dobry 1986, Guzman et al. 1988, Vaid et al. 1989 and Ishihara 1993) have made significant contributions to the understanding of the undrained behavior of saturated sands. The main interest in these studies is to relate the undrained strength of sand to its initial state in order to allow the designer to predict the potential for a saturated sand to liquefy. In other words, most of the investigations focused on the influence of the consolidation pressure and the associated void ratio of the sand on the undrained behavior of the saturated sand under monotonic and cyclic loading.

The undrained behavior of isotropically consolidated saturated sand under monotonic loading is accompanied by a change in the excess porewater pressure which, in turn, leads to different forms of undrained behavior. Unfortunately, no prior study provides a clear picture of mobilized undrained behavior and the associated effective stress path under undrained monotonic loading. The available studies indicate the potential for sand to liquefy and characterize it as liquefiable or nonliquefiable material. The only way to assess the mobilized undrained behavior of a saturated sand (its stress-strain and stress path) under monotonic loading is via laboratory testing. Consolidating the saturated sand to different values of confining pressure or void ratio, a series of isotropically consolidated undrained (ICU) tests allow one to assess the variation in the peak undrained resistance, the residual stress of the saturated sand and the associated levels of strain.

Recently, it has been shown that the undrained response of sand can be assessed from its drained laboratory response (Norris et al. 1997). This study deals specifically with the formulation of drained behavior as a function of state conditions and sand properties, thus reducing the need for laboratory testing. Therefore, the current study provides a general approach to assess the mobilized undrained behavior of saturated sand under monotonic loading whether the sand is loose, medium dense, or dense. Moreover, the present study allows one to characterize the undrained response of the saturated sand, whether the sand is contractive and/or dilative, to define the potential of the sand to liquefy, and the type of the expected liquefaction (complete or limited liquefaction) as seen in Fig. 4.1.

The approach presented here assesses the undrained behavior of saturated sand under monotonic loading and is based on the most basic properties of the sand such as its void ratio, e_c , or the relative density, Dr_c , at the end of consolidation to pressure, σ_{3c} , the roundness of sand grains, ρ , the uniformity coefficient, C_u , the effective angle of the internal friction, ϕ , and the drained axial strain at 50 percent stress level, ϵ_{50} . This work was developed to deal with most types of sand under different levels of confining pressure. The validity of the work presented and the equations formulated are verified by several comparisons with observed results employing Nevada, Ione, Ottawa, Banding, and Fraser sands. The simplicity of this approach makes it an attractive general method to characterize the undrained behavior of sands in a preliminary analysis with no need to run extensive experimental tests.

4.2 METHOD OF ANALYSIS

The technique developed by Norris et al. (1997) employs a series of drained tests, with volume change measurements, on samples isotropically consolidated to the same confining pressure, σ_{3c} , and void ratio, e_c , to which the undrained test is to be subjected. However, the drained tests are rebounded to different lower values of effective confining pressure, $\bar{\sigma}_3$, before being sheared.

During an isotropically consolidated undrained (ICU) test, the application of a deviatoric stress, σ_d , causes the porewater pressure, Δu_d , to build up which results in a reduced effective confining pressure, $\bar{\sigma}_3$, i.e.

$$\bar{\sigma}_3 = \sigma_{3c} - \Delta u_d \quad (4.1)$$

and an associated isotropic expansive volumetric strain, $\epsilon_{v, iso}$, the same as recorded in an isotropically rebounded drained triaxial test. However, in the undrained test, the volumetric change or volumetric strain must be zero. Therefore, there must be a compressive volumetric strain component, $\epsilon_{v, shear}$, due to the deviatoric stress, σ_d . This shear induced volumetric strain, $\epsilon_{v, shear}$, must be equal and opposite to $\epsilon_{v, iso}$,

$$\epsilon_{v, shear} = -\epsilon_{v, iso} \quad (4.2)$$

so that the total volumetric strain, $\epsilon_v = \epsilon_{v, iso} + \epsilon_{v, shear}$, in undrained response is zero. In the isotropically rebounded drained shear test, $\epsilon_{v, iso}$ and then $\epsilon_{v, shear}$ (to match $\epsilon_{v, iso}$) are obtained separately and sequentially; in the undrained test, they occur simultaneously.

During drained isotropic expansion, the resulting axial strain, ϵ_1 , is

$$\epsilon_{1, iso} = \epsilon_{2, iso} = \epsilon_{3, iso} = \frac{1}{3} \epsilon_{v, iso} \quad (4.3)$$

Based on Hooke's Law and effective stress concepts (Norris et al. 1998), the undrained axial strain due to shear (σ_d) and effective stress ($\bar{\sigma}_3$) changes can be related to the drained or effective stress strains as

$$\begin{aligned} (\epsilon_1)_{undrained} &= (\epsilon_1)_{\sigma_d} + (\epsilon_1)_{\Delta \bar{\sigma}_3} = (\epsilon_1)_{drained} + \epsilon_{1, iso} \\ &= (\epsilon_1)_{drained} - \frac{1}{3} \epsilon_{v, iso} \end{aligned} \quad (4.4)$$

Therefore, with isotropically consolidated-rebounded drained triaxial tests available for different $\bar{\sigma}_3$, one can assume a value of $\bar{\sigma}_3$, find $\varepsilon_{v, iso}$ (Fig. 4.2b), enter the ε_v - ε_1 drained shear curves (Fig. 4.2a) at $\varepsilon_{v, shear}$ equal to $\varepsilon_{v, iso}$, and find the drained ε_1 and σ_d on the same confining pressure ($\bar{\sigma}_3$) ε_v - ε_1 and ε_1 - σ_d curves. Then $(\varepsilon_1)_{undrained}$ is established according to Eqn. 4.4 and one point on the undrained σ_d - ε_1 curve can be plotted. The corresponding effective stress path ($\bar{p} = \bar{\sigma}_3 + \sigma_d / 2$ versus $q = \sigma_d / 2$) can also be plotted as shown in Fig. 4.2c. This technique is illustrated in detail by Norris et al. (1995 and 1997).

The technique presented above requires a series of isotropically consolidated drained (ICD) tests be performed to allow one to assess the undrained stress-strain curve of a saturated sand consolidated to a certain confining pressure, σ_{3c} , at a particular value of void ratio, e_c , or relative density, Dr_c . This, in turn, requires a certain level of experience, effort, time and cost. The study presented here establishes a group of applicable equations based on the basic properties of sand in order to yield the following relationships:

- The stress-strain and volume change curves of the isotropically consolidated, drained, triaxial test at different values of confining pressure.
- The isotropically consolidated, rebounded, volume change curve.
- The stress-strain and volume change curves of the isotropically consolidated, rebounded, drained test at different overconsolidation ratios ($OCR = \sigma_{3c} / \bar{\sigma}_3$).

These drained relationships can then be used to predict the undrained response of saturated sand as described above.

4.3 DRAINED BEHAVIOR FORMULATION OF ISOTROPICALLY CONSOLIDATED SAND UNDER DEVIATORIC STRESSES

4.3.1 Drained Stress-Strain (σ_d - ε_1) Relationship

The stress-strain relationship presented here is employed to assess the drained stress-strain curve of the isotropically consolidated sand under shear loading (confining pressure, $\bar{\sigma}_3$, held constant). This

stress-strain relationship was originally established by Norris (1986) and then modified by Ashour et al. (1998). The ratio of deviator stress, σ_d , at axial strain, ϵ_1 , to the failing stress, σ_{df} , is the stress level, SL, which is given as

$$SL = \frac{\sigma_d}{\sigma_{df}} = \frac{\lambda \epsilon_1}{\epsilon_{50}} \exp(-3.707 SL) \quad (4.5)$$

where ϵ_{50} is the value of ϵ_1 at $SL = 0.5$, and 3.707 and λ represent the fitting parameters of the relationship. λ is equal to 3.19 at $\epsilon_1 \leq \epsilon_{50}$ and then varies linearly with the stress level between 3.19 at $\epsilon_1 = \epsilon_{50}$ and 2.14 at $\epsilon_1 = \epsilon_{80}$. If the stress level is greater than 80 percent the stress-strain relationship is given as

$$SL = 0.2 \exp\left[\frac{100 \epsilon_1}{(m \epsilon_1 + q)}\right] \quad (4.6)$$

where $m=59.0$ and $q=95.4 \epsilon_{50}$ are the fitting parameters.

At constant confining pressure, the drained strength, σ_{df} , of a sand is a function of both $\bar{\sigma}_3$ and the frictional angle, ϕ . Accordingly,

$$\sigma_d = SL (\sigma_d)_f = SL \bar{\sigma}_3 \left[\tan^2 \left(45 + \frac{\phi}{2} \right) - 1 \right] \quad (4.7)$$

During the undrained test, $\bar{\sigma}_3$ will vary with the changing porewater pressure but the stress level, SL, at the current $\bar{\sigma}_3$, and shear induced axial strain, ϵ_1 , is given by Eqn. 4.5. Note that ϵ_1 in Eqn. 4.5 is $(\epsilon_1)_{\text{drained}}$ of Eqn. 4.4.

The drained axial strain at 50 percent stress level, ϵ_{50} , is given as

$$(\epsilon_{50})_{\alpha_{3c}} = (\epsilon_{50})_{42.5} \left(\frac{\alpha_{3c}}{42.5} \right)^{0.2} \quad (4.8)$$

where α_{3c} represents the applied consolidation pressure in kPa, and $(\epsilon_{50})_{42.5}$ denotes the drained axial strain at 50 percent stress level under a confining pressure of 42.5 kPa. $(\epsilon_{50})_{42.5}$ is given by Norris (1986) based on correlation with the sand's uniformity coefficient, C_u , and the void ratio, e_c , (or Dr_c), at the applied consolidation pressure.

Given that a simple shear response for an initial isotropic stress state ($\bar{\sigma}_m = \alpha_{3c}$, $K_o = 1$) can be viewed as an expanding Mohr circle about the point α_{3c} , then Eqn. 4.5 can be used to evaluate the modulus reduction relationship, G/G_o , to compare with the long accepted variations (e.g. Seed and Idriss, 1970) as shown for example in Fig. 4.3. Such good agreement gives the proposed formulation added credibility. As shown in Appendix II, the position of the modulus reduction curve will shift with ϵ_{50} which, as judged from Eqn. 4.8, varies with the confining pressure, α_{3c} .

4.3.2 Volume Change in Drained Response Due to Shear Stress ($\epsilon_{v, shear} - \epsilon_1$ Relationship)

The prediction of the volume change of sand through the volumetric strain, $\epsilon_{v, shear}$, due to shear loading is based upon basic information such as $\bar{\sigma}_3$, Dr_c , ϵ_{50} , and ρ . The roundness, ρ , of the sand is determined using a comparator chart e.g. Powers (1953). See Table 4.1 for numerical values for descriptive adjectives, "angular", etc. A number of drained tests performed on different sands (Table 4.2) are used to formulate a series of empirical equations which describe the drained behavior of isotropically consolidated sands.

As seen in Fig. 4.4, the main features that control the shape of the $\epsilon_{v, shear} - \epsilon_1$ relationship are the coordinates and the slopes of the $\epsilon_{v, shear} - \epsilon_1$ curve at points A, B, and C. The initial slope of the $\epsilon_{v, shear} - \epsilon_1$ curve at point A is S_A which is equal to $d\epsilon_{v, shear}/d\epsilon_1$ where ϵ_1 and $\epsilon_{v, shear}$ are equal to zero. The coordinates of peak volumetric strain at point B are $(\epsilon_1)_B$ and $(\epsilon_{v, shear})_B$ where $(\epsilon_{v, shear})_B$ represents $(\epsilon_{v, shear})_{max}$. The slope of the $\epsilon_{v, shear} - \epsilon_1$ curve at point B is S_B and is equal to zero. Finally, at failure, the slope and the coordinates at point C on the $\epsilon_{v, shear} - \epsilon_1$ curve are expressed by S_f and $(\epsilon_1, \epsilon_{v, shear})_C$,

respectively. At point C, S_f is equal to $(d\varepsilon_{v, shear}/d\varepsilon_1)_f$. Beyond point C, the $\varepsilon_{v, shear}-\varepsilon_1$ curve extends linearly at a constant slope equal to S_f .

In order to plot the $\varepsilon_{v, shear}-\varepsilon_1$ curve, a fifth order binomial equation is established based on the slopes and the coordinates at the three major points on the $\varepsilon_{v, shear}-\varepsilon_1$ curve (A, B, and C). The slopes and coordinates at the points A, B and C represent the boundary conditions of Eqn. 4.9.

$$\varepsilon_{v, shear} = a + b\varepsilon_1 + c\varepsilon_1^2 + d\varepsilon_1^3 + e\varepsilon_1^4 + f\varepsilon_1^5 \quad (4.9)$$

Terms a through f are the constants needed to satisfy these boundary conditions. ε_1 and $\varepsilon_{v, shear}$ symbolize the axial strain and the associated volumetric strain due to deviatoric stress of any point on the $\varepsilon_{v, shear}-\varepsilon_1$ curve, respectively. The derivation of Eqn. 4.9 is presented in Appendix II.

The slopes and coordinates at points A, B and C on the $\varepsilon_{v, shear}-\varepsilon_1$ curve at σ_{3c} are obtained using Eqns. 4.10 through 4.15. These equations are empirically developed based on data of isotropically consolidated drained tests on 7 different sands from different environments and obtained by different investigators (Table 4.2). It should be mentioned here that the volume change behavior of any sand is influenced by the method of sample preparation (Ishihara 1993, and Been and Jefferies 1985). The drained tests were performed on loose, medium, and dense sands prepared by different methods. Therefore, the following formulation represents an average for different sample preparation techniques. The sands were isotropically consolidated to different confining pressures (σ_{3c}).

- From Fig. 4.5a, the initial slope, $(S_A)_{\sigma_{3c}}$, at point A on the $\varepsilon_{v, shear}-\varepsilon_1$ curve is given as

$$(S_A)_{\sigma_{3c}} = \lambda_1 = \frac{1}{\exp(\rho^2 + Dr_c)} \quad (4.10)$$

Note that Dr_c in this and the following equations is a decimal value. As noticed in the data recorded by Dakoulas and Yuanhui (1992), Negussey and Vaid (1990), and Been and Jefferies (1985), the variation of the consolidation pressure has no significant effect on the slope S_A .

- The maximum value of the volumetric strain due to applied deviatoric stress, $(\epsilon_{v, shear})_{max}$, is located at point B and is equal to $(\epsilon_{v, shear})_B$. According to the experimental results shown in Fig. 4.5b, $(\epsilon_{v, shear})_B$ at σ_{3c} is obtained as

$$(\epsilon_{v, shear})_{B, \sigma_{3c}} = (\epsilon_{v, shear})_{max, \sigma_{3c}} = 2\lambda_2 = 2 \left[\frac{\epsilon_{s0}^2}{\exp(Dr_c)} \right]_{\sigma_{3c}} \quad (4.11)$$

- From Fig. 4.5c, the axial strain $(\epsilon_1)_B$ which is associated with $(\epsilon_{v, shear})_{max}$ is given as

$$(\epsilon_1)_{B, \sigma_{3c}} = 6\lambda_3 = \frac{6 (\epsilon_{v, shear})_{max, \sigma_{3c}}}{\exp(\rho Dr_c)} \quad (4.12)$$

- Similar to point B, the slope and coordinates at point C on the $\epsilon_{v, shear}-\epsilon_1$ curve can be evaluated based on the data presented in Fig. 4.5. The value of the volumetric strain at point C is assessed using the data plotted in Fig. 4.5d and is obtained as

$$(\epsilon_{v, shear})_{C, \sigma_{3c}} = \lambda_4 = (\epsilon_{v, shear})_{max, \sigma_{3c}} \left[\frac{(\epsilon_1)_{B, \sigma_{3c}}}{(\epsilon_1)_{C, \sigma_{3c}}} \right]^{0.2} [1 + (S_f)_{\sigma_{3c}}] \quad (4.13)$$

- The value of the axial strain at point C (Fig. 4.5e) is related to $(\epsilon_{v, shear})_{max}$, and φ , and is given by

$$(\epsilon_1)_{C, \sigma_{3c}} = 6\lambda_5 = 6 (\epsilon_{v, shear})_{max, \sigma_{3c}} \exp(\tan^2 \varphi) \quad (4.14)$$

- Fig. 4.5f indicates the variation of the slope S_f at point C which is expressed as

$$(S_f)_{\sigma_{3c}} = -\lambda_6 = -\rho^{0.5} Dr_c \tan^2 \varphi \quad (4.15)$$

- Based on the experimental data of the isotropically consolidated drained tests presented in Fig.

4.6, the isotropic volumetric strain, $(\epsilon_v)_c$, to pressure σ_{3c} is given as

$$(\epsilon_v)_c = \lambda_7 = \epsilon_{s0} \exp[Dr_c (1 + \rho)] \quad (4.16)$$

4.4 FORMULATION OF DRAINED REBOUNDED BEHAVIOR

4.4.1 The Isotropic Rebounded Volume Change of Saturated Sand ($\bar{\sigma}_3 - \epsilon_{v, iso}$ Relationship)

Fig. 4.7 presents the observed isotropically consolidated-rebounded behavior of Nevada, Ione (Norris et al. 1997) and Ottawa sands (Dakoulas and Yuanhui 1992) for different values of the consolidation pressure, σ_{3c} (400, 800 and 300 kPa), and overconsolidation ratio (OCR). The observed data of the sands considered are employed to assess an empirical relationship that expresses the rebounded behavior of the sand under decreasing values of the confining pressure (Fig. 4.7). The isotropic rebounded volumetric strain of the saturated sand ($\epsilon_{v, iso}$) is given as

$$\epsilon_{v, iso} = (\epsilon_v)_c - \frac{(\epsilon_v)_c}{OCR^\eta} \quad (4.17)$$

$$\text{where } \eta = \frac{\rho^{0.1}}{4} \exp(0.5 \rho Dr_c) \text{ , and } OCR = \frac{\sigma_{3c}}{\sigma_3} \quad (4.18)$$

4.4.2 Drained Behavior of Isotropically Consolidated-Rebounded Saturated Sand

Two series of isotropically consolidated rebounded drained tests (Norris et al. 1997) performed on two different sands (Nevada and Ione sand) are employed to develop empirical equations in order to describe the drained behavior of isotropically rebounded sand under different values of the overconsolidation ratio (OCR). The drained behavior of consolidated-rebounded sand during shear loading is expressed by the stress-axial strain-volumetric strain relationship due to shear, $\sigma_d - \epsilon_1 - \epsilon_{v, shear}$. The following equations provide the terms of the boundary conditions which are required to plot the $\epsilon_1 - \epsilon_{v, shear}$ relationship at OCR greater than 1. These equations are a function of sand properties and the $\sigma_d - \epsilon_1 - \epsilon_{v, shear}$ relationship at OCR equal to 1 as discussed in the previous section.

In order to assess the drained stress-strain relationship of the rebounded sand under a reduced confining pressure, $\bar{\sigma}_3$, the axial strain at SL of 50 percent is given as

$$(\epsilon_{50})_{\bar{\sigma}_3} = \frac{(\epsilon_{50})_{\sigma_{3c}}}{OCR^{0.5}} \rho^{0.25} \quad (4.19)$$

where ϵ_{50} at σ_{3c} (i.e. OCR =1) is given by Eqn. 4.8. Using $(\epsilon_{50})_{\bar{\sigma}_3}$ in Eqns. 4.5 through 4.7, the drained stress-strain curve of a sand at a rebounded confining pressure, $\bar{\sigma}_3$ (OCR > 1), can be evaluated.

The empirically calculated slopes and coordinates at points A, B, and C on the ϵ_1 - $\epsilon_{v, shear}$ curve of the isotropically consolidated-rebounded drained test at $\bar{\sigma}_3$ (OCR > 1) are used in the determination of constants a through f in Eqn. 4.9 as follows,

- The initial slope at point A

$$(S_A)_{\bar{\sigma}_3} = \frac{(S_A)_{\sigma_{3c}}}{OCR^{0.5}} \left[\frac{(\epsilon_{v, shear})_{\max, \bar{\sigma}_3}}{(\epsilon_{v, shear})_{\max, \sigma_{3c}}} \right]^{0.25} \quad (4.20)$$

- The volumetric strain due to shear at point B

$$(\epsilon_{v, shear})_{\max, \bar{\sigma}_3} = \frac{(\epsilon_{v, shear})_{\max, \sigma_{3c}}}{OCR^\mu} \quad (4.21)$$

$$\mu = \rho^{0.8} \exp \left[\frac{Dr \rho}{OCR} \right] \quad (4.22)$$

- The axial strain at point B

$$(\epsilon_1)_{B, \bar{\sigma}_3} = (\epsilon_1)_{B, \sigma_{3c}} \left[\frac{(\epsilon_{v, shear})_{\max, \bar{\sigma}_3}}{(\epsilon_{v, shear})_{\max, \sigma_{3c}}} \right]^{0.5} \quad (4.23)$$

- Volumetric and axial strains, and the slope at point C

$$(\varepsilon_{v, shear})_{C, \bar{\sigma}_3} = (\varepsilon_{v, shear})_{\max, \bar{\sigma}_3} \frac{(\varepsilon_{v, shear})_{C, \sigma_{3c}}}{(\varepsilon_{v, shear})_{\max, \sigma_{3c}}} \quad (4.24)$$

$$(\varepsilon_1)_{C, \bar{\sigma}_3} = (\varepsilon_1)_{C, \sigma_{3c}} \left[\frac{(\varepsilon_1)_{B, \bar{\sigma}_3}}{(\varepsilon_1)_{B, \sigma_{3c}}} \right]^{0.25} \quad (4.25)$$

An interesting phenomenon reported by Norris et al. (1997) is that all drained rebounded (i.e. overconsolidated) volume change curves exhibit the same slopes, S_p , as that at σ_{3c} (OCR=1).

$$(S_p)_{\bar{\sigma}_3} = (S_p)_{\sigma_{3c}} \quad (4.26)$$

This approach is more accurate if the value of ε_{50} at consolidation pressure, σ_{3c} , is determined from testing rather than reliance on Eqn. 4.8. This, in turn, affects the determination of the undrained response from the drained behavior.

Based on the approach presented, the drained behavior of consolidated and overconsolidated sands can be assessed. Figures 4.8 and 4.9 exhibit a comparison between observed and predicted behavior for Nevada and Ione sand. The assessed stress-strain relationship and volume change curves show good agreement with the experimental results performed by Norris et al. (1997). In addition, the predicted and observed isotropically consolidated and then rebounded volume change response for different sands exhibit a good match as shown in Fig. 4.7.

4.5 LIMITATION FOR DILATIVE BEHAVIOR

The undrained strength of saturated sand under monotonic loading in its dilative mode is limited, in this paper, to its drained strength because negative porewater pressure (i.e. a drained Poisson's ratio, $\nu, > 0.5$) is not considered in this study (see Fig. 4.10a). Once the excess porewater pressure

during the dilative response becomes equal to zero, the effective confining pressure will be equal to the consolidation confining pressure (σ_{3c}), and the undrained response of the sand will be limited by its drained behavior as indicated in Fig. 4.10b. Therefore, the approach presented exhibits a conservative interpretation under monotonic loading when dense sand generates negative excess porewater pressure. The incorporation of negative excess porewater pressure in dense sands using the approach presented is under investigation and will be considered in a separate paper.

4.6 VERIFICATION OF THE PROPOSED APPROACH

The approach developed has been verified through various comparisons to experimental results of different types of sands. Some of these comparisons are presented in this paper, and the properties of these sands are presented in Table 2. The comparison study covers the density of sand from very loose to dense sand under different values of the confining pressure. Most of the undrained stress-strain responses and stress paths assessed, using a computer program, exhibit good agreement with the observed results as seen in the accompanying figures. The approach developed has been verified through various comparisons to experimental results of different types of sands. These comparisons cover the density of sand from very loose to dense sand under different values of the confining pressure. It should be noted that the laboratory tests were run using different techniques of sampling, loading, and data acquisition. Moreover, the testing procedures of some of these tests went through some difficulties which, in turn, affected the accuracy of the published results. The tested samples of sands were prepared with initial void ratios that, usually, do not match the initial void ratios in the field due to the natural sedimentation and then consolidation. Therefore, the isotropic volumetric change measured in the lab may not match the field isotropic volumetric change under the same confining pressure. As a result, the initial void ratio of the tested sample of sand governs the initial structure of the sand sample and the recorded results.

4.6.1 Nevada Sand

As mentioned by Norris et al. (1995, 1997), samples for test series 1 on Nevada sand were prepared using a pouring tube filled with dry sand resting on the sample base inside a vacuum forming mold. The tube with a mesh at its bottom was raised at a constant rate leaving behind a loose structure of the sand. The samples were 71 mm in diameter by 152 mm high. This method of sampling is

similar to the dry deposition sample preparation technique. The sample was saturated at a back pressure of 100 kPa and then consolidated to an effective confining pressure of 400 kPa. The average relative density at the end of the consolidation was 15.2% and the effective angle of internal friction was 32 degrees. The value of ϵ_{50} at the consolidation pressure σ_{3c} was equal to 0.94%. However, ϵ_{50} can be estimated by using Figure 4.11 and Eqn. 4.12.

Figures 4.11a and 4.11b exhibit a comparison between the undrained behavior of Nevada sand monitored in the lab (Norris et al. 1995, 1997) and the predicted undrained behavior using the stress-strain-volume change characterization technique presented here. The technique developed provides an undrained stress-strain relationship in excellent agreement with the measured values over a long range of axial strain, as seen in Figure 4.11b. Nevada sand shows a limited liquefaction response associated with a residual strength (phase transformation) of approximately 100 kPa at values of axial strain range between 4 to 6 percent. The residual strength is followed by a substantial growth in the strength.

By comparison, the assessed effective stress path presented in Figure 4.11a provides a very good prediction for the undrained strength of Nevada sand during the contractive and dilative behavior of the sand.

4.6.2 Ione Sand

Ione sand was used by Norris et al. (1995, 1997) to study its undrained behavior and its potential to liquefy. The samples employed were prepared using sand wetted to 0.05% moisture, drawn through a pouring tube with a mesh at its bottom. The prepared sample was 71 mm in diameter and 152 mm high. The sample was saturated under a back pressure of 100 kPa. The sample volume was carefully measured after sample formation (at 50 kPa) and its volumetric change was recorded during the isotropic consolidation from 50 to 800 kPa. The void ratio and the relative density were assessed at the end of the consolidation ($\sigma_{3c} = 800$ kPa). The average relative density at the end of the consolidation was approximately 32% and the effective angle of internal friction was 28 degrees. The value of ϵ_{50} under the consolidation pressure σ_{3c} was equal to 1.55%. However, ϵ_{50} can be estimated by using Figure 4.8 and Eqn. 4.11.

Figures 4.12a and 4.12b exhibit a comparison between the observed and the predicted undrained stress-strain behavior of Ione sand. Based on the properties of Ione sand mentioned above and listed in Table 4.2, the established approach efficiently assesses the constitutive relationship of Ione sand. The mobilized undrained response of Ione sand which is plotted in Figure 4.12b shows good agreement with the recorded values at the low and high levels of sand strain. The undrained behavior of Ione sand yields a limited liquefaction response at the residual strength followed by a slight increase in the undrained strength of the sand at the higher values of axial strain.

The method presented provides excellent assessment for the effective stress path of Ione sand. Figure 4.12a exhibits the match between the observed and predicted values of the effective stress path during the contractive and dilative behavior of Ione sand, and the location of the inflection point on the stress path.

4.6.3 Ottawa Sand

The test results of the monotonic undrained behavior of Ottawa sand which were recorded by Vaid et al. (1989) are used to verify the developed approach. The properties of Ottawa sand used by Vaid et al. (1989) are similar to those of the sand used by Negussey and Vaid (1990). The tested samples were 63 mm in diameter by 126 mm high and prepared by water pluviation technique. The initial relative density of all samples after forming at a pressure of 20 kPa was 32.5%. The sand was monotonically loaded after consolidation to a confining pressure of 196 kPa (2 kg/cm²). The effective angle of internal friction was taken in the range of 33 to 37 degree based on the value given by Vaid and Chern (1983), and Dakoulas and Yuanhui (1992), and according to the values of the associated relative density. The relative densities of the samples at the consolidation pressure range from 36% to 62.5% as seen in Figure 4.13.

Figure 4.13a shows the undrained stress-strain relationship under monotonic loading and confining pressure of 2 kg/cm². The response of Ottawa sand relies on the relative density at the end of consolidation (D_{r_c}). Samples 1, 2 and 3 experience contractive behavior followed by dilative behavior. However, the determined drop in sand strength between the peak of the undrained strength and the residual strength over the three sets of tests ranges between approximately 30% to

15%. It should be mentioned that the initial relative density of the tested sand has a significant influence on the undrained behavior of the sand.

The recorded behavior of samples 4 and 5 indicate dilative behavior as a result of the high relative density. The undrained stress-strain relationship assessed for sample set 4 experiences a slight contractive response before dilative response takes over. The response predicted is still in reasonable agreement with the observed behavior. Sample 5 exhibits consistent dilative behavior over both the experimental tests and as predicted by the technique proposed.

The stress paths assessed from the tested samples are presented in Figure 4.13b. The developed method allows assessment of the effective stress paths of Ottawa sand efficiently. Figure 4.13b exhibits clearly the mobilized strength of Ottawa sand during the contraction and/or dilatancy stages of loose, medium dense and dense conditions.

4.6.4 Fraser River Sand

The results presented in Fig. 4.14 were obtained from tests performed on Fraser River sand (Vaid and Thomas 1995). This sand grain sizes ranging from 0.074 mm to 0.6 mm. Maximum and Minimum void ratios are 1.00 and 0.68. The sand used has $D_{50}=0.3$ mm, C_u (uniformity coefficient) = 1.5, and $Dr = 19\%$. Triaxial specimens used were 63 mm diameter and 126 mm high, and reconstituted by water pluviation.

The observed and predicted undrained response of Fraser River sand is presented in Fig. 4.14. The experimental tests were performed by Vaid and Thomas (1995). The data presented describe the stress-strain relationship and effective stress path of the sand at relative density (Dr_c) of 19% under different values of consolidation pressure ($\sigma_{3c} = 1200, 400$ and 200 kPa). Figure 4.14 shows reasonable agreement between predicted and observed response.

4.6.5 Banding Sand

Banding sand was used by Castro (1969) to perform a series of undrained triaxial tests under monotonic and cyclic loading. The tested specimens were 35 mm diameter and 89 mm high and

lubricated ends permitted all samples to expand laterally at the end when strained axially during the test. However, the non-uniformities of strains due to water migration within the sample during the undrained test caused a variation in the void ratio in the sample. The sand sample showed a dramatic increase in relative density above the average value (Dr_c) at the top and a substantial drop below the average value of Dr_c in the middle portion. This behavior yields complete liquefaction observed with most of the results presented by Castro (1969) for loose and medium dense Banding sand.

The results of Banding sand presented in Figure 4.15 cover relative densities from 21% (loose sand) to 64% (medium dense sand), and consolidation pressures from 0.3 kg/cm² to 4 kg/cm². The values of ϵ_{50} and the angle of internal friction of each tested sample are measured from the drained stress-strain curve under the associated consolidation pressure (Castro 1969).

The technique employed provides an assessment for the undrained strength of the Banding sand. The assessed undrained stress-strain responses exhibit good agreement with the observed results such as the tests seen in Figures 4.15a, b and c. Generally, the ultimate and residual strength predicted are in good agreement with the measured values.

In some cases such as in Figures 4.18a and b, the tested samples experience complete liquefaction while the response predicted exhibits limited liquefaction. Such behavior occurs as a result of the non-uniform distribution of the excess porewater pressure and void ratio throughout the sample inducing a low relative density zone at the middle of the sample (Castro 1969). Therefore, some planes of failure develop in the middle of the sample thus creating complete liquefaction in the lab that may not occur in the field.

4.7 SUMMARY AND CONCLUSION

This chapter has provided the formulation for assessing the drained and drained rebounded response ($\epsilon_v - \bar{\sigma}_3$ and $\sigma_d - \epsilon_1 - \epsilon_v$) for sand for use in assessment of its undrained behavior ($\sigma_d - \epsilon_1$ and stress path). A general approach has been established to assess the undrained stress-strain curve and effective stress path under monotonic loading from drained triaxial tests. The wide range in diversity

of the responses as well as properties of the sands required that the dependence upon important sand properties and conditions be evaluated. Appropriate formulation of drained and drained rebounded (i.e. overconsolidated) triaxial test response is developed that, in turn, allows the assessment of developing liquefaction and the undrained behavior of saturated sands. The formulation presented is a function of the void ratio, confining pressure and basic properties of sand such as relative density, uniformity coefficient, and roundness which are typically available to the designer or can be obtained from visual inspection. The formulation of drained behavior is based upon reported experimental drained test results that were obtained from different investigators using different testing techniques. The developed formulas allow one to predict the potential of sand to liquefy, the type of liquefaction (limited or complete liquefaction) or dilative behavior, the peak and residual strength values, as well as the whole undrained stress-strain curve and effective stress path. The developed approach has been validated using several comparisons with published results of undrained triaxial tests on different sands (Nevada, Ione, Banding, Ottawa and Fraser sand). The simplicity of this approach makes it an attractive general method (in a computer program) to characterize the undrained behavior of sands (loose, medium or dense).

CHAPTER 5

LATERAL LOADED PILE RESPONSE IN LIQUEFIED SOIL

5.1 INTRODUCTION

This chapter provides the methodology to assess the response of an isolated pile in sand under an applied pile head load/moment combination assuming undrained conditions in the sand. The degradation in soil strength due to the free-field excess porewater, generated by the earthquake, is considered along with the near-field excess porewater pressure generated by lateral loading from the superstructure. Current design procedures assume slight or no resistance for the lateral movement of the pile in the liquefied soil which is a conservative practice. Alternatively, if liquefaction is assessed not to occur, some practitioners take no account of the increased free-field porewater pressure, and none consider the additional near-field porewater pressure due to inertial interaction loading from the superstructure; a practice that is unsafe in loose sands. The strain wedge (SW) model, developed to evaluate drained response (a nonlinear three-dimensional model of a flexible pile in soil), has been extended to incorporate the undrained response of a laterally loaded pile in sand. The chapter characterizes the reduction in pile response due to a drop in sand strength and Young's modulus as a result of developing liquefaction in the sand.

5.2 ANALYSIS PROCEDURE OF LATERALLY LOADED PILE IN SAND UNDER LIQUEFACTION CONDITIONS

This chapter combines three different techniques to analyze the response of a laterally loaded pile in saturated sands under undrained conditions and developing liquefaction.

- Evaluation of the excess porewater pressure generated in the free-field ($u_{xs, ff}$), Fig. 5.1, due to the earthquake shaking based on Seed's method (Seed et al. 1983). This excess porewater pressure reduces the effective stress and, therefore, the corresponding soil resistance for subsequent undrained load application.

- Assessment of the excess porewater pressure ($u_{xs, nf}$) in the near-field soil region (adjacent to the pile, Fig. 5.1) induced by the lateral load from the superstructure. Undrained formulation for saturated sand presented by Ashour and Norris (1999) is employed to assess the undrained stress-strain relationship at any level of loading.
- $u_{xs, ff}$ and $u_{xs, nf}$ calculated using the previous techniques are incorporated with the strain wedge (SW) model analysis (Ashour et al. 1998) to predict the response of a laterally loaded pile. The SW model is extended to treat the undrained conditions in sand as presented later.

The assessed value of the free-field excess porewater pressure ratio, r_u , induced by the earthquake is obtained using Seed's method (Seed et al. 1983). This $u_{xs, ff}$ is calculated conservatively at the end of earthquake shaking corresponding to the number of equivalent uniform cycles produced over the full duration of the earthquake. Thereafter, the lateral load (from the superstructure) is applied at the pile head that generates additional porewater pressure ($u_{xs, nf}$) in the soil immediately around the pile, given the degradation in soil strength already caused by $u_{xs, ff}$. Note that $u_{xs, ff}$ is taken to reduce the vertical effective stress from its pre-earthquake state ($\bar{\sigma}_{v0}$), i.e. $\bar{\sigma}_v = (1 - r_u) \bar{\sigma}_{v0}$. Thereafter, the undrained behavior (e.g. relative superstructure excitation) due to an inertial induced lateral load is assessed using undrained stress-strain formulation in the SW model. Thus, the procedure accounts for both of $u_{xs, ff}$ and $u_{xs, nf}$. It should be noted that these procedures incorporate the whole undrained stress-strain curve (at any level of loading) not only the residual strength of the sand (Fig. 5.2).

While this scenario takes the equivalent load from the superstructure (P_o) to occur at the largest value of $u_{xs, ff}$, the designer may wish to evaluate the effect of this load at an earlier time during shaking and is free to do so (using a portion of $u_{xs, ff}$). This analysis provides the pile head load-deflection (P_o - Y_o) and pile head load-maximum bending moment (P_o - M_{max}) relationship corresponding to different levels of anticipated load, P_o . As a result, the designer can calculate the equivalent static load during the earthquake and obtain the corresponding Y_o and M_{max} values from the predicted P_o - Y_o and P_o - M_{max} curves, respectively.

The technique presented yields the undrained p-y curves along the deflected length of the pile

showing a distinct change from the corresponding drained soil-pile interaction response. The undrained SW model takes into account the effect of pile properties as well as the properties of the sand on the resulting nonlinear p-y curves and, hence, the pile head response. The analysis procedure considers the developing or mobilized wedge of resisting soil as part of its nonlinear deflection compatible evaluation. An associated computer program gives the pile-head load, the associated pile-head deflection and the maximum moment value as well as undrained p-y curves (as desired).

5.3 FREE-FIELD EXCESS POREWATER PRESSURE, $u_{xs, ff}$

Seed et al. (1983) developed a simplified procedure for evaluating the liquefaction potential of sand for level ground conditions based on the sand's corrected standard penetration test (SPT) blow count, $(N_1)_{60}$. The free-field porewater pressure increase ($u_{xs, ff}$) in the sand or silty sand soils due to the equivalent history of earthquake shaking can likewise be assessed. The procedure requires knowledge of the total and effective overburden pressure (σ_{vo} and $\bar{\sigma}_{vo}$, respectively) in the sand layer under consideration, the magnitude of the earthquake (M), the associated maximum ground surface acceleration (a_{max}) at the site, and the percentage of fines in the sand (Seed et. al 1985). The cyclic stress ratio, CSR [$(\tau_h)_{ave} / \bar{\sigma}_{vo}$], induced by the earthquake at any depth is computed as

$$CSR = \frac{(\tau_h)_{ave}}{\bar{\sigma}_{vo}} = 0.65 \frac{a_{max}}{g} \frac{\sigma_{vo}}{\bar{\sigma}_{vo}} r_d \quad (5.1)$$

where $(\tau_h)_{ave}$ is the magnitude of the uniform sinusoidal shear stress on horizontal and vertical planes of N equivalent cycles of excitation, g is the acceleration of gravity, and r_d is the stress reduction coefficient varying from 1 at the ground surface to a value of 0.9 at a depth of 9.6 m. The stress reduction coefficient (r_d) versus depth is given in Fig. 5.3 of Seed and Idriss (1971).

Curves of the cyclic resistance ratio (CRR) necessary to cause liquefaction in an M = 7.5 earthquake versus the corrected blow count, $(N_1)_{60}$, are given by (an updated) Fig. 5.4 of Seed et al. (1985) for different fines contents. Youd and Idriss (1997) provide a summary of different scaling factors and their equations suggested by various investigators to convert this resistance ratio (of 15 cycles at M = 7.5) to that of the desired earthquake M of N cycles. A curve midway in the recommended range

is employed herein (Fig. 5.5).

The factor of safety against liquefaction at the end of N cycles of excitation of an earthquake of magnitude M is taken as the ratio, CRR / CSR . Even if this ratio does not drop to a value of unity (i.e. failure), a free-field excess porewater pressure will result. If N cycles of CSR are induced, but N_1 cycles are required to liquefy the sand at this same stress ratio, then the excess porewater pressure ratio (r_u) generated is given in Fig. 5.6 (DeAlba et al. 1976) as a function of N / N_1 . Given r_u , the free-field excess porewater pressure generated is

$$u_{xs,ff} = r_u \bar{\sigma}_{vo} \quad (5.2a)$$

and the resulting reduced vertical effective stress is

$$\bar{\sigma}_v = (1 - r_u) \bar{\sigma}_{vo} \quad (5.2b)$$

5.4 NEAR-FIELD EXCESS POREWATER PRESSURE, $u_{xs,nf}$

The technique for assessing undrained response developed by Norris et al. (1997) and formulated by Ashour and Norris (1999) employs a series of drained tests (with volume change measurements) on samples isotropically consolidated to the same confining pressure, σ_{3c} ($= \bar{\sigma}_{vo}$), and void ratio, e_c , to which the undrained test is to be subjected. However, the drained tests are rebounded to different lower values of effective confining pressure, $\bar{\sigma}_3$, before being sheared (Fig. 5.7).

During an isotropically consolidated undrained (ICU) test, which represents the state in the saturated sand around the pile, the application of a deviatoric stress, σ_d , produced by the lateral load from the superstructure causes the near-field porewater pressure ($u_{xs,nf}$) to build up which results in a reduced effective confining pressure, $\bar{\sigma}_3$ (Fig. 5.7b), i.e.

$$\bar{\sigma}_3 = \sigma_{3c} - u_{xs,nf} \quad (\text{effect of near-field porewater pressure only}) \quad (5.3a)$$

In order to simulate the effect of $u_{xs,ff}$ combined with $u_{xs,nf}$, the confining pressure is reduced from

σ_{3c} under undrained conditions, for free-field excitation ($u_{xs,ff}$), before the pile induced σ_d and $u_{xs,nf}$ are taken to occur. Accordingly, Figs. 5.7b and 5.7c are modified as seen in Fig. 5.8 and expressed as

$$\bar{\sigma}_3 = (\sigma_{3c} - u_{xs,ff}) - u_{xs,nf} \quad (\text{free- and near-field porewater pressure}) \quad (5.3b)$$

Due to σ_d , an isotropic expansive volumetric strain ($\epsilon_{v,iso}$) develops the same as recorded in an isotropically rebounded drained triaxial test. However, in the undrained test, the volumetric change or volumetric strain must be zero. Therefore, there must be a compressive volumetric strain component ($\epsilon_{v,shear}$) due to this superstructure-pile induced deviatoric stress, σ_d . The shear related volumetric strain, $\epsilon_{v,shear}$, must be equal and opposite to $\epsilon_{v,iso}$, i.e.

$$\epsilon_{v,shear} = -\epsilon_{v,iso} \quad (5.4)$$

so that the total volumetric strain, $\epsilon_v = \epsilon_{v,iso} + \epsilon_{v,shear}$, in undrained response is zero. In the isotropically consolidated-rebounded drained triaxial test, $\epsilon_{v,iso}$ and then $\epsilon_{v,shear}$ (to match $\epsilon_{v,iso}$) are obtained separately and sequentially; in the undrained test, they occur simultaneously, but with the same end results (Norris et al. 1997).

During drained isotropic expansion, the resulting axial strain, ϵ_1 , is

$$\epsilon_{1,iso} = \epsilon_{2,iso} = \epsilon_{3,iso} = \frac{1}{3} \epsilon_{v,iso} \quad (5.5)$$

Based on Hooke's Law and effective stress concepts (Norris et al. 1998), the undrained axial strain due to shear (σ_d) and effective stress ($\bar{\sigma}_3$) changes can be related to the drained or effective stress strains as

$$(\epsilon_1)_{undrained} = (\epsilon_1)_{\sigma_d} + (\epsilon_1)_{\Delta\bar{\sigma}_3} = (\epsilon_1)_{drained} + \epsilon_{1,iso}$$

$$= (\epsilon_1)_{drained} - \frac{1}{3} \epsilon_{v,iso} \quad (5.6)$$

Therefore, with isotropically consolidated-rebounded drained triaxial tests available for different $\bar{\sigma}_3$, one can assume a value of $\bar{\sigma}_3$, find $\epsilon_{v,iso}$ (Fig. 5.7b), enter the ϵ_v - ϵ_1 drained shear curves (Fig. 5.7a) at $\epsilon_{v, shear}$ equal to $\epsilon_{v, iso}$, and find the drained ϵ_1 and σ_d on the same $\bar{\sigma}_3$ confining pressure ϵ_v - ϵ_1 and ϵ_1 - σ_d curves. Then $(\epsilon_1)_{undrained}$ is established according to Eqn. 5.6 and one point on the undrained σ_d - ϵ_1 curve can be plotted. The corresponding effective stress path ($\bar{p} = \bar{\sigma}_3 + \sigma_d/2$ versus $q = \sigma_d/2$) can also be plotted as shown in Fig. 5.7c.

The technique presented above (Norris et al. 1997) requires a series of isotropically consolidated drained (ICD) tests be performed to allow one to assess the undrained stress-strain curve of a saturated sand consolidated to a certain confining pressure, σ_{3c} , at a particular value of void ratio, e_c , or relative density, Dr_c . Alternatively, Ashour and Norris (1999) have established a group of equations, based on readily assessed properties of sand, that yield all the relationships presented in Fig. 5.7 and as described as follows:

- The stress-strain and volume change curves (σ_d - ϵ_1 - ϵ_v) of the isotropically consolidated, drained, triaxial test (OCR = 1)
- The isotropically consolidated, rebounded, volume change curve
- The stress-strain and volume change curves of the isotropically consolidated, rebounded, drained test (σ_d - ϵ_1 - ϵ_v) at different overconsolidation ratios (OCR = $\sigma_{3c} / \bar{\sigma}_3 \geq 1$).

These formulations (Ashour and Norris 1999) are employed in this chapter to assess the whole undrained stress-strain curve of saturated sand (Fig. 5.2). The SW model representation of deformation in the soil is predicated upon triaxial test stress-strain response at constant confining pressure (σ_{3c}) corresponding to the initial effective overburden pressure ($\bar{\sigma}_{vo}$). Therefore, the predicted undrained stress-strain curve is employed in the SW model analysis to analyze the response of a laterally loaded pile in saturated sand under undrained conditions and developing liquefaction. The calculated undrained response of sand is function of

- the relative density of sand ($D_{r,c}$) at the corresponding consolidation pressure (σ_{3c});
- the shape of the grains of sand (roundness parameter, ρ);
- the angle of internal friction (φ);
- the drained axial strain at a deviatoric stress level of 50% (ϵ_{50}); and
- the consolidation pressure (σ_{3c}) which represents the original vertical effective stress in sand ($\bar{\sigma}_0$).

As described by Eqn. 5.3b, the effective confining pressure $\bar{\sigma}_3$ will be zero when r_u in the free-field reaches 1. As a result, the liquefied sand may exhibit increasing undrained deviatoric strain (ϵ_1) associated with, approximately, zero deviatoric stress (σ_d) before it dilates, as seen in Fig. 5.9 (Seed 1979, and Vaid and Thomas 1995). It should be noted that the denser the sand (e.g. Fig. 5.9b), the less strain before dilative response occurs. Such dilative behavior of liquefied sand is employed in the current procedure. However, details of such post liquefaction, stress-strain characterization will be presented in a separate work.

5.5 UNDRAINED STRAIN WEDGE MODEL FOR SAND

The basic purpose of the SW model is to relate stress-strain-strength behavior of the soil in the wedge to one-dimensional Beam on Elastic Foundations (BEF) parameters. The SW model is, therefore, able to provide a theoretical link between the more complex three-dimensional soil-pile interaction and the simpler one-dimensional BEF characterization. SW model response and BEF characterization reflect the following interdependence:

- the horizontal soil strain (ϵ) and stress change ($\Delta\sigma_h$) in the developing passive wedge in front of the pile (in the SW model) to the deflection pattern (y versus depth, x) and the soil-pile reaction (p) of the pile, respectively, in BEF characterization
- the nonlinear variation in the Young's modulus ($E = \Delta\sigma_h/\epsilon$) of the soil (in the SW model) to the nonlinear variation in the modulus of soil subgrade reaction ($E_s = p/y$) associated with BEF characterization.

The analytical relations that reflect soil-pile interaction response characterized by the SW model are presented in detail by Ashour et al. (1998). The SW model allows appropriate evaluation of BEF

parameters to solve the following fourth-order ordinary differential equation,

$$EI \left(\frac{d^4 y}{d^4 x} \right) + Q \left(\frac{d^2 y}{d^2 x} \right) + E_s(x)y = 0 \quad (7)$$

EI indicates the pile bending stiffness, Q symbolizes the axial load, y represents the lateral deflection of the pile at depth x, and E_s is the soil-pile reaction. Note that $E_s(x)y$ is the soil-pile reaction p, because E_s is the secant slope of the p-y curve at depth x.

5.6 CONFIGURATION OF THE PASSIVE SOIL WEDGE

The SW model is based on the mobilized passive wedge in front of the pile (Fig. 5.10) which is characterized by base angle, β_m , the current passive wedge depth h, and the spread of the wedge via the fan angle, φ_m (the mobilized effective stress friction angle). The horizontal stress change at the passive wedge face, $\Delta\sigma_h$, and side shear, τ , act as shown. A basic assumption associated with the SW model is that the deflection pattern of the pile can be taken to be linear over the controlling depth of the mobilized passive wedge of soil near the pile top resulting in a linearized deflection angle, δ , as seen in Fig. 5.11.

The SW model subdivides the soil profile and the loaded pile into sublayers and segments of constant thickness as shown in Fig. 5.11. Each sublayer of soil is considered to behave as a uniform soil and have its own properties according to the sublayer location and soil type. However, the depth, h, of the deflected portion of the pile is controlled by the stability analysis of the pile under the conditions of soil-pile interaction. The effects of the soil and pile properties are associated with the soil-pile reaction along the pile by the Young's modulus of the soil, the stress level in the soil, the pile deflection, and the modulus of subgrade reaction between the pile segment and each soil sublayer (Ashour et al. 1998).

The shape of the wedge in any soil layer depends upon the properties of that layer and, therefore, would seem to satisfy the nature of a set of independent Winkler "soil" springs in BEF analysis (Fig. 5.12). However, the mobilized depth (h) of the passive wedge at any time is a function of the various soils (and their stress levels) and the bending stiffness (EI) and the head fixity conditions (fixed, free,

or other) of the pile. This, in turn, affects the resulting p-y response in a given soil layer, therefore, the p-y response is not a unique function of the soil alone.

The governing equations of the mobilized passive wedge shape are applied within each soil sublayer (i) of a given deposit. The configuration of the wedge (Figs. 5.10 and 5.11) at any instant of load is a function of the stress level in the sublayer of sand and, therefore, its mobilized friction angle, φ_m .

$$(\Theta_m)_i = 45 - \frac{(\varphi_m)_i}{2} ; \quad (\beta_m)_i = 45 + \frac{(\varphi_m)_i}{2} \quad (5.8)$$

The width, \overline{BC} , of the wedge face at any depth is

$$(\overline{BC})_i = D + (h - x_i) 2(\tan \beta_m)_i (\tan \varphi_m)_i \quad (5.9)$$

where h symbolizes the current full depth of the passive wedge in front of the pile; x_i represents the depth from the top of the pile or passive wedge to the middle of the sublayer under consideration; D indicates the width of the pile cross-section (see Fig. 5.10). The equations above are applied at the middle of each sublayer.

5.7 STRAIN WEDGE MODEL UNDER UNDRAINED CONDITIONS

Under undrained conditions, the major principal stress change ($\Delta\sigma_h$) in the wedge is in the direction of pile movement, and it is equivalent to the deviatoric stress in the isotropically consolidated undrained (ICU) triaxial test as shown in Fig. 5.11 assuming that the horizontal direction in the field is taken as the axial direction in the (ICU) triaxial test. The vertical stress change ($\Delta\sigma_v$) and the perpendicular horizontal stress change ($\Delta\sigma_{ph}$) are equal and taken to be zero. Corresponding to the (ICU) triaxial compression test, deviatoric stress is increased, while the effective confining pressure decreases due to the positive induced excess porewater pressure, Δu_d . Note that Δu_d represents $u_{x_s, nf}$ of the near-field region.

The approach presented by Ashour and Norris (1999) evaluates the deviatoric stress-axial strain response of sand under undrained conditions. Therefore, it provides the SW model with the capability of assessing the response of a laterally loaded pile in saturated sand under undrained

conditions. As presented above, the SW model is based on the concepts of the triaxial test. The near-field build-up of the porewater pressure around the pile affects the vertical ($\bar{\sigma}_{vo}$) and the horizontal effective stresses ($\bar{\sigma}_h$) which are initially assumed to be equal, i.e.

$$\bar{\sigma}_{ho} = K \bar{\sigma}_{vo} = \bar{\sigma}_{vo} = \sigma_{3c} \quad ; \quad k = 1 \text{ (due to pile installation)} \quad (5.10)$$

The cycles of earthquake loading will generate excess porewater pressure in the free-field ($u_{xs,ff}$) that will reduce the effective stress in sand (Eqn. 5.2) according to its location below ground surface. Once the excess porewater pressure ($u_{xs,nf}$) increases due to the pile loading, the confining pressure in the sand around the pile reduces to

$$\bar{\sigma}_v = \bar{\sigma}_3 = (\sigma_{3c} - u_{xs,ff}) - u_{xs,nf} \quad (5.11)$$

where

$$\bar{\sigma}_h = \bar{\sigma}_v + \Delta\sigma_h$$

$u_{xs,nf}$ ($= \Delta u_d$) is a function of stress level. Therefore, the assessment of the mobilized strength of the sand ($\sigma_d = \Delta\sigma_h$) as a function of the axial strain (major strain) under undrained conditions allows the determination of the sand resistance and pile deformation at the associated undrained horizontal strain, ϵ_u which is equal to $(\epsilon_1)_{undrained}$ in Eqn. 5.6. The current value of undrained Young's modulus in sand sublayer (i) which is associated with ϵ_u is given as

$$(E_u)_i = \left[\frac{\Delta\sigma_h}{\epsilon_u} \right]_i = \left[\frac{\sigma_d}{\epsilon_u} \right]_i \quad (5.12)$$

Both the vertical strain (ϵ_z) and the horizontal strain perpendicular to pile movement (ϵ_{ph}) are equal and are given as

$$\epsilon_z = \epsilon_{ph} = -\nu \epsilon_u$$

where ν is the Poisson's ratio of sand under undrained conditions (equal to 0.5).

The major principal effective stress change, $\Delta\sigma_h$, in the passive wedge is in the direction of pile movement and is equivalent to the deviatoric stress change in the undrained triaxial test, σ_d (assuming that the horizontal direction in the field is taken as the axial direction in the triaxial test).

The mobilized effective stress fanning angle, φ_m , of the passive wedge in front of the pile is related to the stress level or the strain in the sand. Knowing the soil strain, ε_u , the deviatoric stress, σ_d , and the instant associated effective confining pressure, $\bar{\sigma}_3$, φ_m can be determined from the associated effective stress-strain curve and effective stress path. Based on the approach presented in Ashour and Norris 1999, both the stress level, SL_u , and the mobilized angle of internal friction, φ_m , associated with the effective stress, $\bar{\sigma}_3$, and soil strain, ε_u , under undrained conditions can be calculated, i.e.

$$(SL_u)_i = \left[\frac{\Delta\sigma_h}{(\Delta\sigma_{hr})\bar{\sigma}_i} \right]_i = \frac{(\sigma_d)_i}{(\bar{\sigma}_3)_i \left[\tan^2 \left(45 + \frac{\varphi_i}{2} \right) - 1 \right]} \quad (5.13)$$

Since $\sigma_d = (\bar{\sigma}_3)_i \left[\tan^2 \left(45 + \frac{(\varphi_m)_i}{2} \right) - 1 \right]$, then

$$(SL_u)_i = \frac{\tan^2 \left(45 + \frac{(\varphi_m)_i}{2} \right) - 1}{\tan^2 \left(45 + \frac{\varphi_i}{2} \right) - 1} \quad (5.14)$$

Note that SL_u is stress level relating the effective stress $\sigma_d (= \Delta\sigma_h)$ to $\sigma_{dr} (= \Delta\sigma_{hr})$; where $\Delta\sigma_{hr}$ is the peak of the associated drained (i.e. current $\bar{\sigma}_3$) effective stress-strain curve (Fig. 5.7a).

The initial and subsequent values of confining pressure are not equal along the depth of the passive wedge of sand in front of the pile. Therefore, at the same value of horizontal soil strain (ε_u), the

undrained resistance of the sand surrounding the pile varies throughout the depth of the passive wedge of sand providing different values of stress level. Such behavior requires the determination of the mobilized undrained resistance of the sand along the depth of the passive wedge. The SW model provides the means to divide the sand layer into equal-thickness sublayers in order to calculate the undrained sand response at each sublayer (i) according to the location and the properties of sand of that sublayer.

5.7.1 Soil-Pile Interaction in the SW Model Under Undrained Conditions

By applying the drained SW model procedures for sand presented by Ashour et al. (1998), the modulus of subgrade reaction of the sand under undrained conditions, E_{su} , at any sublayer (i) can be determined based on the associated values of E_u and SL_u . The SW model relies on calculating the modulus of subgrade reaction, E_{su} , which reflects the soil-pile interaction at any level during pile loading or soil strain. In any sublayer (i), E_{su} is expressed as

$$(E_{su})_i = \frac{P_i}{y_i} \quad (5.15)$$

Corresponding to a horizontal slice of (a soil sublayer) at a depth x (see Fig. 5.10), horizontal equilibrium and the soil-pile reaction, p_i (line load), under the undrained conditions is expressed as

$$p_i = (\Delta\sigma_h)_i \overline{BC}_i S_1 + 2\tau_i D S_2 \quad (5.16)$$

$\Delta\sigma_h$ represents the mobilized undrained resistance in sand sublayer (i). Shape factors S_1 and S_2 are equal to 0.75 and 0.5, respectively, for a circular pile cross section, and equal to 1.0 for a square pile (Briaud et al. 1984). Side shear stress, τ , under undrained conditions is given as

$$\tau_i = (\bar{\sigma}_3)_i \tan(\phi_s)_i; \quad \tan(\phi_s)_i = 2 \tan t(\varphi_m)_i \quad (5.17)$$

φ_s indicates the angle of friction for side shear response which mobilizes faster than φ_m ($\varphi_s \leq \varphi$). The assessed p-y curve for the laterally loaded pile in sand under undrained conditions should be softer than that of the drained case. However, the p-y curve for medium dense sand (dilative at large strain) could be slightly lower than or equal to that in drained conditions. Because negative porewater pressure is not included in the technique employed here, the p-y curve under undrained

conditions would never be stiffer than the drained one. Therefore, this approach is conservative relative to dense sands.

Alternatively, one can rearrange Eqn. 5.10 as

$$A_i = \frac{p_i/D}{(\Delta\sigma_h)_i} = \frac{\overline{BC}_i S_1}{D} + \frac{2\tau_i S_2}{(\Delta\sigma_h)_i} \quad (5.18)$$

Parameter A symbolizes the ratio between the equivalent pile face stress, p/D , and soil stress $(\Delta\sigma_h)$ at the face of the passive wedge. It is a function of pile and wedge dimensions, applied strains, and soil properties. By combining the equations of the passive wedge geometry (Eqns. 5.8 and 5.9) and the side shear stress (Eqn. 5.17) with the above relationship, one finds that

$$A_i = S_1 \left(1 + \frac{(h - x_i) 2(\tan\beta_m \tan\varphi_m)_i}{D} \right) + \frac{2S_2 (\bar{\sigma}_3)_i (\tan\varphi_s)_i}{(\Delta\sigma_h)_i} \quad (5.19)$$

where the values φ_m , $\bar{\sigma}_3$, φ_s , and $\Delta\sigma_h$ are calculated from the undrained effective stress behavior of the sand.

By comparison with the drained modulus of subgrade reaction, E_s , in sand presented in Ashour et al. (1999), the undrained modulus of subgrade reaction, E_{su} , is given as

$$(E_{su}) = \frac{p_i}{y_i} = \frac{D (A \varepsilon_u E_u)_i}{\delta (h - x_i)} = \frac{(A E_u)_i}{(h - x_i)} D (\Psi_u)_i \quad (5.20)$$

Ψ_u is a parameter that relates δ to ε_u . Using the concepts presented by Ashour et al. (1998) and based on Equations 2.37 through 2.40, the relationship between ε_u and δ can be expressed as

$$\Psi_u = \frac{\varepsilon_u}{\delta} \quad (5.21)$$

or

$$\Psi_u = \frac{2}{(1 + \nu_u) \sin 2\Theta_m} \quad (5.22)$$

The parameter Ψ_u varies with the undrained Poisson's ratio of the soil (ν_u) and the soil's mobilized angle of internal friction (ϕ_m) and the mobilized passive wedge angle (Θ_m).

Undrained Poisson's ratio for sand is equal to 0.5, while the base angle, Θ_m , can vary between 45° (for $\phi_m = 0$ at $\epsilon = 0$) and 25° (for, say, $\phi_m = 40^\circ$ at failure), respectively. For this range in variation for ν and ϕ_m , the parameter Ψ for sand varies between 1.33 and 1.74 with an average value of 1.55.

It should be noted that Eqn. 5.20 is based upon the undrained response of sand using the undrained stress-strain relationship (ϵ_u , σ_d and E_u) and values of the parameters A and Ψ_u for undrained conditions. Once the values of E_{su} at any level of loading along the length of the deflected portion of a pile are calculated, the laterally loaded pile and the three-dimensional passive wedge in front of the pile can be transformed to a Beam on Elastic Foundations (BEF) problem (Eqn. 5.7) as shown in Fig. 5.12. The laterally loaded pile analysis represents an iterative solution that satisfies the equilibrium between the lateral load, soil-pile resistance, soil strain, and the associated pile deflection at any level of loading. The evaluation of the modulus of subgrade reaction (E_{su}) as a function of soil and pile properties is the key point in the SW model analysis. Thereafter, a numerical technique such as the finite element or the finite difference method can be utilized to solve the BEF problem.

5.8 GROUP EFFECT ON THE RESPONSE LATERALLY LOADED PILES IN LIQUEFYING SANDS

As seen in Fig. 5.13, the interference among the individual piles is a function of the area of the overlap zones which varies with the level of loading and the location of the soil sublayers (i.e. the geometry of the soil passive wedge). As mentioned in Chapter 3, the overlap shear zones produce increase the stresses (i.e. strains) in the passive wedge of soil in front of the pile in question. Consequently, the total strain, ϵ_v , in the passive wedge (due to the pile head load, P_o , and the interference among the piles) will induce a pile-head deflection larger than that of the single pile under the same lateral load P_o .

The major difference between the drain and undrained analysis of the pile group is the soil stress-strain relationship. The undrained stress-strain relationship assessed in Chapter 4 is employed in the

analysis of the pile group in order to predict the changes in soil resistance at ε_t . This procedure is applied at each sand sublayer to reflect the undrained behavior of sand in that sublayer at the current level of loading and the accompanying shape of the passive wedge. It should be noted that the shape and geometry of the passive wedge of liquefied soil are based on the accompanying undrained stress-strain relationship which affects, in turn, the area of the overlapping among the piles in the group. While the strains (stresses) increase in the overlap zones, the excess porewater pressure may increase too according to the density of sand.

$$\varepsilon_t = \varepsilon_u + \Delta\varepsilon_u \quad (5.23)$$

It should be noted that the group effect on the pile response (compared to the single pile), in the liquefying soil (undrained condition), is much less than that one under the drained conditions. As a result of sand dilatancy, the gap between the drained and undrained group effect decreases by increasing the density of sand. Thus, compared to the undrained response of the single pile in loose sand, there is no much reduction in the capacity of an individual pile in a group of piles embedded in the same liquefiable loose sand.

Figures 5.14 through 5.16 show the effect of the interference among the piles in the group (working load reduction factor) on the average pile-head response of the pile group. 2D and 4D pile spacings among the piles of a 3 x 3 pile group are assumed. The pile group is, also, assumed to be driven in loose, medium and dense saturated banding sands which have relative densities of 37, 64 and 82 percent. The pile employed is a long pile of 0.304-m diameter and pile bending stiffness of 31300 kn-m². The results presented in Figs. 5.14 through 5.16 reflect only the effect of the near-field excess porewater pressure ($u_{xs,nf}$) on the undrained response of the pile group compared to the drained and undrained ones of the single pile.

As seen in Figures 5.14 through 5.16, the close pile spacing (2D) has an effect on the reduction factor of an average pile in the group under the undrained conditions. However, this influence reduces significantly by increasing the pile spacings to 4D or larger. It should be noted that the excess porewater pressure in the near-filed reduces the pile-head capacity of the single pile in loose sand

(highly liquefiable soil), and the interference among the individual piles in the group induces additional reduction for the pile group capacity. However, the increase in sand density will limit the influence of both of the $u_{xs, nf}$ and the piles interference in the pile group, as shown in Figs 5.14b, 5.15b and 5.16b.

5.9 SUMMARY

The procedure presented yields the undrained response of a laterally loaded pile in liquefiable soil incorporating the influence of both the developing excess porewater pressure in the free-field (due to the ground acceleration) and that additional near-field pore pressure (due to the lateral load from the superstructure). The technique reflects the effect of undrained conditions in the soil on the assessed (soil-pile reaction) p-y curves based on the reduced soil-pile interaction response (modulus of subgrade reaction). Compared to pile response under drained conditions, the approach proposed shows a dramatic reduction in pile head capacity can occur due to developing liquefaction. The flexibility and capability of this procedure will reduce the uncertainty of dealing with the behavior of laterally loaded piles in liquefiable soils. It will allow the designer to assess realistic responses of laterally loaded piles in liquefiable soils based on the local site conditions and the seismic zone.

CHAPTER 6

CASE STUDIES AND APPLICATIONS

6.1 INTRODUCTION

This chapter presents some examples and full-scale load tests in liquefying soil to highlight the capabilities and the limitations of the proposed technique. Unfortunately, the number of full-scale load tests in liquefying soils available in the literature is very limited because of the cost to run such tests and the sophistication of the test procedure. The first application in this chapter is an illustrative example that highlights the versatility of proposed procedures. This example reflects the significance of the different types of excess porewater pressures (free- and near-field) in the analysis of laterally loaded piles. The second application is a comparison study with full-scale lateral load tests in a liquefying soil. The tests were conducted on a single pile and a pile group on Treasure Island, San Francisco Bay, California. The good comparisons obtained from these tests validate and build ones' confidence in the proposed procedures. A design problem from the literature is presented as the third example. This design problem was analyzed using the computer program LPILE for drained conditions and SW model to obtain softer p-y curves as a result of soil liquefaction.

6.2 RESPONSE OF A SINGLE PILE IN UNIFORM MEDIUM TO LOOSE SANDY SOIL

The example presented reflects the effect of undrained conditions on the behavior of a laterally loaded free-head pile similar to the pile used in the Mustang Island test (Reese et al. 1974) but driven into a sand similar to Banding sand which was tested by Castro (1969) and studied by Ashour and Norris (1999). This example shows clearly the differentiation between the p-y curves under drained and undrained conditions. The undrained loading conditions solved involve the consideration of excess porewater pressure in the free-field ($u_{xs, ff}$), the near-field ($u_{xs, nf}$), and a combination of both of them ($u_{xs, ff} + u_{xs, nf}$).

The pile is a free-head steel pipe pile of 0.6 m diameter, 21.3 m length, and bending stiffness, EI , $166.7 \text{ MN}\cdot\text{m}^2$. The pile is assumed to be driven in a saturated loose to medium sand (similar to Banding sand) and to have a relative density (D_r) of 37% (SPT corrected blow count of 6, Tokimatsu and Seed, 1987), an angle of internal friction of 32.5 degrees, an effective unit weight of 9.4 kN/m^3 , and a strain $(\epsilon_{50})_{42.5}$ (reference strain) of 0.85% (Castro 1969, and Ashour and Norris 1999). The sand employed is assumed to be clean sand. The maximum ground acceleration (a_{max}) at the ground surface at the site for assessment of $u_{x_s, \text{ff}}$ is equal to 0.08g.

The sand employed exhibits undrained contractive type of behavior followed by dilative response as seen in Fig. 6.1. Figure 6.1 shows that each sublayer has its own undrained resistance ($\sigma_d - \epsilon_u$) according to its location. In addition, the sand has an increasing peak undrained resistance with depth which occurs at the high point on the associated effective stress path but below the Mohr-Coulomb failure envelope.

The consideration of undrained conditions in the analysis of the laterally loaded pile driven in loose to medium sand results in a varied drop in the pile-head load capacity compared to that of drained (i.e. static) conditions (Fig. 6.2). The consideration of the different excess porewater pressures in free- and/or near-field ($u_{x_s, \text{ff}}$ and $u_{x_s, \text{nf}}$) affects the resistance of sand significantly. It is obvious from Fig. 6.2 that the reduction in pile response under undrained conditions does not have the same pattern and is a function of the level of lateral loading and the type of excess porewater pressure. Note that use of $u_{x_s, \text{nf}}$ alone might reflect the undrained response of a pile in sand due to (say) a ship impact load (no earthquake).

The pile-head load-displacement curves shown in Fig. 6.3 reflect the effect of a varying ground surface acceleration (and $u_{x_s, \text{ff}}$) on the undrained response of the pile. Note that a value of 0.00g implies there is only $u_{x_s, \text{nf}}$. It should be noted that the sand approaches complete liquefaction ($r_u = 1$) under free-field conditions at $a_{\text{max}} = 0.15\text{g}$. Figure 6.4 shows the distribution of the drained and undrained lateral deflection (y) and the associated bending moment (M) along the loaded pile under different values of the ground acceleration.

The induced drop in soil resistance along the height of the passive wedge of sand in front of the pile produces a softer p-y curve compared to that assessed under drained conditions as shown in Fig. 6.5. The incorporation of different values of a_{\max} (and $u_{x_s, ff}$) with the near-field water pressures results in substantial changes in the shapes of the p-y curve at the same depth (3 m below ground surface).

6.3 TREASURE ISLAND, SAN FRANCISCO BAY, FULL-SCALE LOAD TEST ON SINGLE PILE AND PILE GROUP

This example presents a comparison between the results obtained by using the SW model and the data observed from full-scale field tests in liquefied soil on Treasure Island in San Francisco Bay, California (Ashford and Rollins, 1999). A series of lateral load tests on a full size CISS pile (cast in steel shell) and pile group were conducted in liquefied soil to improve the understanding of the lateral load behavior of long piles in liquefied soil. Both static and cyclic tests were conducted in non-liquefied soil, and then in liquefiable soil after a surface layer 3 to 6 m thick was liquefied by blasting techniques.

The soil profile at the Treasure Island testing site consists of hydraulically placed fill to a depth of 11 m, underlain by natural sandy silts and San Francisco Bay Mud to depths that exceed 20 m. The hydraulic fill consists of loose to fine silty sands or sandy silts with thin interbeds of lean clay (Bennett 1994). The water table is 1.2 to 1.8 m below the ground surface. Figures 6.6 and 6.7 show the soil boring log for the single pile, and the 4-pile group and the 0.6-m CISS pile test areas, respectively. The soil was liquefied by carrying out controlled blasts at that site without densifying the soil in the test area. Figure 6.8 exhibits the dissipation of the excess porewater pressure ratio, r_u , at 2.7 m depth at the location of the pilot liquefaction study. More details on the procedures of liquefying the soil at the test site are reported by (Ashford and Rollins, 1999). The soil properties employed in the SW model analysis is listed in Exam1.sws file which is attached to the program.

The drained and undrained lateral load tests presented in this case study were performed on 0.324-m diameter pipe pile ($EI = 44500 \text{ kN-m}^2$), 0.6-m diameter CISS pile (cast in steel shell, $EI = 448320 \text{ kN-m}^2$), and 0.310-m wide H-pile ($EI = 49000 \text{ kN-m}^2$). All tests piles had free-head conditions and were laterally loaded 0.8 m above ground surface. The tested piles had different values of bending

stiffness which are calculated and presented with each test as seen in the accompanying figures.

The predicted and observed drained response of the three piles compare favorably as seen in Figs. 6.9 through 6.11. While the pipe pile (0.324-m diameter) exhibits a bending stiffness less than that of the H-pile, both piles experienced approximately the same (observed) drained responses.

It should be noted that the procedures followed in the Treasure Island test (liquefying the soil around the pile and then loading the pile laterally) are similar to the procedures presented in Chapter 5. The assessed undrained behavior of the test piles is based on the procedures presented herein, and includes the effect of both excess porewater pressure components ($u_{xs, ff} + u_{xs, nr}$).

The piles were cyclically loaded after the first blast at the site. The observed undrained points, which are shown in Figs. 6.9 through 6.11, represent the peaks of the cyclic undrained response of these piles. It should be mentioned that the good agreement between the measured and predicted undrained response is based on an assumed maximum ground acceleration, a_{max} , of 0.08g in Figs. 6.9 and 6.11, and an a_{max} of 0.1g in Fig. 6.10 (H-pile). These values of ground surface acceleration generate high excess porewater pressures ($u_{xs, ff}$) in most of the sand layers and complete liquefaction in other layers. These values of a_{max} (0.08g and 0.1g) employed in the analysis cause excess porewater pressure ratios (r_u) equal to unity in most of the soil profile and the best match with the measured free-field excess porewater pressure pattern induced in the field (Fig. 6.8).

The pile group (2 x 2 CISS 0.324 m diameter) was loaded statically until one pile reached an absolute displacement of 38 mm at the loading point. Good agreement between the observed and predicted static loading is shown in Fig. 6.12.

After this test, the charges were set off. Ten seconds later, the post-blast loading sequence began. The piles were cycled to 75, 150, and then 225 mm absolute displacement at the loading point, and then cycled 9 times at 225 mm displacement. Figure 6.12 shows a very good match between the predicted and observed undrained behavior of the pile group. An a_{max} of 0.08g was used for the predicted group case. The observed points plotted in Fig. 6.12 represent the largest values of the

pile head load - load displacement path during the cyclic loading.

The procedure presented in this report may be conservative because it takes the soil to be completely undrained (no excess porewater dissipation during shaking or loading of the pile) and the sand around the pile (near-field region) to be a clean sand.

6.4 SINGLE PILE BEHAVIOR IN LAYERED SOIL THAT INCLUDES A HIGHLY LIQUEFIABLE LAYER OF SOIL

This example has been presented by Wang and Reese (1998) to analyze the behavior of a laterally loaded pile in liquefied soil by reducing the traditional (Matlock-Reese) p-y curve. The modification of the traditional drained p-y curve is based on the use of the residual strength of the liquefied soil. A drilled pier with a diameter of 1.2 m, a penetration length of 18.3 m, and bending stiffness of 2.30×10^6 kN-m² is assumed to be driven in the soil profile shown in Fig. 6.13. The pier in question is subjected to an axial load of 100 kN and one external pile-head moment of 316 kN-m in the direction of the lateral load.

The second layer of soil below the ground surface (5.2 m thick) is a liquefiable layer with a residual strength of 7.2 kN/m². The second layer of soil which consists of a submerged loose sands will liquefy under an earthquake of magnitude 7 on Richter scale.

Figure 6.14 shows a comparison between the drained and undrained responses of the loaded pier which are obtained using the SW model and, separately, the data assessed by Wang and Reese (1998) using LPILE and modified traditional p-y curves for sand. It should be noted that the soil reaches its residual strength at large values of soil strain. Also, the traditional p-y curve is developed based on the data collected from drained tests. There was no detail given on how the drained p-y curves were modified based on the residual strength of soil.

A maximum ground acceleration of 0.15g is assumed in the SW model solution. As a result, the excess porewater pressure ratio (r_u) in the liquefiable layer approaches 100% and develops complete liquefaction in this layer upon pile head load applications.

The results of p-y method, which is shown in Fig. 6.14, are assessed at a low level of loading (very small soil strain) and has a significant difference between the results of LPILE and the SW model. It should be noted that the p-y method does not provide reliable results at the low level of loading and soil strain. Also, the pile analyzed in the current case does not respond as a long pile but, rather, an intermediate pile. Therefore, the pile length must be increased to allow the employment of the Matlock-Reese p-y curves in the analysis.

APPENDIX I.

REFERENCES

- Ashford, S. A., and Rollins, K. (1999). "Full-Scale Behavior of Laterally Loaded Deep Foundations in Liquefied Sands." Report No. TR - 99/03, Structural Engineering Dept., University of California, San Diego
- Ashour, M., Norris, G., and Pilling, P. (1998). "Lateral Loading of a Pile in Layered Soil Using the Strain Wedge Model," *Journal of Geotechnical and Geoenvironmental Engineering*, ASCE, Vol. 124, No. 4, pp. 303-315.
- Ashour, M. and Norris, G. (1999). "Liquefaction and Undrained Response Evaluation of Sands from Drained Formulation." *Journal of Geotechnical and Geoenvironmental Engineering*, ASCE, Vol. 125, No. 8, pp. 649-658.
- Ashour, M., Pilling, P., Norris, G., and Perez, H. (1996). "Development of Strain Wedge Model Program for Pile Group Interference and Pile Cap Contribution Effects." CCEER Report No. 96-4, Civil Engrg Dept., University of Nevada, Reno.
- Been, K., and Jefferies, M. G. (1985). "A State of Parameter for Sands," *Geotechnique* 35, No. 2, pp. 99-112.
- Briaud, J. L., Smith, T., and Mayer, B. (1984). "Laterally Loaded Piles and the Pressuremeter: Comparison of Existing Methods." *Laterally Loaded Deep Foundations*, ASTM, STP 835, pp. 97-111.
- Casagrande, A., "Liquefaction and Cyclic Deformation of Sands a Critical Review," Fifth Panamerican Conference on Soil Mechanics and Foundation Engineering, Buenos Aires, Argentina, November, 1976.
- Castro, G., and Poulos, S. (1977). "Factors Affecting Liquefaction and Cyclic Mobility," *Journal of Geotechnical Engineering Division*, ASCE, Vol. 103, No. GT6, pp. 501-516.
- Castro, G. (1969). "Liquefaction of Sands," *Ph.D. Thesis*, Division of Engineering and Applied Physics, Harvard University, Cambridge, Mass.
- Castro, G., Poulos, S., France, J., and Enos, J. (1982), "Liquefaction Induced by Cyclic Loading," Report to National Science Foundation, Washington, D.C., No. NSF/SEE-82018.
- Cox, W. R., Reese, L. C., and Grubbs, B. R. (1974). "Field Testing of Laterally Loaded Piles in Sand." *The Sixth Annual Offshore Technology Conference*, Houston, Texas, OTC 2079, pp. 459-472.
- Coyle, H. M. and Reese, L. C. (1966). "Load Transfer for Axially Loaded Piles in Clay." *Journal of Soil Mechanics and Foundations Division*, ASCE, Vol. 92, NO. SM2.

Dakoulas, P., and Yuanhui, S. (1992). "Fine Ottawa Sand: Experimental Behavior and Theoretical Predictions," *Journal of Geotechnical Engineering*, ASCE, Vol. 118, No. 12, pp. 1906-1923.

DeAlba, Pedro, Seed, H. B., and Chan, Clarence K. (1976). "Sand Liquefaction in Large-Scale Simple Shear Tests." *Journal of Geotechnical Division*, ASCE, Vol. 102, No. GT9, Proc. Paper 12403, pp. 909-927.

Norris, G., Zafir, Z., and Siddharthan, R. (1998). "An Effective Stress Understanding of Liquefaction Behavior." *Journal of Environmental & Engineering Geoscience*, Vol. 4, No. 1 pp. 93-101.

Evans, Jr. L. T., and Duncan, G. M. (1982). "Simplified Analysis of Laterally Loaded Piles." UC Berkeley, Rept. No. UCB/GT/82-04, 245 pp.

Fukushima, S., and Tatsuoka, F. (1984). "Strength and Deformation Characteristics of Saturated Sand at Extremely Low Pressures," *Journal of Soils and Foundations*, No. 4, Vol. 24, pp. 30-48.

Gowda, P. (1991). "Laterally Loaded Pile Analysis for Layered Soil Based on the Strain Wedge Model." M. S. Thesis, University of Nevada, Reno.

Ishihara, K. (1993). "Liquefaction and Flow Failure During Earthquakes," *Geotechnique* 43, No. 3, pp. 351-415.

Ishihara, K., Tatsuoka, F., and Yasuda, S. (1975). "Undrained Deformation and Liquefaction of Sand under Cyclic Stresses," *Journal of Soils and Foundations*, No. 1, pp. 29-44.

Lee, K. L., and Seed, H. B. (1967). "Drained Strength Characteristics of Sands," *Journal of the Soil Mechanics and Foundations Division*, ASCE, Vol. 93, No. SM6, pp. 117-141.

Matlock, H. and Reese, L. C. (1961). "Generalized Solution for Laterally Loaded Piles." *Journal of Soil Mechanics and Foundations Division*, ASCE, Vol. 86, No. SM5, pp. 673-694.

Matlock, H. (1970). "Correlations for Design of Laterally Loaded Piles in Soft Clay." *The 2nd Annual Offshore Technology Conference*, Houston, Texas, OTC 1204, pp. 577-607.

Mohamad, R., and Dobry, M. (1986) "Undrained Monotonic and Cyclic Triaxial Strength of Sand," *Journal of Geotechnical Engineering*, ASCE, Vol. 112, No. 10, pp. 941-958.

Negussey, D., and Vaid, Y. P. (1990). "Stress Dilatancy of Sand at Stress Ratio States," *Journal of Soils and Foundations*, No. 1, Vol. 30, pp. 155-166.

Norris, G., Siddharthan, R., Zafir, Z., and Madhu, R. (1997). "Liquefaction and Residual Strength of Sands from Drained Triaxial Tests," *Journal of Geotechnical Engineering*, ASCE, Vol. 123, No. 3, pp. 220-228.

Norris, G., Madhu, R., Valceschini, R., and Ashour, M. (1995). "Liquefaction and Residual Strength of Loose Sands from Drained Triaxial Tests," Report No. CCEER-95-2, Civil Engineering Dept. University of Nevada, Reno, Submitted to Army Corps of Engineers.

Norris, G., Zafir, Z., and Siddharthan, R. (1998). "An effective Stress Understanding of Liquefaction Behavior," *Journal of Environmental & Engineering Geoscience*, Vol. 4, No. 1 pp. 93-101.

Norris, G. M. (1986). "Theoretically Based BEF Laterally Loaded Pile Analysis." *Proceedings, Third International Conference on Numerical Methods in Offshore Piling, Nantes, France*, pp. 361-386.

Norris, G. M. (1977). "The Drained Shear Strength of Uniform Quartz Sand as Related to Particle Size and Natural Variation in Particle Shape and Surface Roughness." Ph.D. Thesis, University of California, Berkeley, 523 pp.

Norris, G., Siddharthan, R., Zafir, Z., and Madhu, R. (1997). "Liquefaction and Residual Strength of Sands from Drained Triaxial Tests," *Journal of Geotechnical Engineering, ASCE*, Vol. 123, No. 3, pp. 220-228.

Norris, G. M. (1986). "Theoretically Based BEF Laterally Loaded Pile Analysis," *Proceedings, Third International Conference on Numerical Methods in Offshore Piling, Nantes, France*, pp. 361-386.

Powers, M. C. (1953). "A New Roundness Scale for Sedimentary Particles," *Journal of Sedimentary Petrology*, Vol. 23, No. 2, pp. 117-119.

Reese, L. C. (1958). "Discussion of "Soil Modulus for Laterally Loaded Piles." by Bramlette McClelland and John A. Focht, Jr., *Transactions, ASCE*, Vol. 123, pp. 1071.

Reese, L. C. (1983). "Behavior of Piles and Pile Groups Under Lateral Load." Report to the U.S. Department of Transportation, Federal Highway Administration, Office of Research, Development, and Technology, Washington, D.C.

Reese, L. C., Cox, W. R., and Koop, F. D. (1974). "Analysis of Laterally Loaded Piles in Sand," *The Six Annual Offshore Technology Conference, Houston, Texas, May 6-8, OTC 2080*, pp. 473-483.

Reese, L. C. and Sullivan, W. R. (1980). "Documentation of Computer Program COM624, Parts and II, Analysis of Stresses and Deflections for Laterally Loaded Piles Including Generation of p-y Curves." *Geotechnical Engineering Software GS80-1, Geotechnical Engineering Center, Bureau of Engineering Research, University of Texas at Austin, August, 1980*.

Reese, L. C. (1977). "Laterally Loaded Piles: Program Documentation." *Journal of Geotechnical Engineering, ASCE*, Vol. 103, No. GT4, pp. 287-305.

Reese, L. C., Cox, W. R., and Koop, F. D. (1974). "Analysis of Laterally Loaded Piles in Sand." *The*

Six Annual Offshore Technology Conference, Houston, Texas, OTC 2080, pp. 473-483.

Reuss, R., Wang, S. T., Reese, L. C. (1992). "Tests of Piles Under Lateral Loading at the Pyramid Building, Memphis, Tennessee." *Geotechnical News*, Vol. 10, No. 4, December, pp. 44-49.

Seed, H. B. (1979). "Considerations in the Earthquake-Resistance Design of Earth and Rockfill Dams." *Geotechnique* 29, No. 3, pp. 215-263.

Seed, H. B., and Idriss, I. M. (1970). "Soil Moduli and Damping Factors for Dynamic Response Analyses," Report No. EERC 70-10, College of Engineering, University of California, Berkeley, California.

Seed, H. B. and Lee, K. L. (1967). "Undrained Strength Characteristics of Cohesionless Soil," *Journal of the Soil Mechanics and Foundations Division, ASCE*, Vol. 93, SM6, pp. 333-360.

Seed, H. B., Idriss, I.M., and Arango, I. (1983). "Evaluation of Liquefaction Potential Using Field Performance Data," *Journal of Geotechnical Division, ASCE*, Vol. 109, No. 3, pp. 458-482.

Seed, H. B., Tokimatsu, K., Harder, L. F., and Chung, R. M. (1985). "Influence of SPT Procedures in Soil Liquefaction Resistance Evaluations." *Journal of Geotechnical Division, ASCE*, Vol. 111, No. 12, pp. 1425-1445.

Skempton, A. W. (1954). "The Pore Pressure Coefficients A and B." *Geotechnique*, 4, pp. 148.

Tokimatsu, K., and Seed, H. B. (1987). "Evaluation of Settlement in Sands Due to Earthquake Shaking." *Journal of Geotechnical Division, ASCE*, Vol. 113, No. 8, pp. 861-878.

Tomlinson, M. J. (1957). "The Adhesion of Piles Driven in Clay Soils." *Proceedings of Fourth International Conf. on Soil mechanics and Foundation Engrg*, Vol. II, London, pp. 66-71.

US Army Corps of Engineers. (1996). "Design of Sheet Pile Walls." *Technical Engineering and Design Guides As Adapted from the*, No. 15, ASCE Press.

Vaid, Y. P. and Thomas, J. (1995). "Liquefaction and Post-liquefaction Behavior of Sand," *Journal of Geotechnical Engineering, ASCE*, Vol. 121, No. 2, pp. 163-173.

Vaid, Y. P., Chung, E. K. F., and Kuerbis, R. H. (1989). "Preshearing and Undrained Response of sand," *Journal of Soils and Foundations*, No. 4, Vol. 29, pp. 49-61.

Wang, S. T., and Reese, L. C. (1998). "Design of Pile Foundations in Liquefied Soils." *Special Geotechnical Special Publication No. 75, ASCE, Geotechnical earthquake Engineering and Soil Dynamics Conference, Seattle, Washington*, Vol. 2, August, 1998, pp. 1331-1343.

Wu, T. H. (1966). *Soil Mechanics*, Boston, Allyn and Bacon Inc., pp. 169.

Youd, T. L., and Idriss, I. M. (1997). "Evaluation of Liquefaction Resistance of Soils.", *Technical*

Report, NCEER-97-0022.

APPENDIX II. (Simple Shear Characterization)

An expanding Mohr circle about an initial isotropic stress state ($\bar{\sigma}_m = \sigma_{3c}$, $K_o = 1$) can be considered as a two-dimensional representation of an increasing simple shear stress state. While the normal stress on horizontal and vertical planes remains constant (equal to σ_{3c}), the corresponding $\bar{\sigma}_3$ and $\bar{\sigma}_1$ become

$$\bar{\sigma}_1 = \sigma_{3c} + \tau_{\max} ; \quad \bar{\sigma}_3 = \sigma_{3c} - \tau_{\max} \quad (\text{II.1})$$

and

$$\tau_{\max} = \frac{\sigma_d}{2} ; \quad \sigma_d = SL \sigma_{df} = SL \bar{\sigma}_3 \left[\tan^2 \left(45 + \frac{\phi}{2} \right) - 1 \right] \quad (\text{II.2})$$

$$\gamma_{\max} = \varepsilon_1 (1 + \nu) ; \quad G = \frac{\tau_{\max}}{\gamma_{\max}} = \frac{\sigma_d/2}{\varepsilon_1 (1 + \nu)} = \frac{E}{2(1 + \nu)} \quad (\text{II.3})$$

where ν , γ and G represent the Poisson's ratio, the shear strain and the shear modulus, respectively.

From Equation 4.5,

$$E = \frac{\sigma_d}{\varepsilon_1} = \frac{\sigma_{df}}{\varepsilon_{50}} \lambda \exp(-3.707 SL) \quad (\text{II.4a})$$

and

$$E_i = \frac{\sigma_{df}}{\epsilon_{50}} \lambda \quad \text{at } SL = 0 \quad (\text{II.4b})$$

Therefore, the Young's modulus reduction, E/E_i , is simply

$$\frac{E}{E_i} = \exp(-3.707 SL) \quad (\text{II.5})$$

Corresponding to this, the shear modulus reduction, G/G_o , is

$$\frac{G}{G_o} = \frac{E/[2(1 + \nu)]}{E_i/[2(1 + \nu_i)]} = \frac{E}{E_i} \frac{(1 + \nu_i)}{(1 + \nu)} \quad (\text{II.6})$$

where E/E_i is given by Equation II.5. If one takes ν to vary linearly with SL from $\nu_i = 0.1$ at $SL = 0$ to, say, $\nu = 1/2$ at $SL = 1/2$, then G/G_o vs. γ can be obtained in the following fashion:

1. Choose SL
2. Assess ϵ_1 , ν and γ_{\max}
3. Assess E/E_i and G/G_o
4. Plot G/G_o vs. γ_{\max}
5. Repeat steps 1-4

Figure 3 was constructed in this fashion for a value of $\epsilon_{50} = 0.003$ at $\alpha_{3c} = 100$ kPa, and $\nu = 0.1 + 0.8SL$, for SL from 0.0 to 0.5.

APPENDIX III.

The ε_1 - $\varepsilon_{v, \text{shear}}$ relationship (Fig. 4) is expressed by a fifth order binomial equation as follows:

$$y = a + bx + cx^2 + dx^3 + ex^4 + fx^5 \quad (\text{III.1})$$

The slope of any point on the ε_1 - $\varepsilon_{v, \text{shear}}$ relationship is given as

$$\bar{y} = b + 2cx + 3dx^2 + 4ex^3 + 5fx^4 \quad (\text{III.2})$$

where term x represents the axial strain ε_1 , y symbolizes the volumetric strain due to shear $\varepsilon_{v, \text{shear}}$ and \bar{y} indicates the slope of a point on the curve of ε_1 - $\varepsilon_{v, \text{shear}}$ relationship ($d\varepsilon_1 / d\varepsilon_{v, \text{shear}}$)

- Boundary conditions at point A

$$x = 0 \quad y = 0 \quad \bar{y} = S_A \quad (\text{III.3})$$

By substituting the above conditions in Equations III.1 and III.2

$a = 0$	$b = S_A$	(III.4)
---------	-----------	---------

Therefore, Equations III.1 and III.2 can be rewritten as

$$y = S_A x + cx^2 + dx^3 + ex^4 + fx^5 \quad (\text{III.5})$$

$$\bar{y} = S_A + 2cx + 3dx^2 + 4ex^3 + 5fx^4 \quad (\text{III.6})$$

- Boundary conditions at point B

$$x = x_B \quad y = y_B \quad \bar{y} = 0 \quad (\text{III.7})$$

Therefore,

$$y_B = S_A x_B + cx_B^2 + dx_B^3 + ex_B^4 + fx_B^5 \quad (\text{III.8})$$

$c = \frac{y_B}{x_B^2} - \frac{S_A}{x_B} - dx_B - ex_B^2 - fx_B^3 \quad (\text{III.9})$

and

$$\bar{y}_B = S_A + 2cx_B + 3dx_B^2 + 4ex_B^3 + 5fx_B^4 = 0 \quad (\text{III.10})$$

$$S_A + \frac{2y_B}{x_B} - 2S_A - 2dx_B^2 - 2ex_B^3 - 2fx_B^4 + 3dx_B^2 +$$

$$4ex_B^3 + 5fx_B^4 = 0 \quad (\text{III.11})$$

$$-S_A + \frac{2y_B}{x_B} + dx_B^2 + 2ex_B^3 + 3fx_B^4 = 0 \quad (\text{III.12})$$

$d = \frac{S_A}{x_B^2} - \frac{2y_B}{x_B^3} - 2ex_B - 3fx_B^2 \quad (\text{III.13})$
--

By substituting for constant d (Equation III.13) in Equation III.9, constant c can be written as

$$c = \frac{3y_B}{x_B^2} - \frac{2S_A}{x_B} + ex_B^2 + 2fx_B^3 \quad (III.14)$$

- Boundary conditions at point C

$$x = x_C \quad y = y_C \quad \bar{y} = S_C = S_f \quad (III.15)$$

Therefore,

$$y_C = S_A x_C + cx_C^2 + dx_C^3 + ex_C^4 + fx_C^5 \quad (III.16)$$

By substituting for Constants c and d (Equations III.13 and III.14) into Equation III.16

$$y_C = S_A x_C + \left[\frac{3y_B}{x_B^2} - \frac{2S_A}{x_B} + ex_B^2 + 2fx_B^3 \right] x_C^2 + \left[\frac{S_A}{x_B^2} - \frac{2y_B}{x_B^3} - 2ex_B - 3fx_B^2 \right] x_C^3 + ex_C^4 + fx_C^5 \quad (III.17)$$

$$y_C = \left[S_A x_C + \frac{3y_B x_C^2}{x_B^2} - \frac{2S_A x_C^2}{x_B} + \frac{S_A x_C^3}{x_B^2} - \frac{2y_B x_C^3}{x_B^3} \right] +$$

$$e \left[x_B^2 x_C^2 - 2x_B x_C^3 + x_C^4 \right] + f \left[2x_B^3 x_C^2 - 3x_B^2 x_C^3 + x_C^5 \right] \quad (\text{III.18})$$

Equation III.18 can be expressed in short hand fashion as

$$y_C = M + eN + fO \quad (\text{III.19})$$

where terms M, N and O symbolize the parentetic terms in equation III.18

Consequently, constant e is given as

$$e = \frac{[y_C - M - fO]}{N} \quad (\text{III.20})$$

Using Equation III.20, the constants c and d (Equations III.13 and III.14) can be expressed as

$$c = \frac{3y_B}{x_B^2} - \frac{2S_A}{x_B} + x_B^2 \frac{[y_C - M - fO]}{N} + 2fx_B^3 \quad (\text{III.21})$$

$$d = \frac{S_A}{x_B^2} - \frac{2y_B}{x_B^3} - 2x_B \frac{[y_C - M - fO]}{N} - 3fx_B^2 \quad (\text{III.22})$$

The slope at point C is defined as S_f and represents the sixth boundary condition (equation III.15). By substituting into Equation III.6

$$S_f = S_A + 2cx_C + 3dx_C^2 - 4ex_C^3 + 5fx_C^4 \quad (\text{III.23})$$

By substituting for constants c, d and e (Equations III.20 through III.22) in Equation III.23

$$S_f = S_A + \left[\frac{6y_B x_C}{x_B^2} - \frac{4S_A x_C}{x_B} + 2x_C x_B^2 \frac{[y_C - M - fO]}{N} + 4fx_B^3 x_C \right] +$$

$$\left[\frac{3S_A x_C^2}{x_B^2} - \frac{6y_B x_C^2}{x_B^3} - 6x_B x_C^2 \frac{[y_C - M - fO]}{N} - 9fx_B^2 x_C^2 \right] +$$

$$\left[4x_C^3 \frac{[y_C - M - fO]}{N} \right] + 5fx_C^4 \quad (\text{III.24})$$

$$S_f = \left[S_A + \frac{6y_B x_C}{x_B^2} - \frac{4S_A x_C}{x_B} + \frac{3S_A x_C^2}{x_B^2} - \frac{6y_B x_C^2}{x_B^3} \right] +$$

$$2x_C x_B^2 \frac{[y_C - M - fO]}{N} - 6x_B x_C^2 \frac{[y_C - M - fO]}{N} +$$

$$4x_C^3 \frac{[y_C - M - fO]}{N} + f[4x_B^3 x_C - 9x_B^2 x_C^2 + 5x_C^4] \quad (\text{III.25})$$

$$f \left[6x_B x_C^2 - 2x_B^2 x_C - 4x_C^3 \right] \frac{O}{N} + f P \quad (\text{III.26})$$

where

Q and P denote the first and last parenthetic terms in Equation III.25.

Therefore,

$$f = \frac{S_f - Q - \frac{[y_C - M]}{N} [2x_B^2 x_C - 6x_B x_C^2 + 4x_C^3]}{P + [6x_B x_C^2 - 2x_B^2 x_C - 4x_C^3] \frac{O}{N}} \quad (\text{III.27})$$

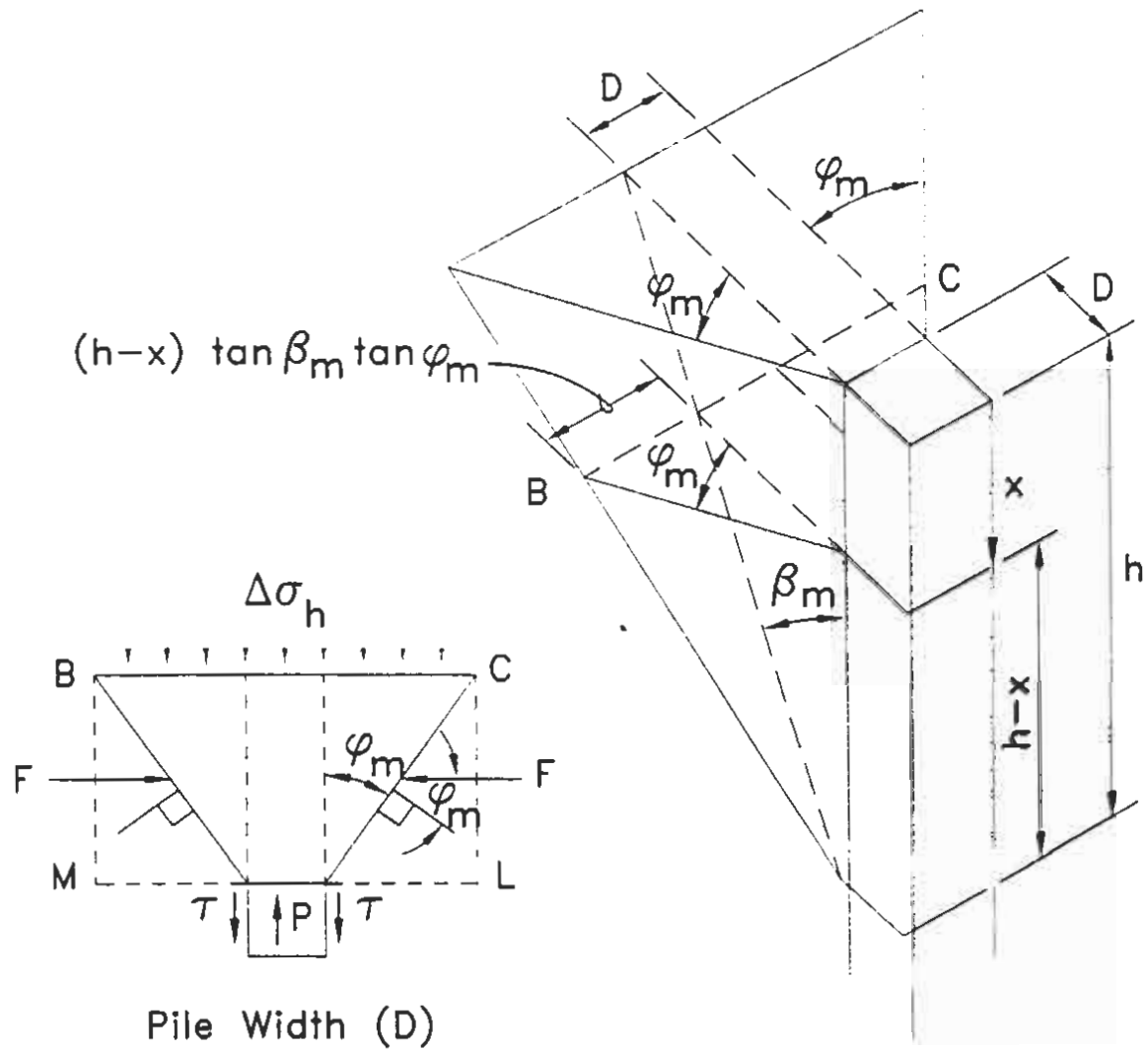
According to Equation III.27, constant f can be evaluated as a function of the slopes and coordinates of points A, B and C on the $\epsilon_1 - \epsilon_{v, \text{shear}}$ relationship (Fig. 4). Having constant f, all other constants (c, d and e) of Equation III.5 can be determined using Equations III.20 through III.22.

Table 4.1 Roundness Classes (Powers 1953)

Grade Terms	Class Intervals	Geometric Means
Very angular	0.12 - 0.17	0.14
Angular	0.17 - 0.25	0.21
Subangular	0.25 - 0.35	0.30
Subrounded	0.35 - 0.49	0.41
Rounded	0.49 - 0.70	0.59
Well rounded	0.70 - 1.00	0.84

Table 4.2 The Properties of Sands Employed to Develop the Approach Presented

Material	Roundness (ρ)	e_{max}	e_{min}	C_u	Ref.
Nevada Sand (subrounded, clean, fine, white quartz, foundry sand)	0.45	0.856	0.548	1.6	Norris et al. (1995, 1997)
Ione Sand (subangular, clean, fine, grayish quartz, glass sand)	0.29	1.000	0.717	1.4	Norris et al. (1995, 1997)
Toyoura Sand (angular, uniform, Japanese sand)	0.21	0.977	0.605	1.46	Fukushima and Tatsuoka. (1984)
Sacramento River Sand (SRS) (subangular to subrounded, uniform, feldspar and quartz sand)	0.35	1.03	0.61	1.4	Lee and Seed (1967)
Banding Sand (subrounded to subangular, uniform, clean, fine quartz sand)	0.33	0.84	0.50	1.80	Castro (1969)
Kogyuk Sand (350/2) (subrounded to subangular, uniform, medium quartz sand)	0.40	0.829	0.47	1.80	Been and Jefferies (1985)
Ottawa Sand (rounded, medium uniform quartz sand ASTM C-109)	0.55	0.82	0.50	1.50	Negusse and Vaid (1990)
	0.55	0.95	0.57	1.66	Dakoulas and Yuanhui (1992)



SLICE OF WEDGE AT DEPTH x

Fig. 2.1 The Basic Strain Wedge in Uniform Soil

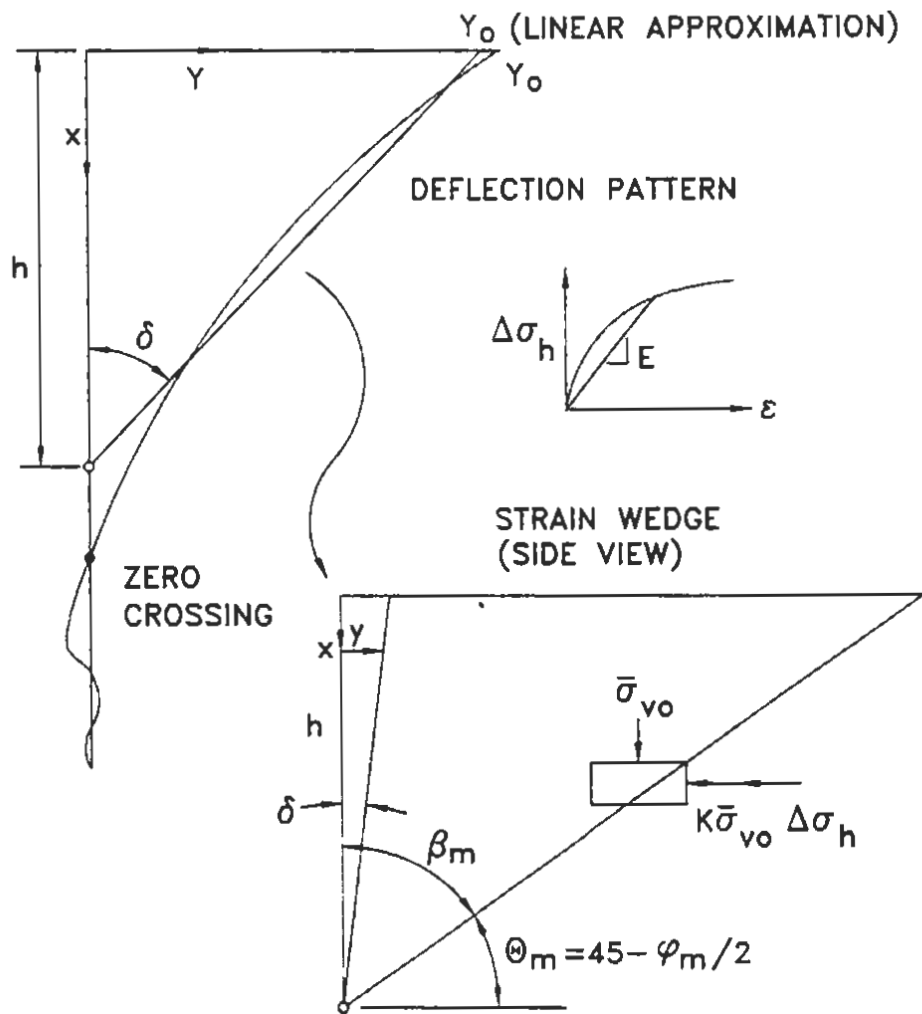


Fig. 2.2 Deflection Pattern of Laterally Loaded Long Pile and the Associated Strain Wedge

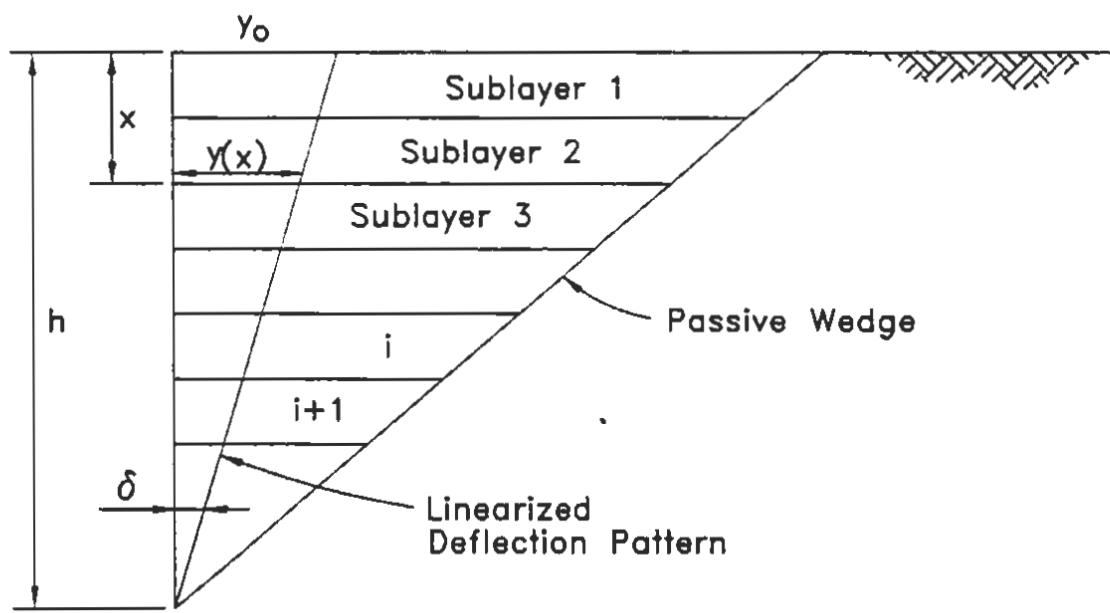
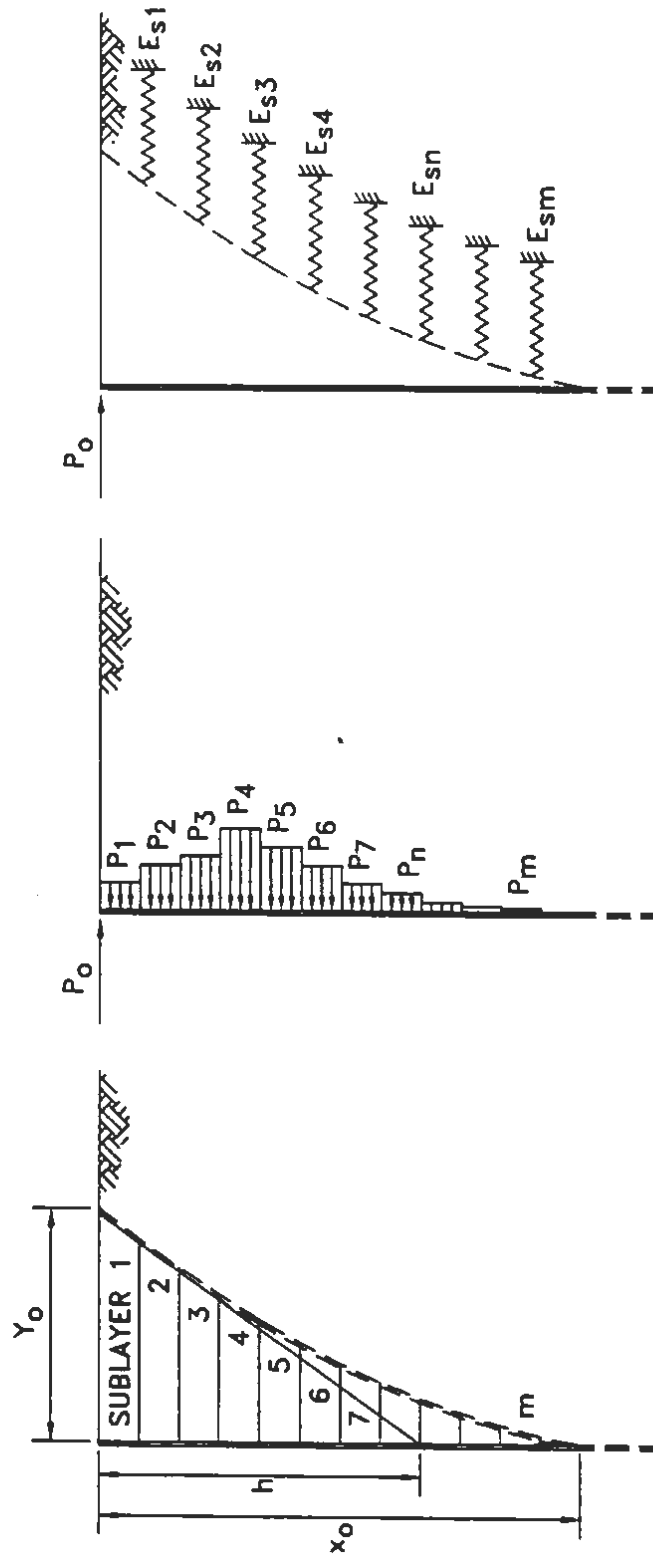


Fig. 2.3 The Linearized Deflection Pattern of the Pile Embedded in Soil in the Multi-Sublayer Strain Wedge Model



(a) PILE DEFLECTION PATTERN (b) SOIL REACTION DISTRIBUTION ALONG THE PILE (c) SOIL-PILE MODELING

Fig. 2.4 Soil-Pile Interaction in the Multi-Sublayer Technique

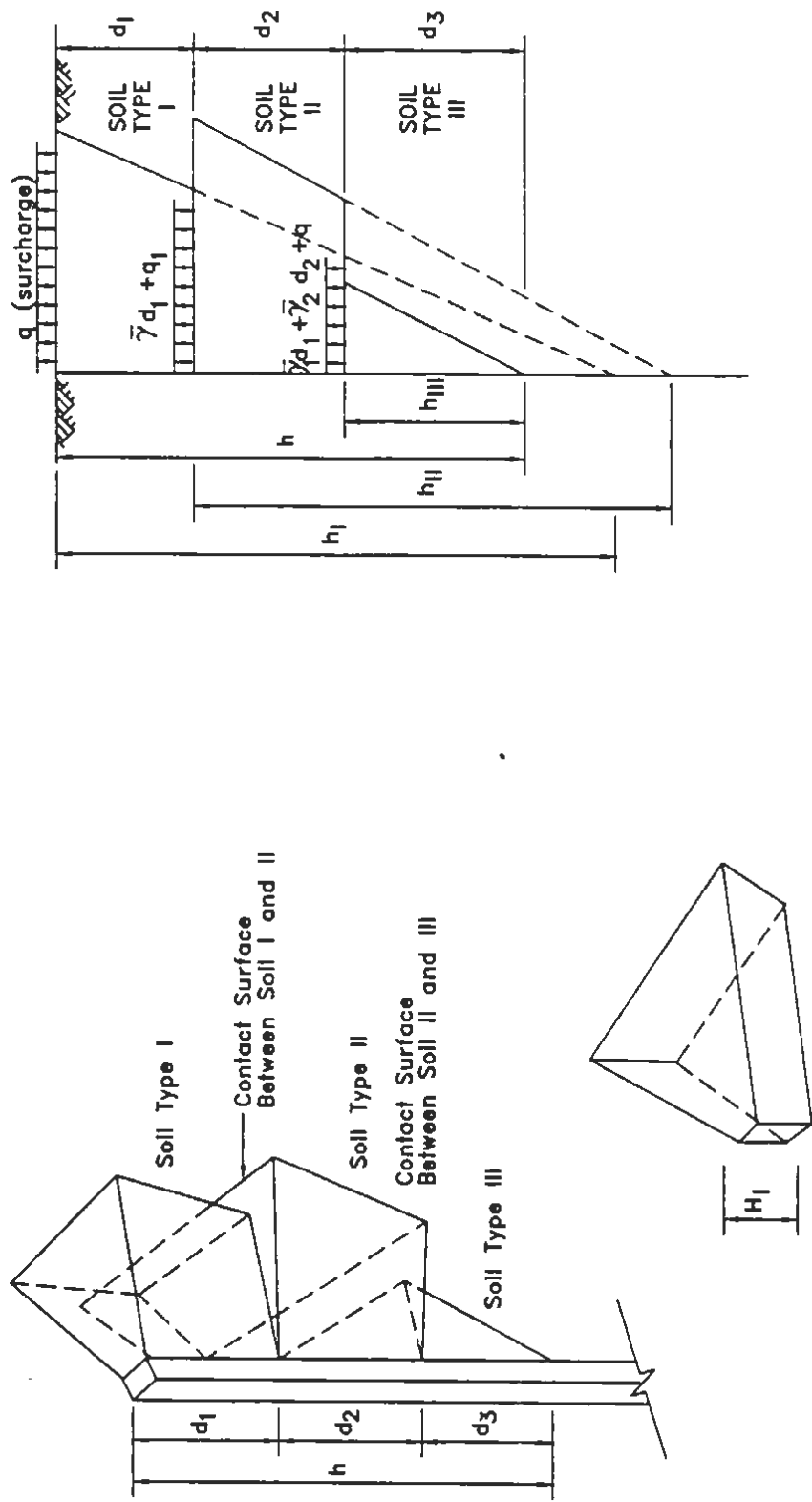


Fig. 2.5 The Proposed Geometry of the Compound Passive Wedge

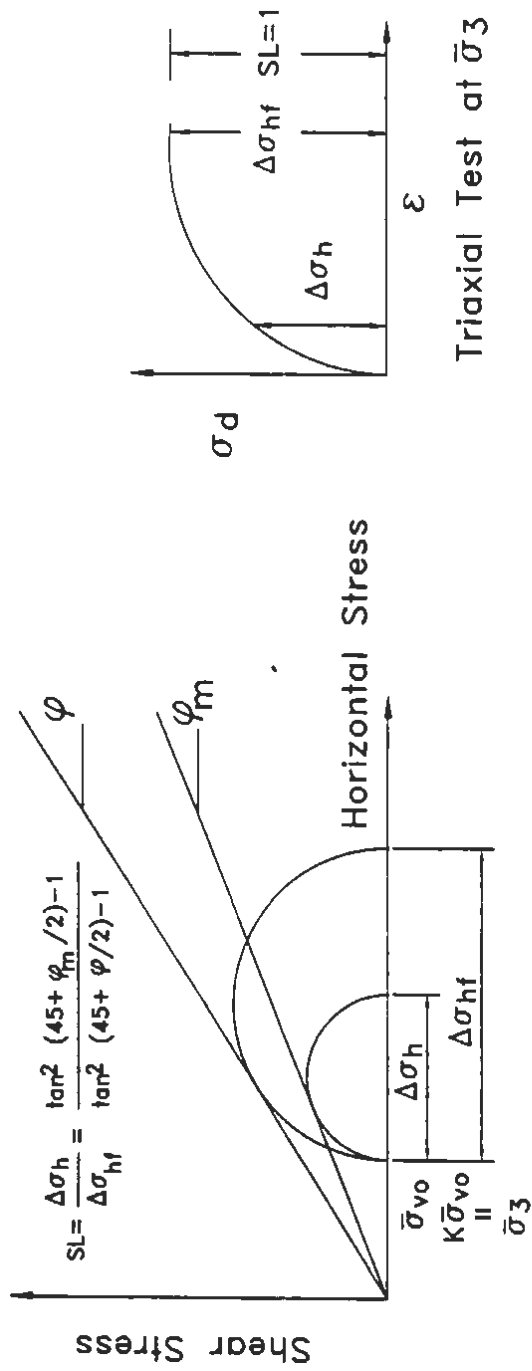
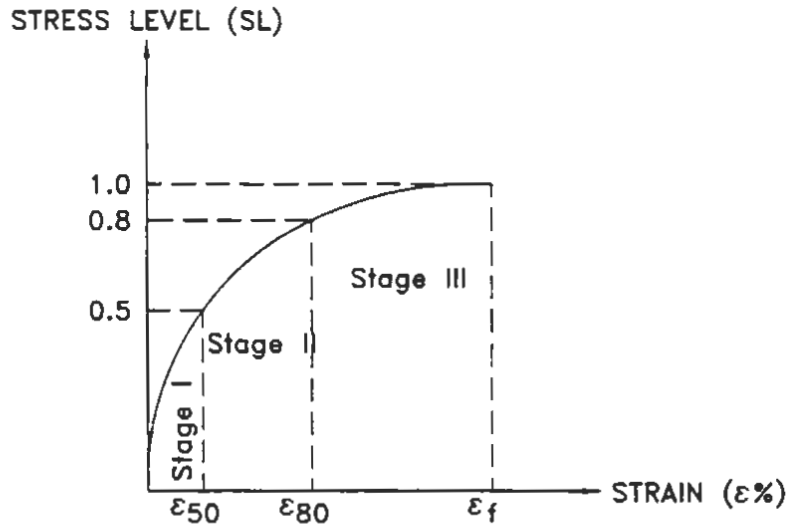
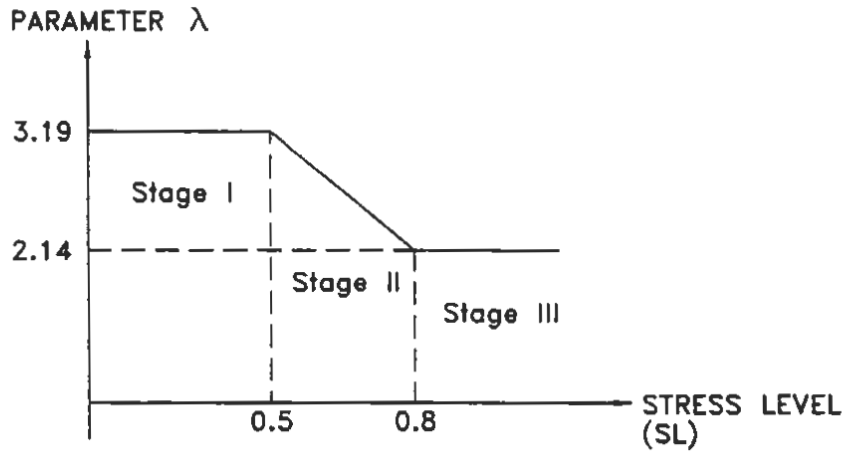


Fig. 2.7 Relationship Between Horizontal Stress Change, Stress Level, and Mobilized Friction Angle



(a) THE DEVELOPED HYPERBOLIC STRESS-STRAIN RELATIONSHIP IN SOIL



(b) THE VARIATION OF THE FITTING PARAMETER λ VERSUS STRESS LEVEL (SL)

Fig. 2.8 The Developed Stress-Strain Relationship in Soil

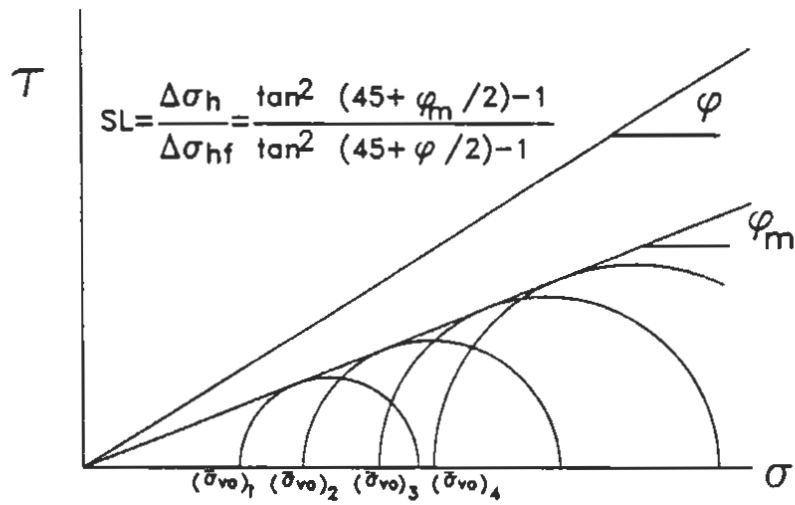
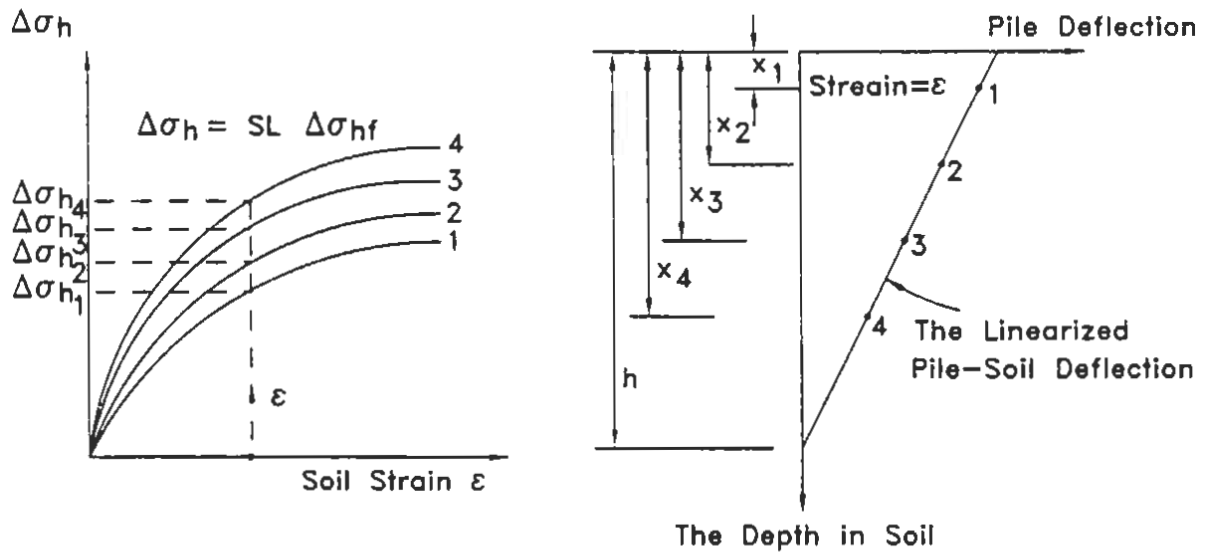
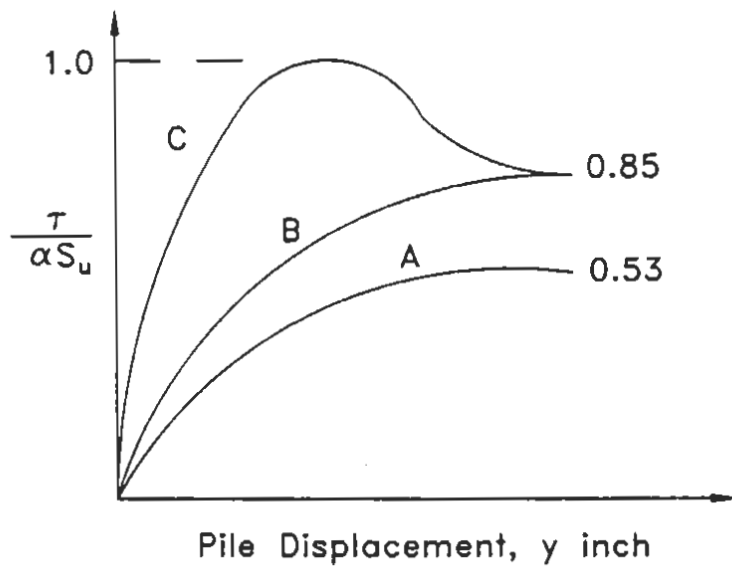
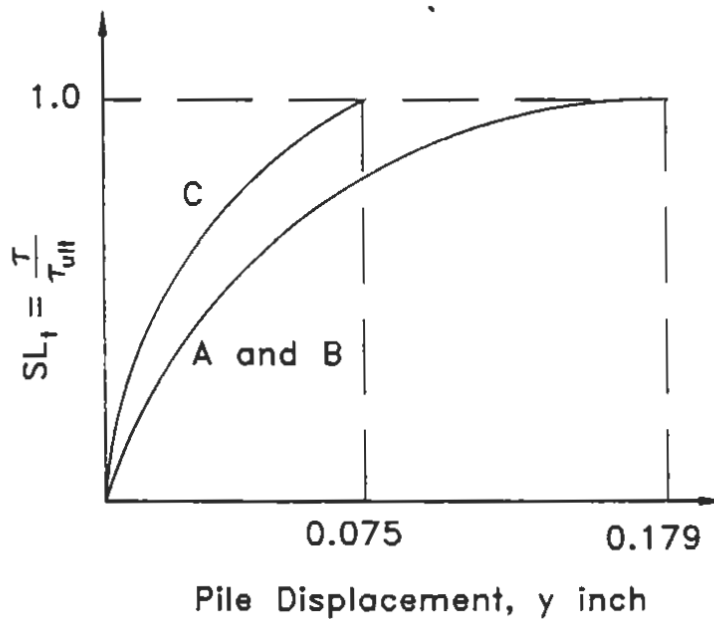


Fig. 2.9 The Nonlinear Variation of Stress Level Along the Depth of Soil at Constant Strain ϵ



(a) Coyle-Reese Shear Stress Transfer Curve (t-z Curve)



(b) The Normalized t-z Curves

Fig. 2.10 The Employed Side Shear Stress-Displacement Curve in Clay

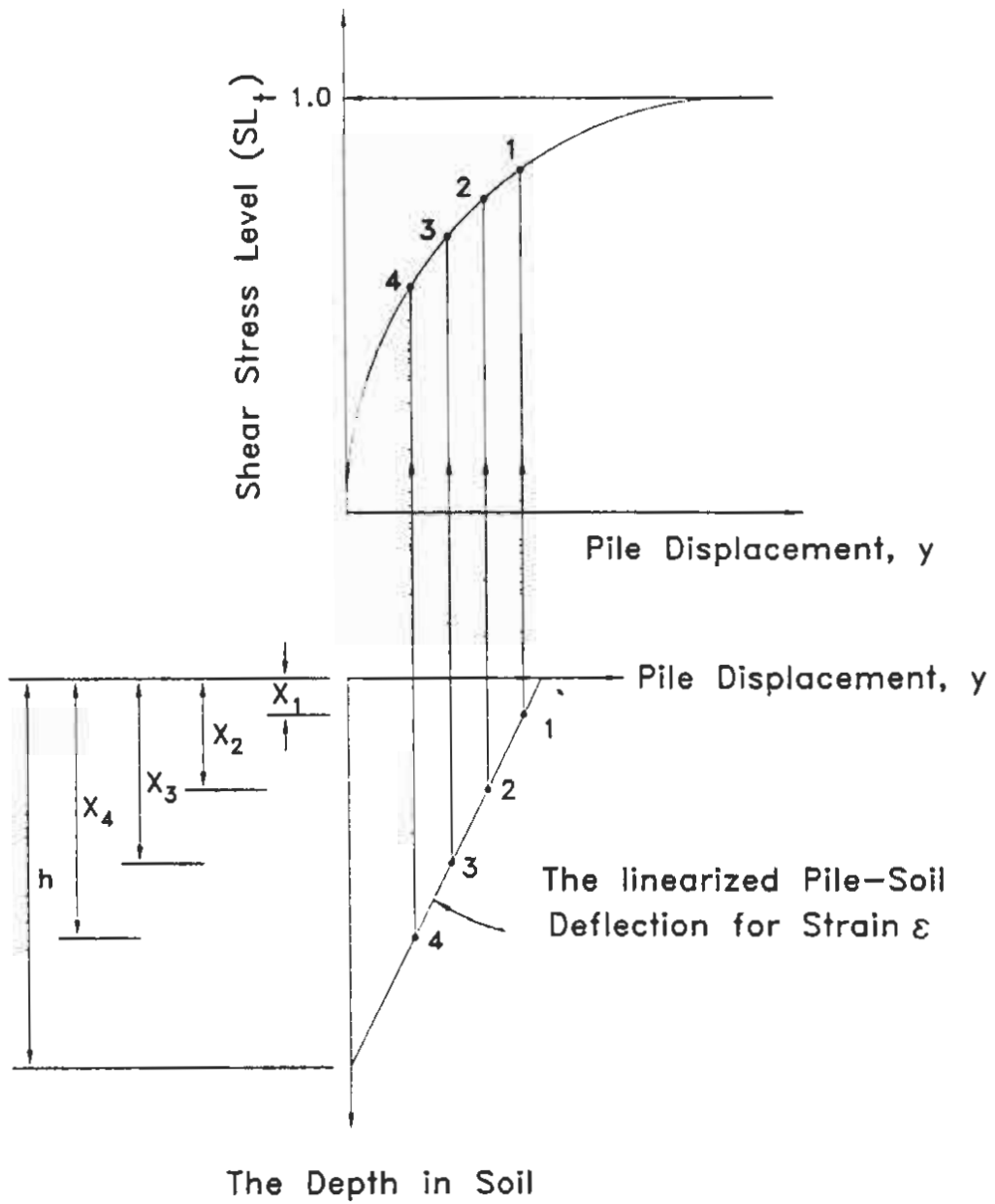


Fig. 2.11 The Nonlinear Variation of Side Shear Stress Level (SL_t) Along the Depth of Soil for Constant Strain ϵ in the Wedge

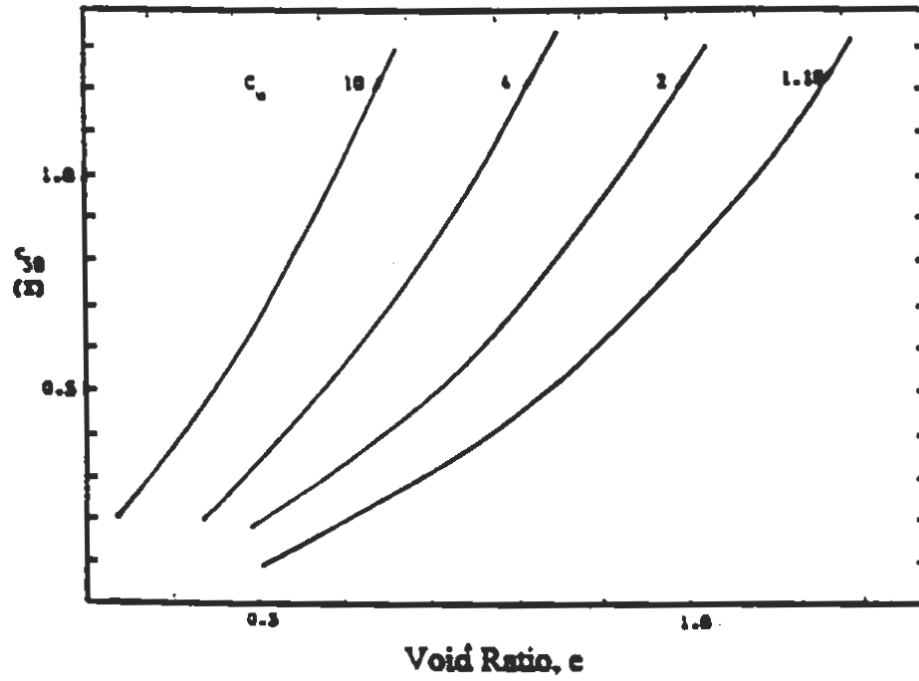


Fig. 2.12 Relationship Between ϵ_{50} , Uniformity coefficient (C_u) and Void Ratio (e) (Norris 1986)

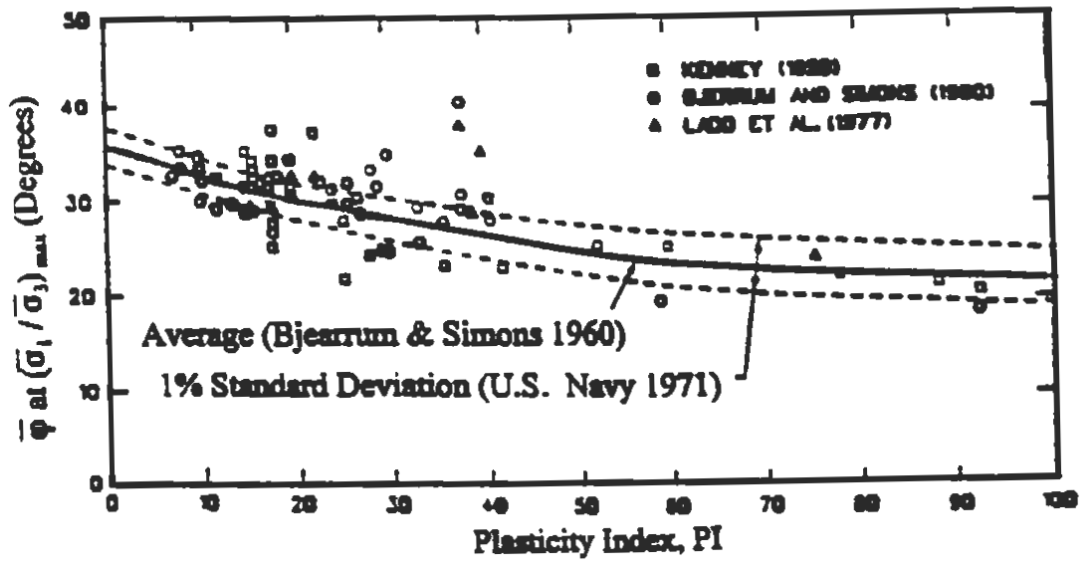


Fig. 2.13 Relationship Between Plasticity Index (PI) and $\bar{\phi}$ (US Army Corps of Engineers 1996)

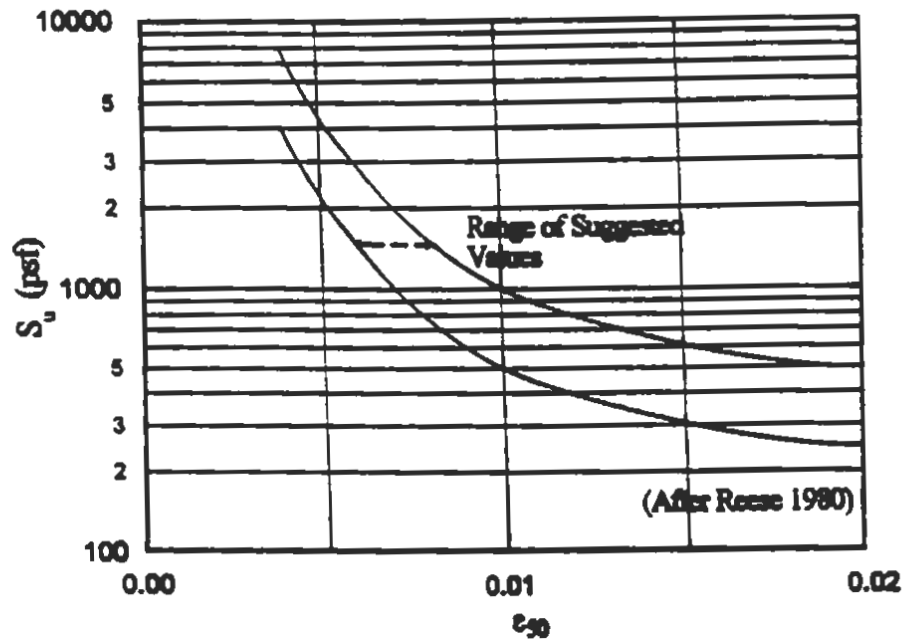


Fig. 2.14 Relationship Between ϵ_{50} and Undrained Shear Strength, S_u (Evans and Duncan 1982)

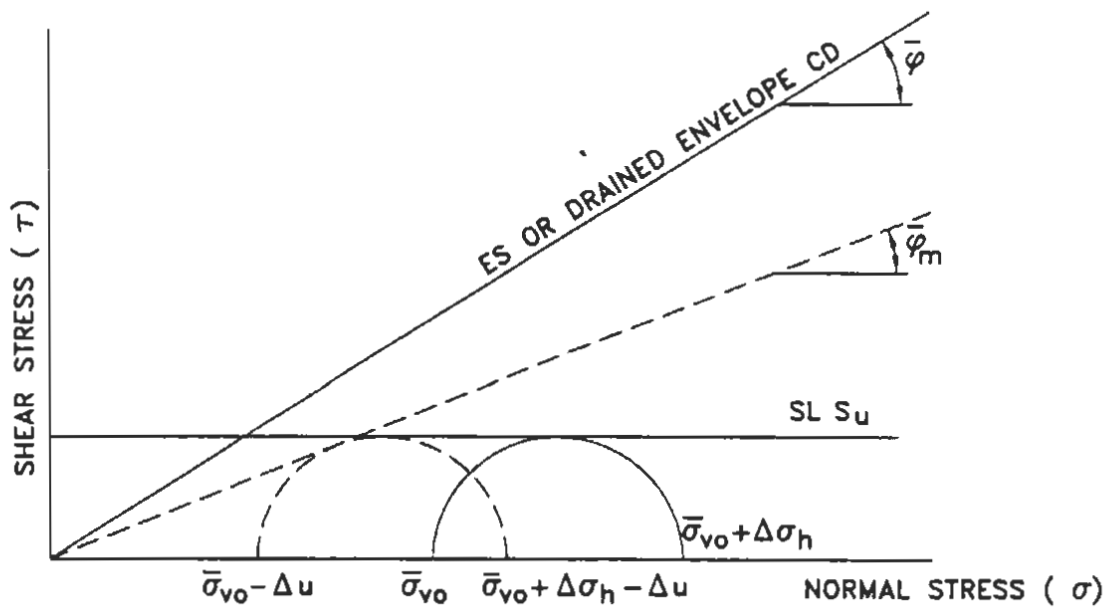
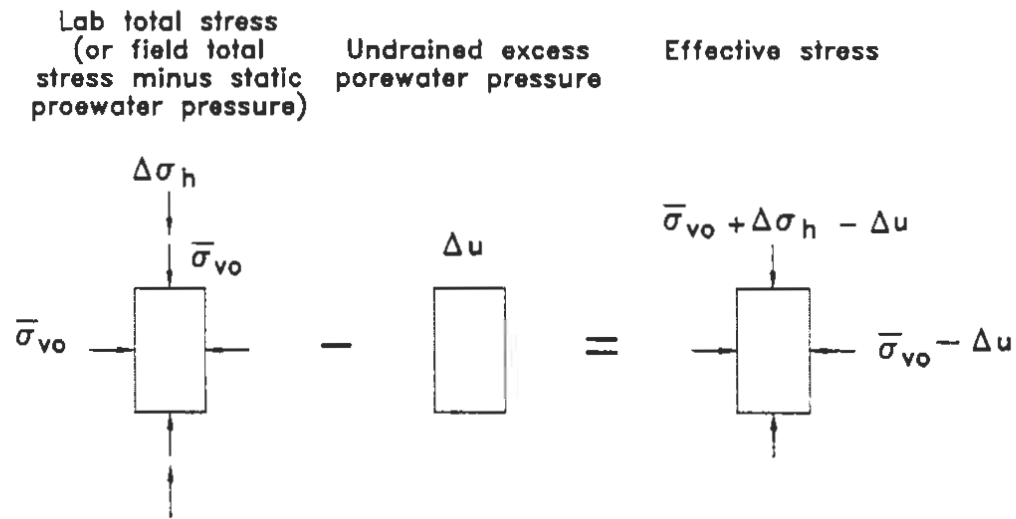


Fig. 2.15 Relationship Between Effective Stress and Total Stress Conditions

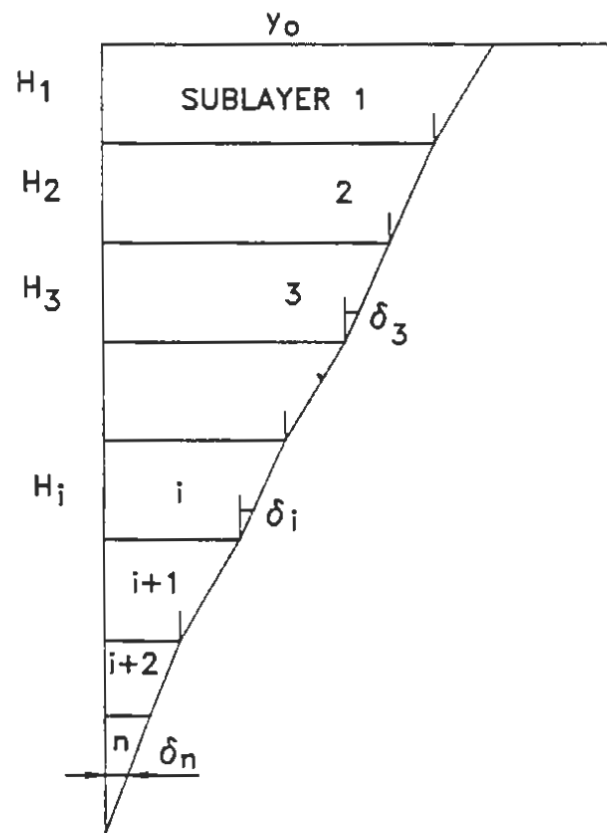


Fig. 2.16 The Assembling of Pile Head Deflection Using the Multi-Sublayer Technique

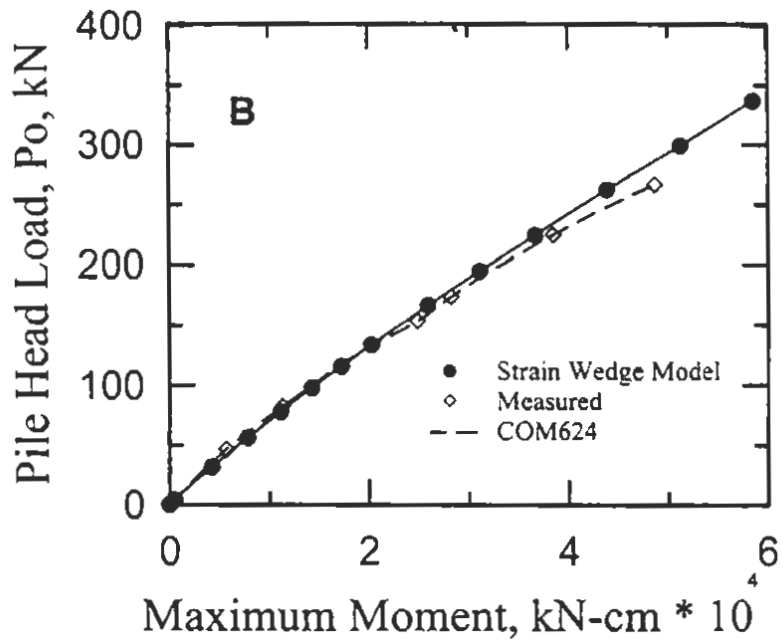
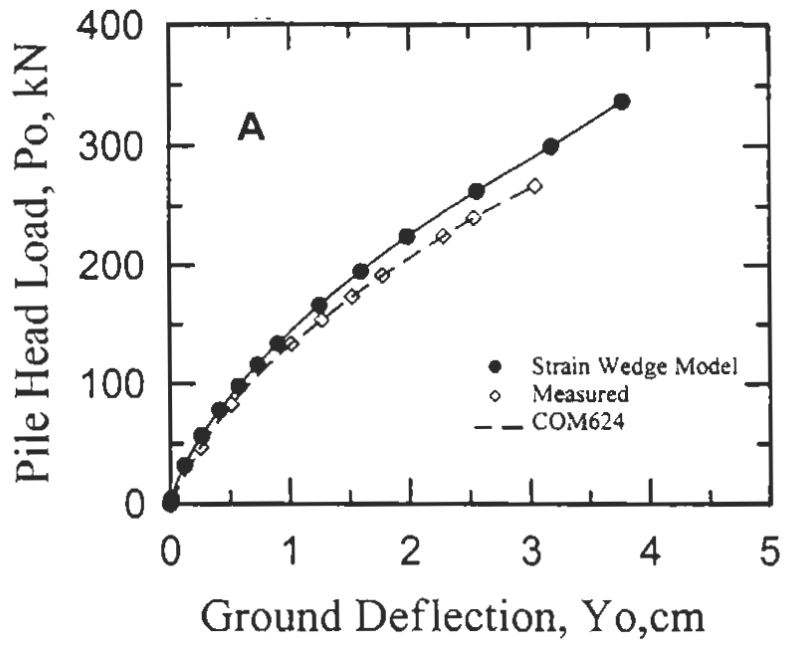


Fig. 2.17 The Measured and Predicted Response of a Laterally Loaded Pile in Sand at the Mustang Island Test.

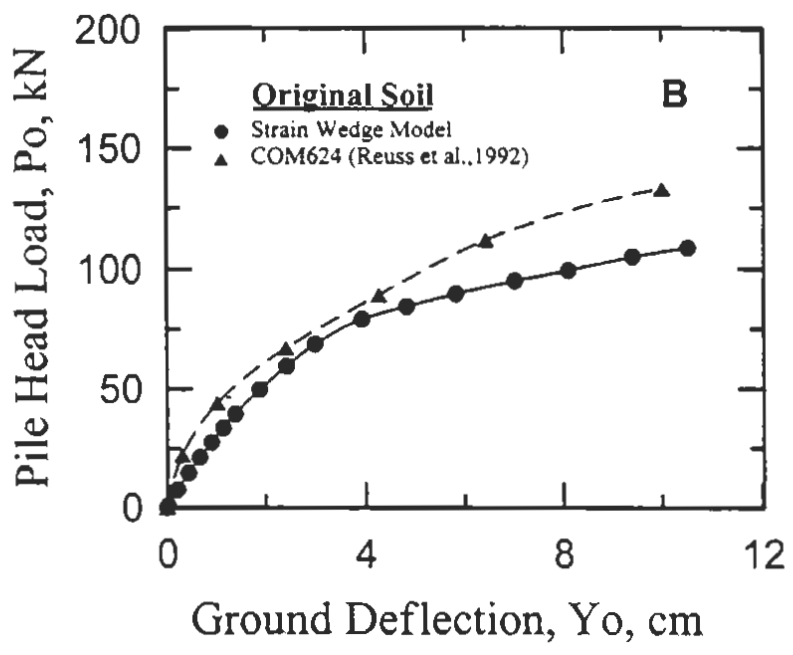
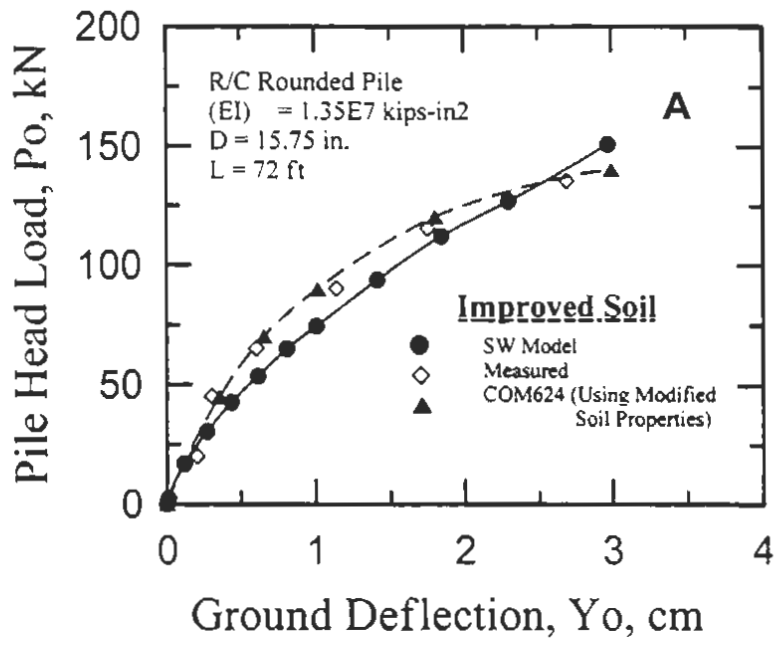


Fig. 2.18 The Measured and the Predicted Response of the Loaded Pile in the Improved and the Original Soils at the Pyramid Building, Memphis, Test.

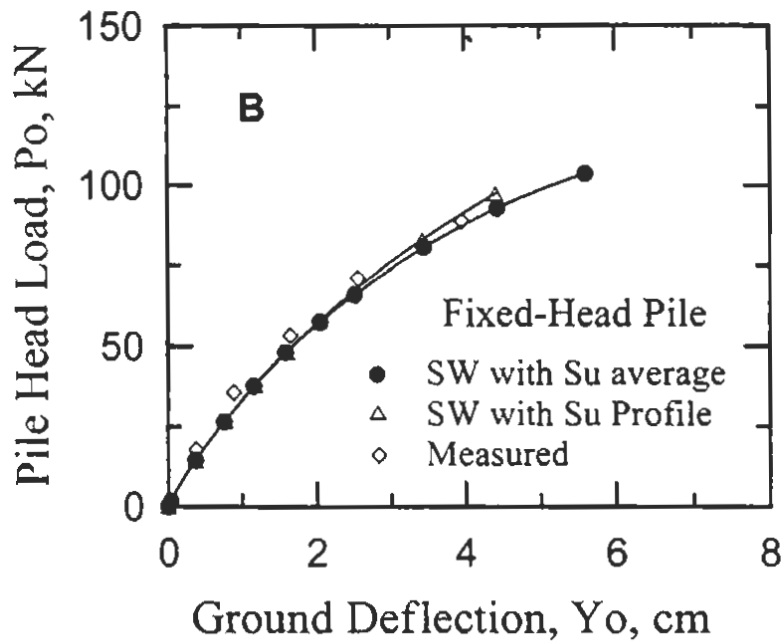
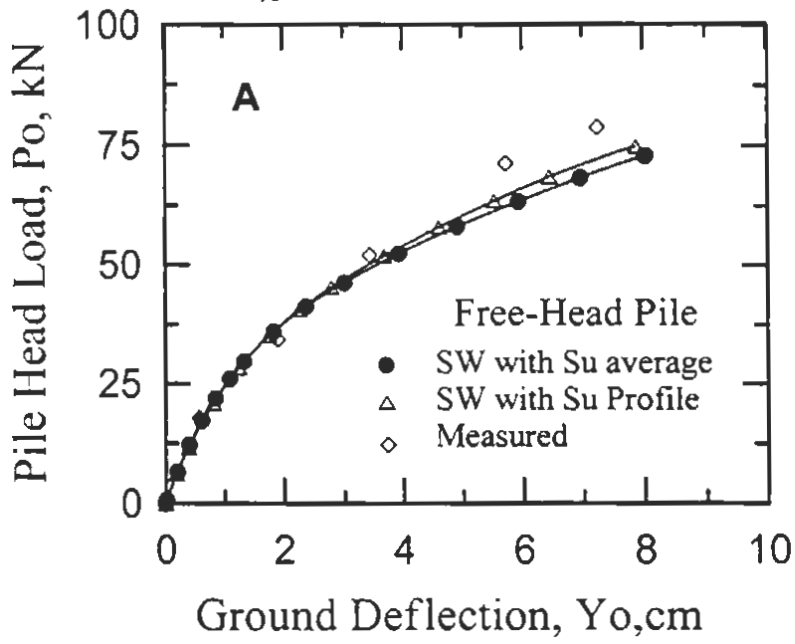


Fig. 2.19 The Measured and the SW Model Results of the Loaded Pile at the Sabine River Test.

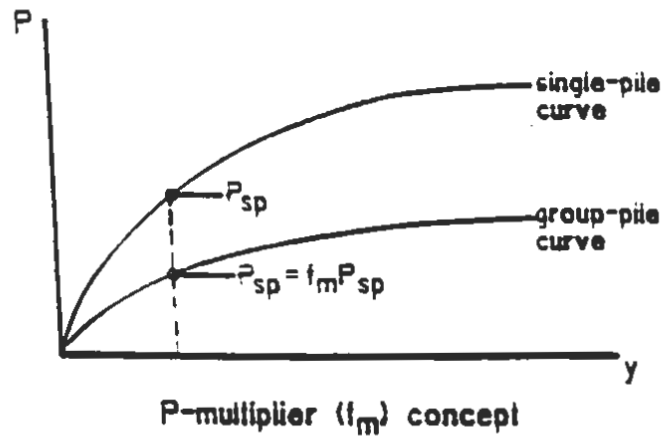


Fig. 3.1 p-Multiplier (f_m) Concept (Brown et al. 1988)

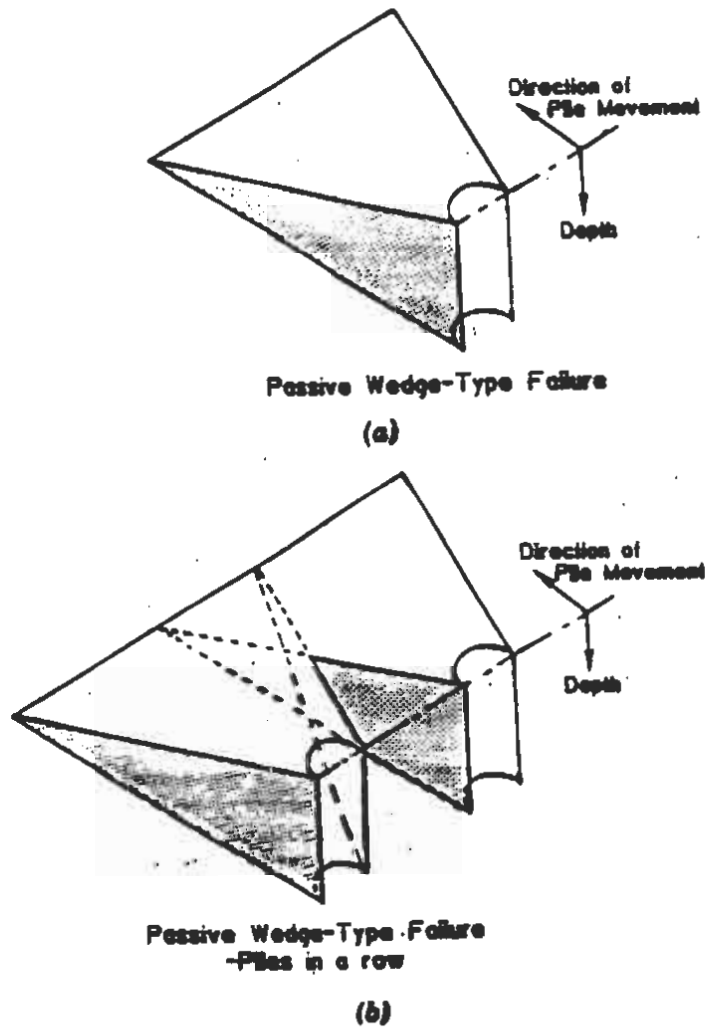


Fig. 3.2 Overlapping Shear Zones in Front Line (Brown et al. 1988)

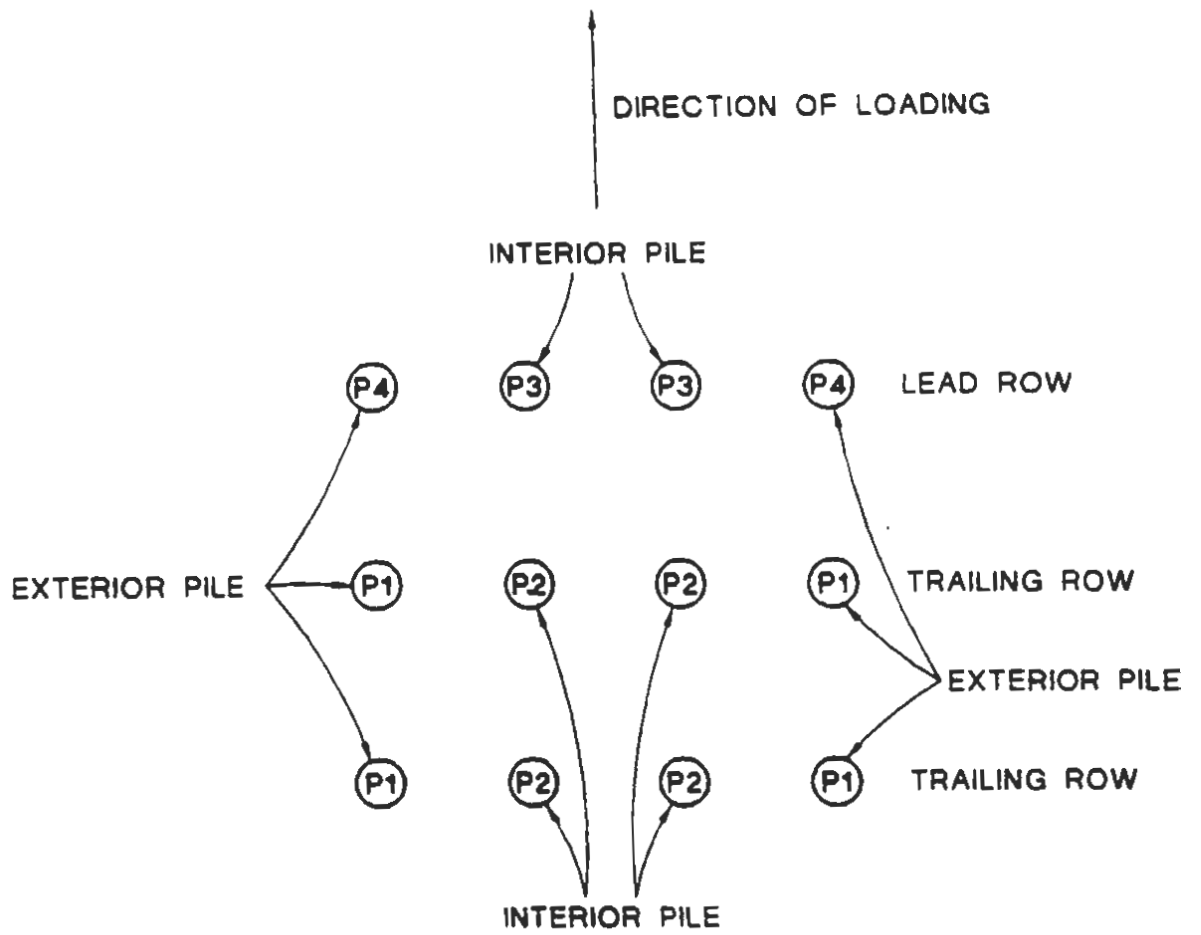
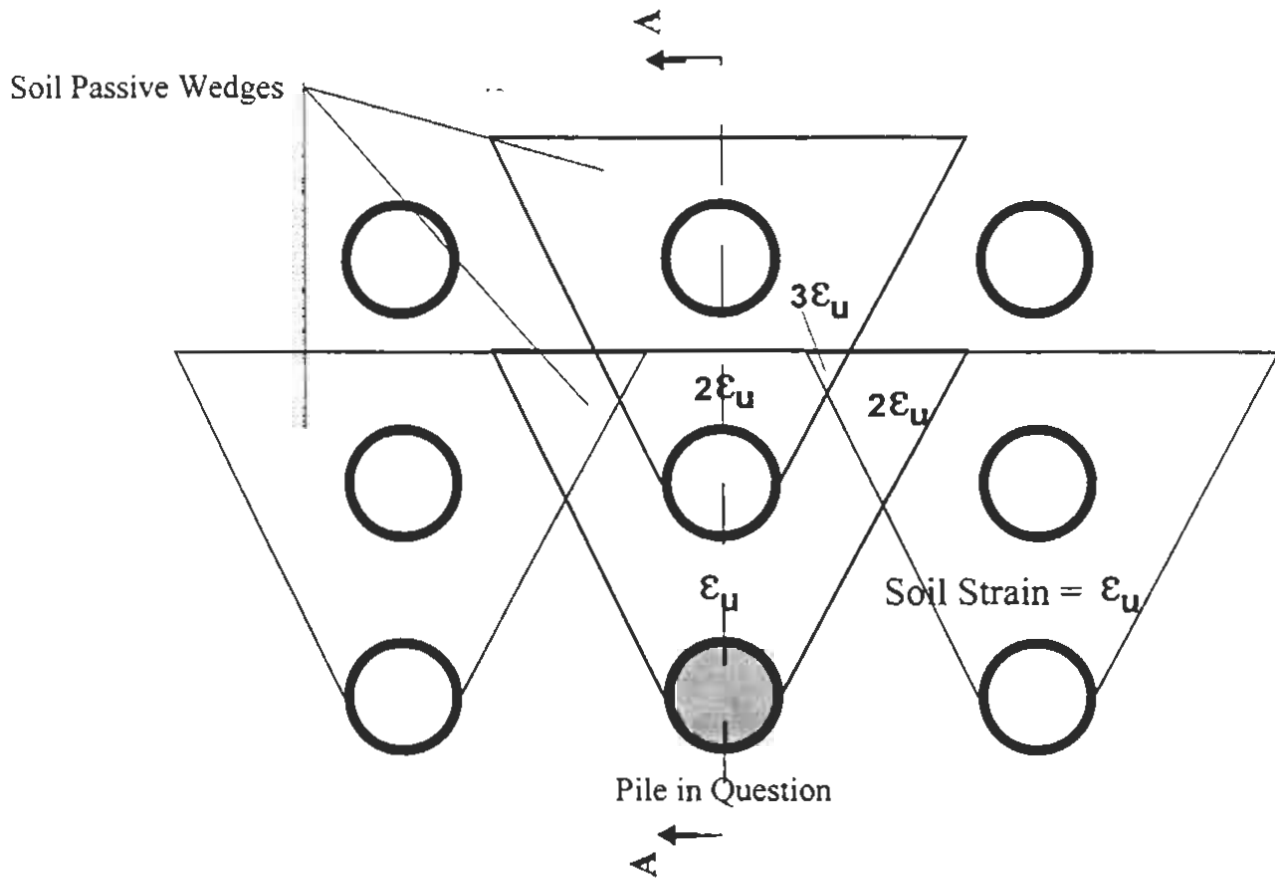
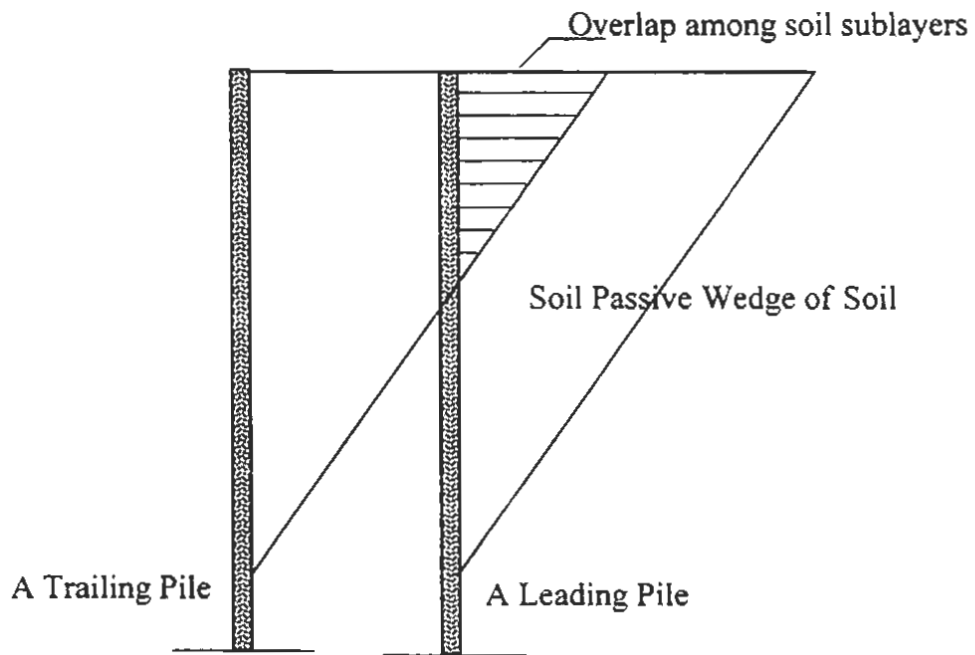


Fig. 3.3 Definition of Terms for a Pile Group

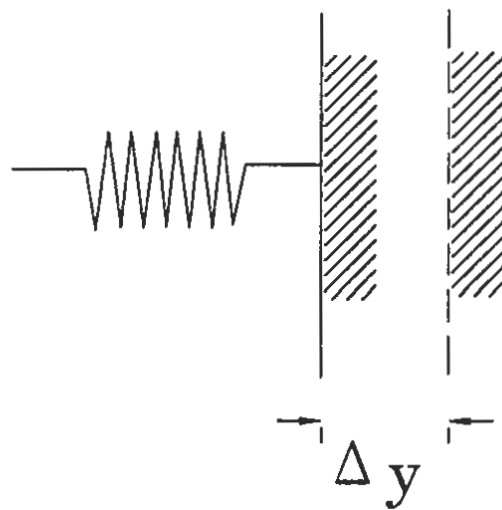
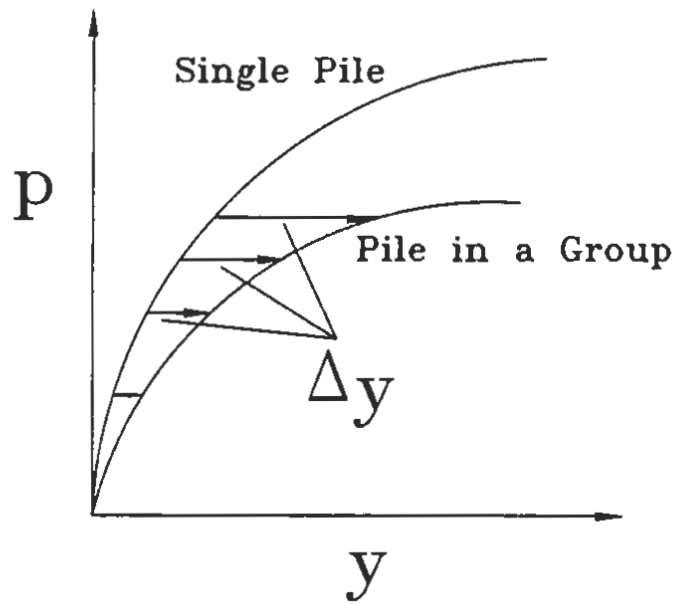


a) A Plan Cross Section View of Pile Interference



b) An Elevation Cross Section View of Pile Interference (A-A)

Fig. 3.4 Overlap Shear Zones Due to Pile Interference



Additional Displacement of Soil and Pile Due to Overlapping Stresses

Fig. 3.5 Modified p - y Curve of an Individual Pile in a Pile Group and Its Model

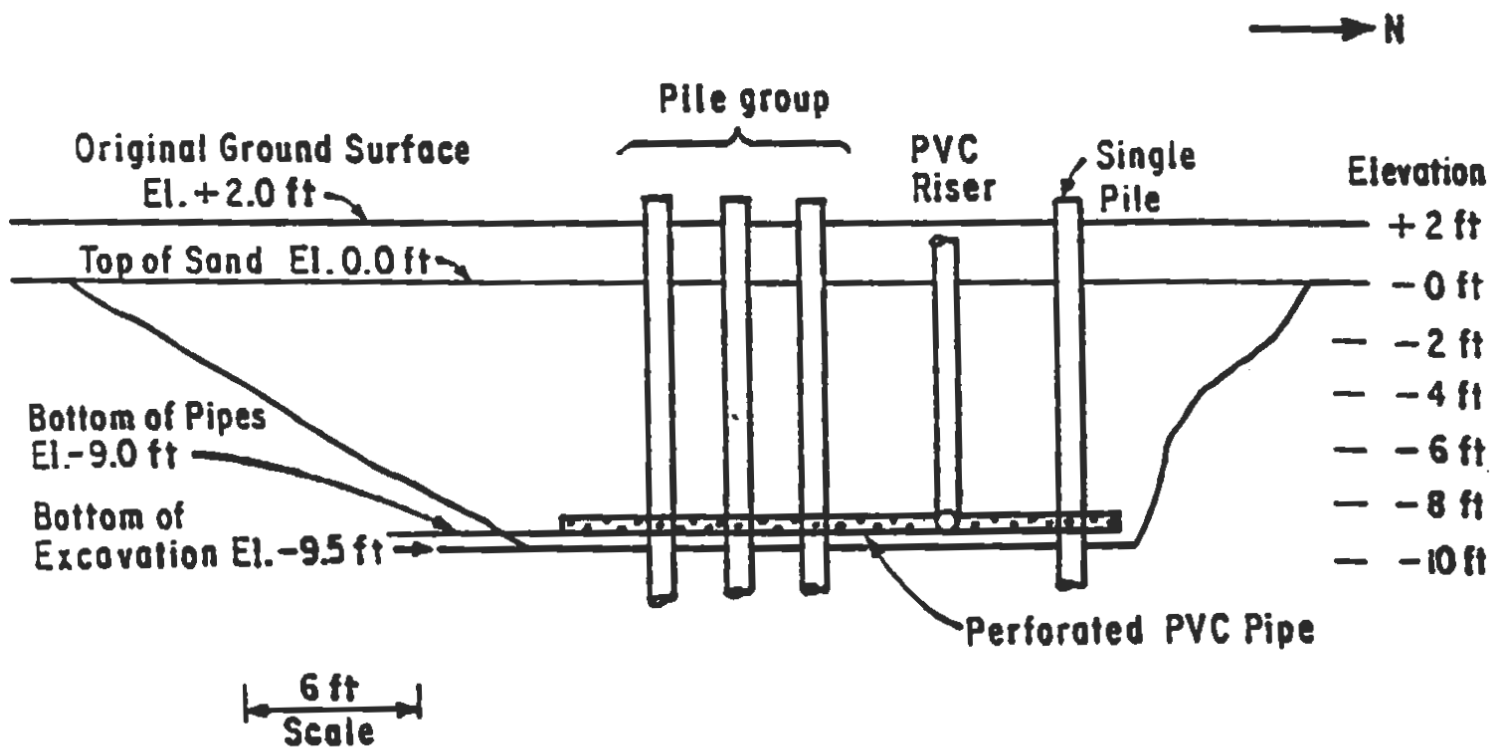


Fig. 3.6 Elevation View of Excavation and Pipe System, University of Houston, Texas, Full-Scale Load Test (Morrison et al, 1986)

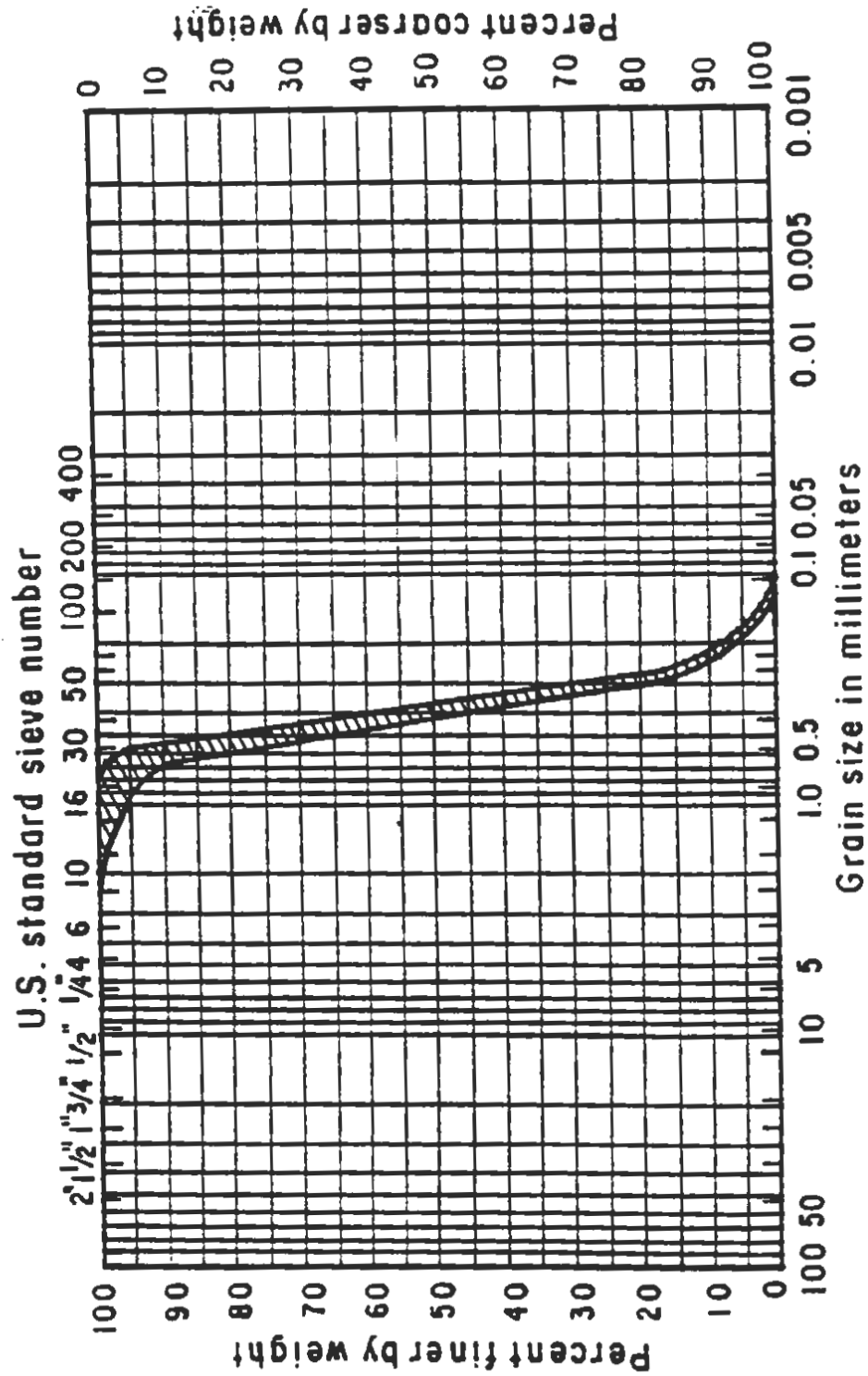


Fig. 3.7 Grain-Size Distribution of Sand, University of Houston, Texas, Full-Scale Load Test (Morrison et al, 1986)

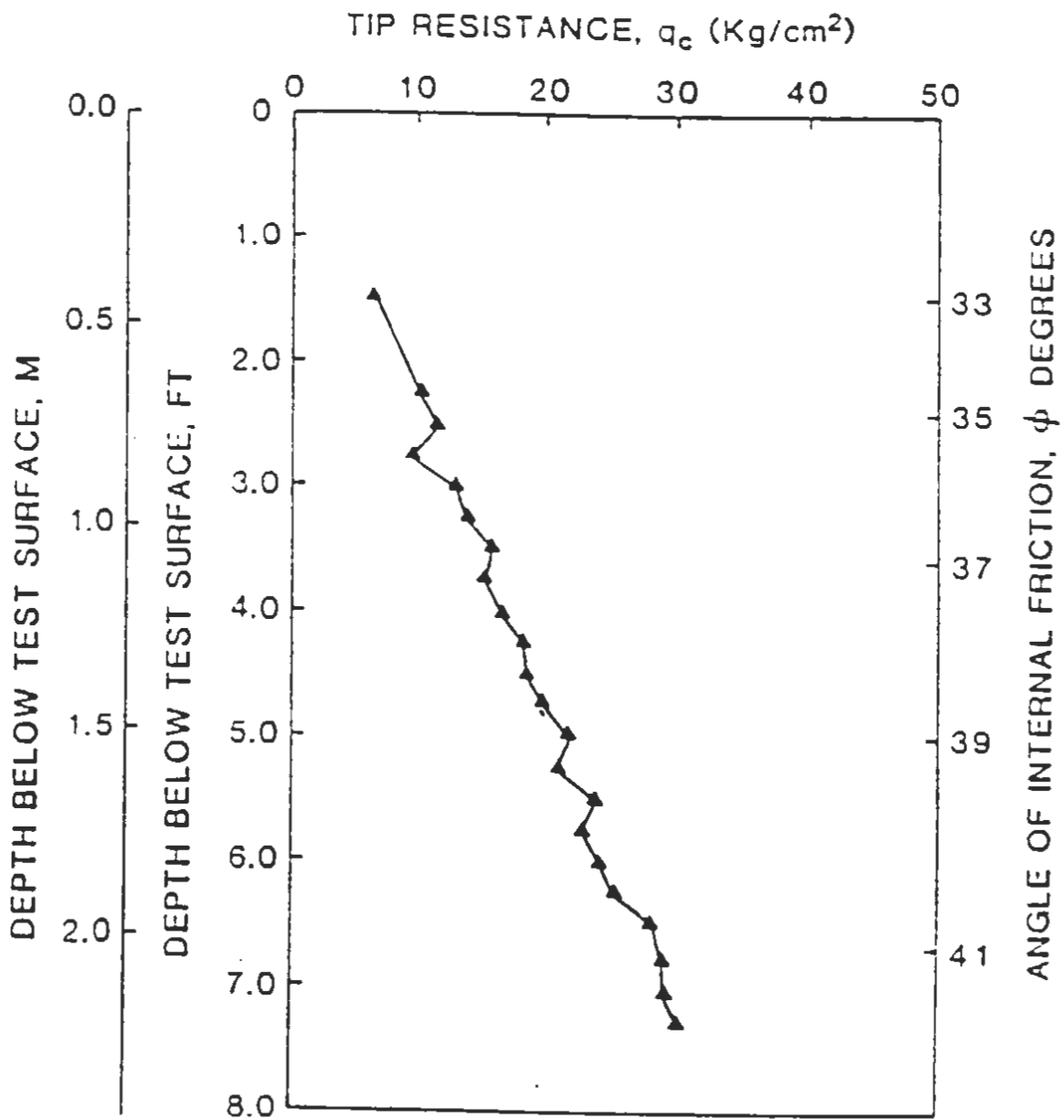


Fig. 3.8 Angle of Internal Friction Versus Depth Based on CPT-2 Penetration Test, University of Houston, Texas, Full-Scale Load Test (Ochoa and O'Neill, 1986)

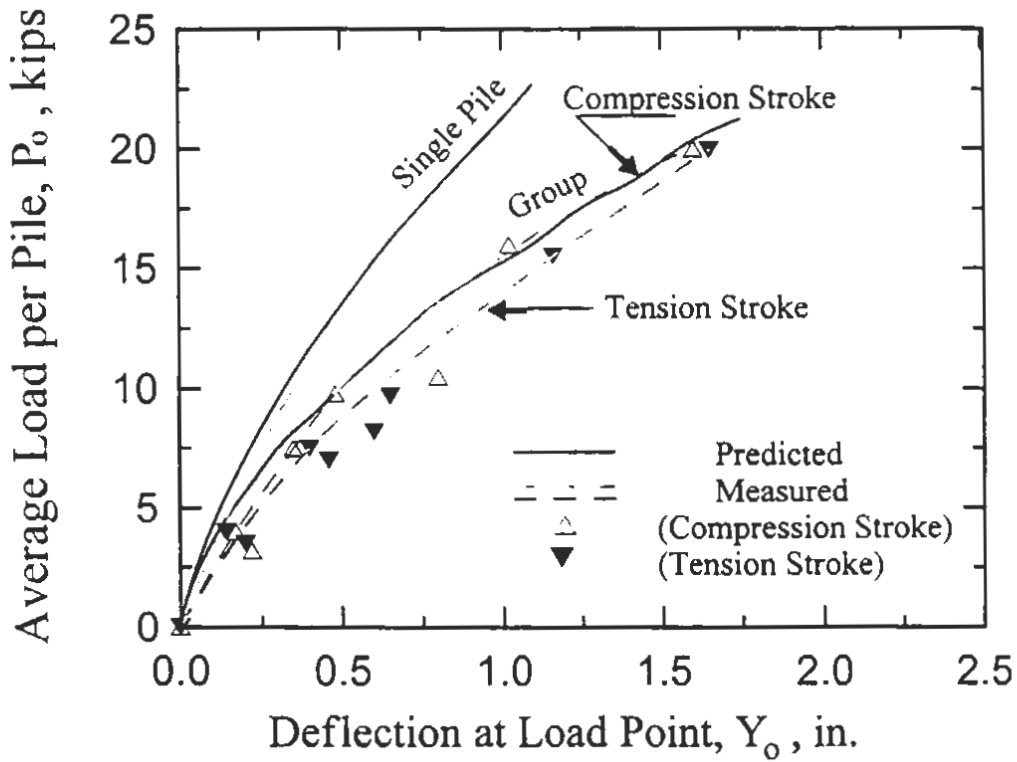


Fig. 3.9 lateral Load vs. Deflection at the Pile Head (Morrison and Reese 1986)

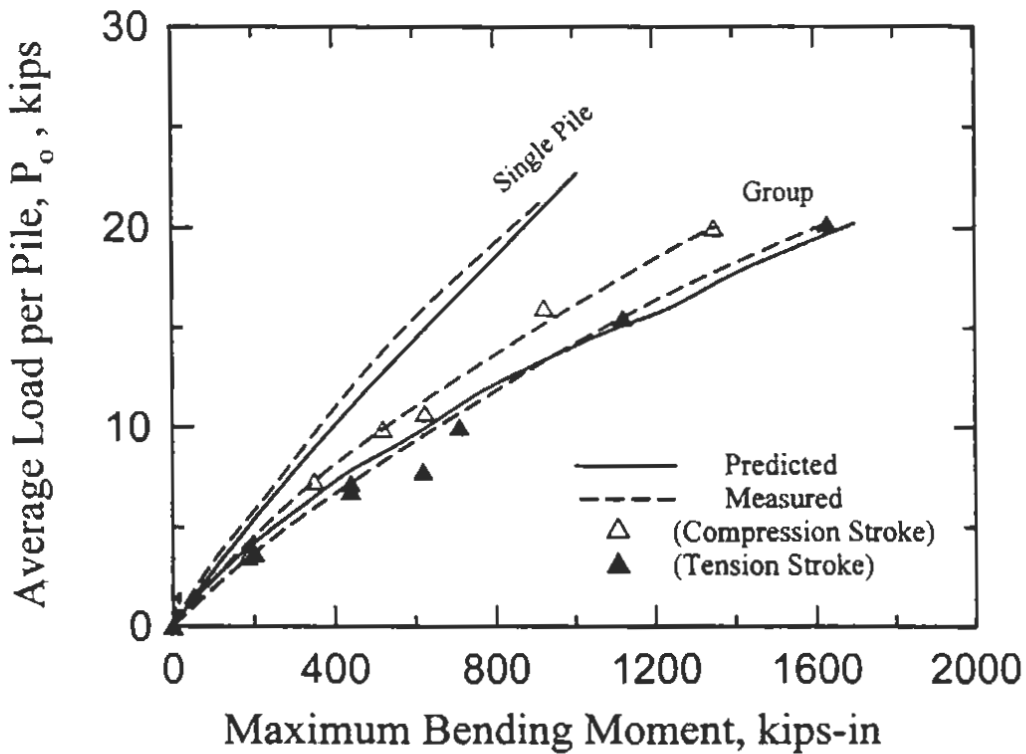
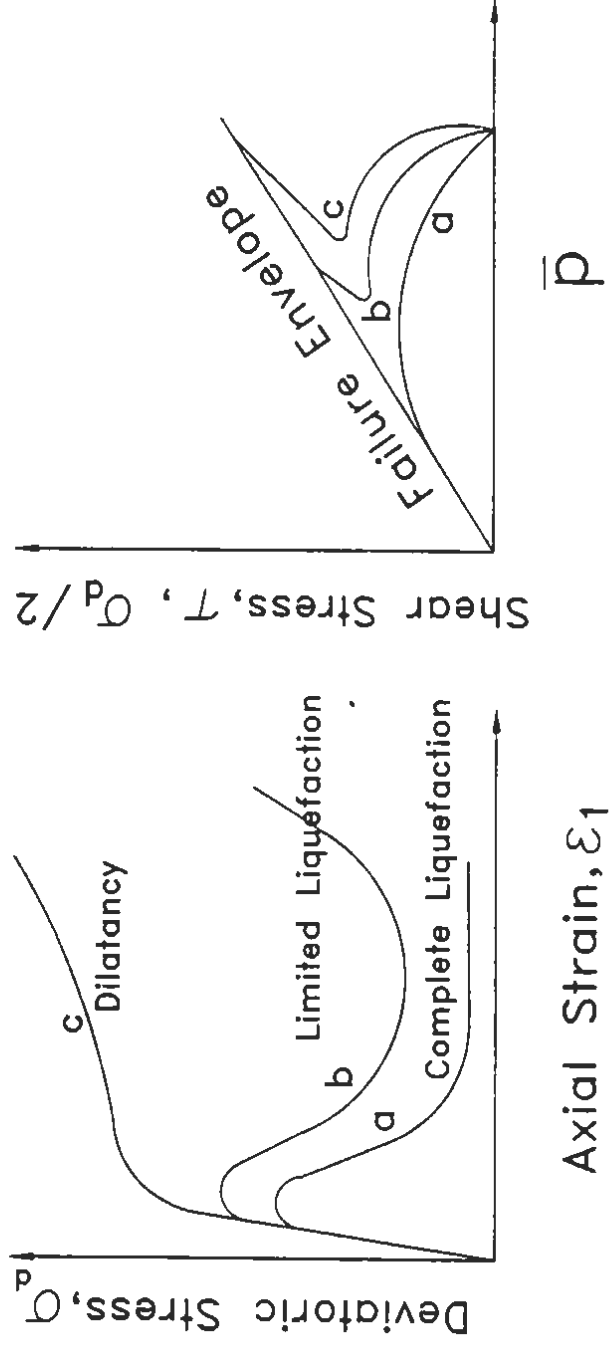


Fig. 3.10 Pile-Head Load vs. Maximum Moment (Morrison and Reese 1986)



Typical Stress-Strain Curves Stress Path

Fig. 4.1 Undrained Behavior of Saturated Sand Under Monotonic Loading

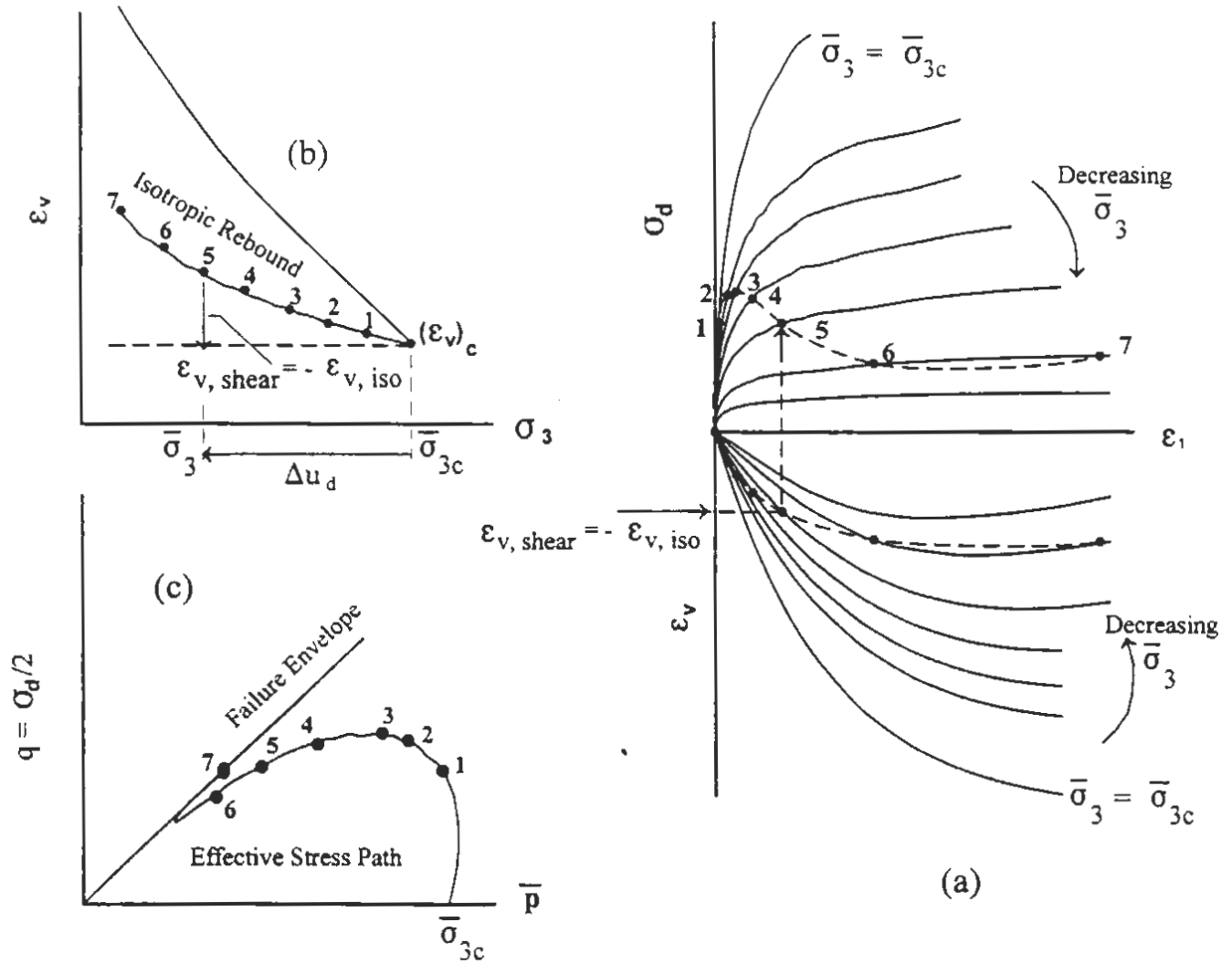


Fig. 4.2 Interrelationships Among (a) Drained and Undrained Stress-Strain Behavior (b) Isotropic Consolidation Rebound, and (c) Effective Stress Path

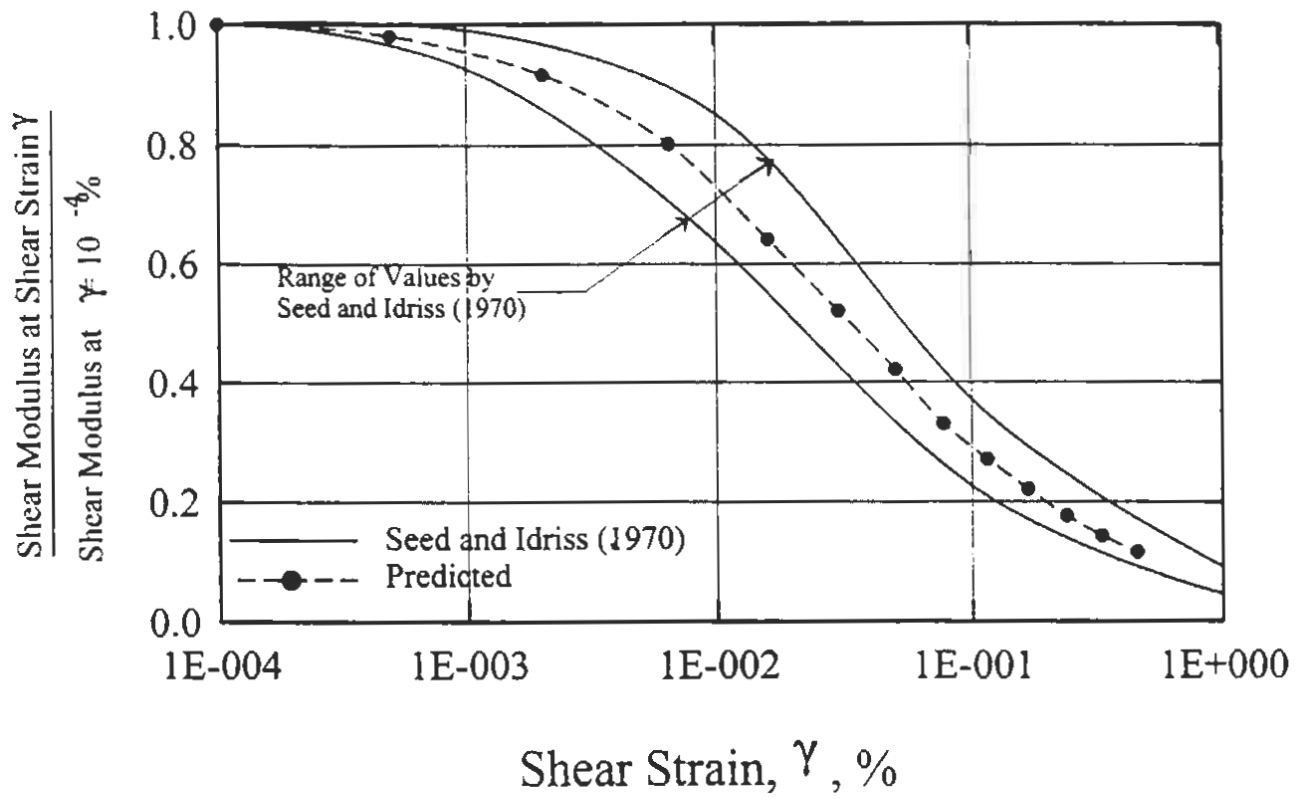


Fig. 4.3 Variation of Shear Modulus with Shear Strain for Sands

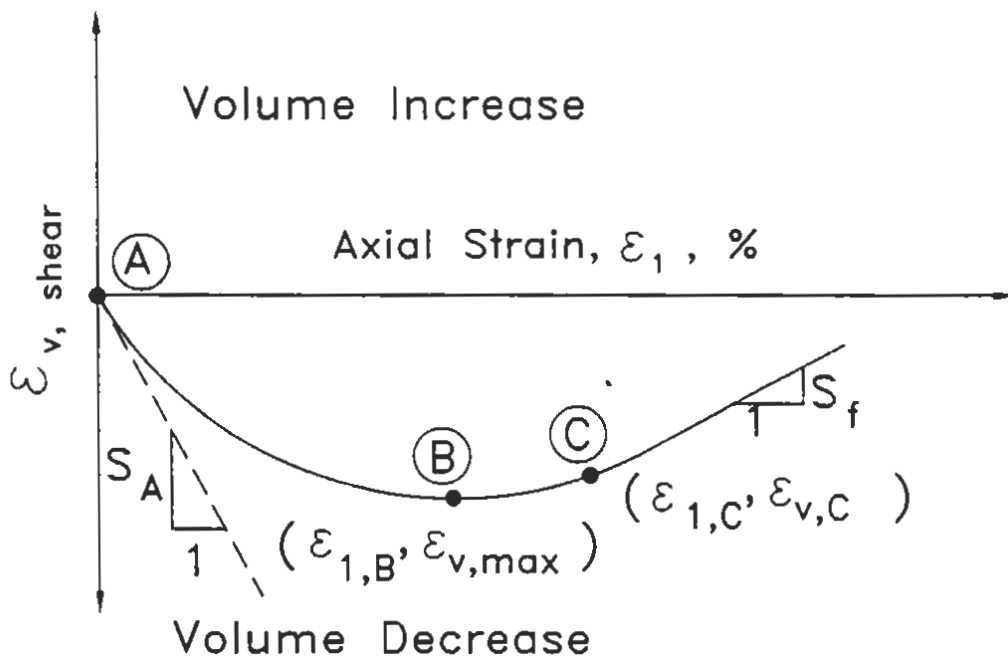


Fig. 4.4 Volumetric Strain Curve Due to Shear vs. Axial Strain and its Major Points

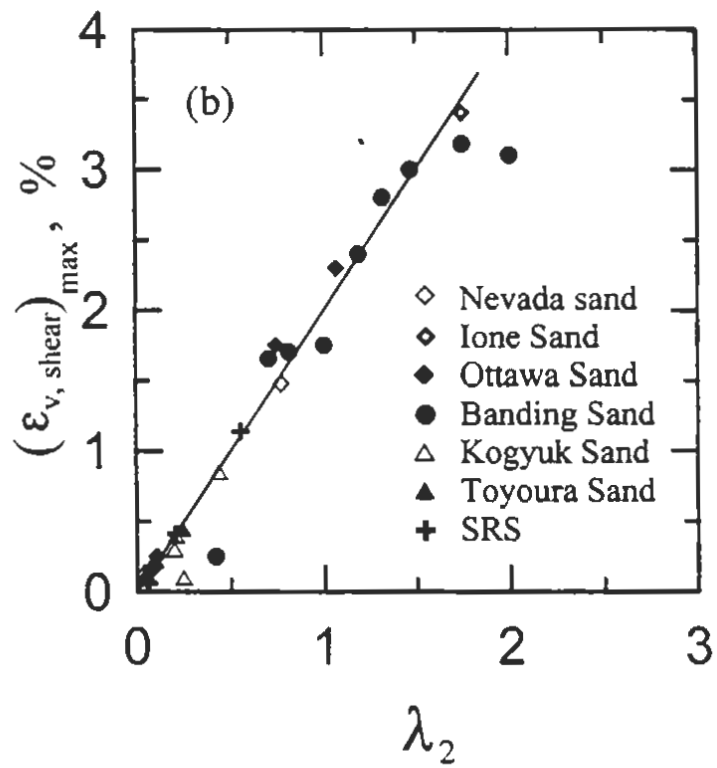
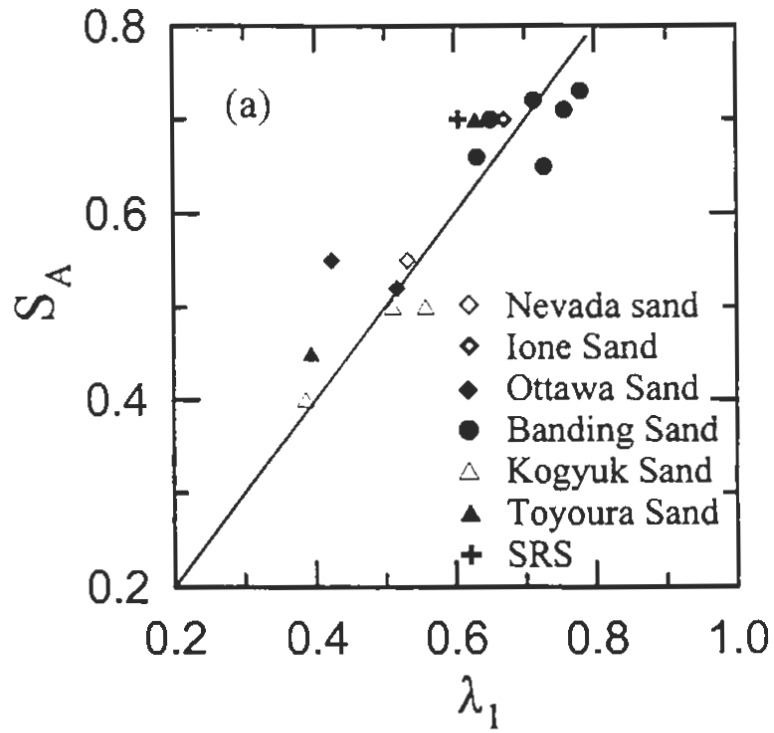


Fig. 4.5 Sand Properties vs. Axial and Volumetric Strains, and Slops at the Major Points on the Volumetric Strain Curve Due to Shear Stresses

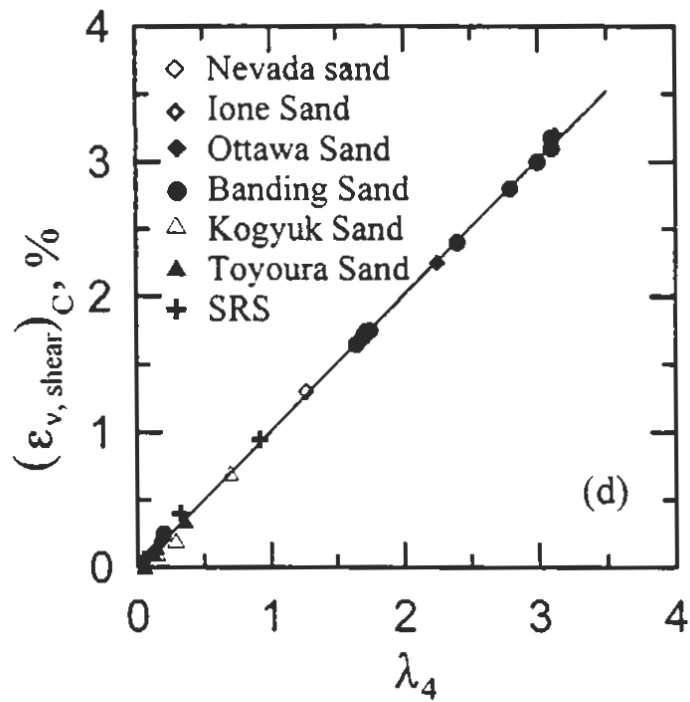
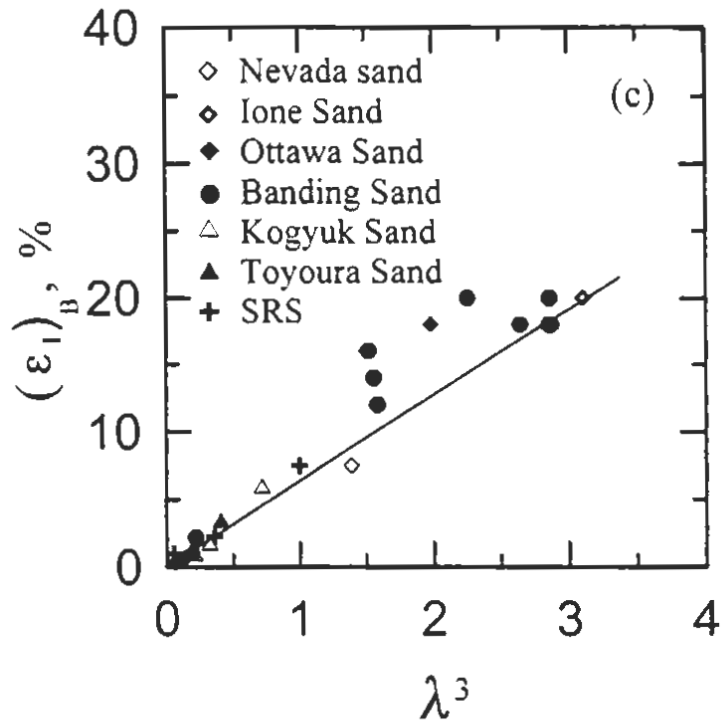


Fig. 4.5 Sand Properties vs. Axial and Volumetric Strains, and Slops at the Major Points on the Volumetric Strain Curve Due to Shear Stresses

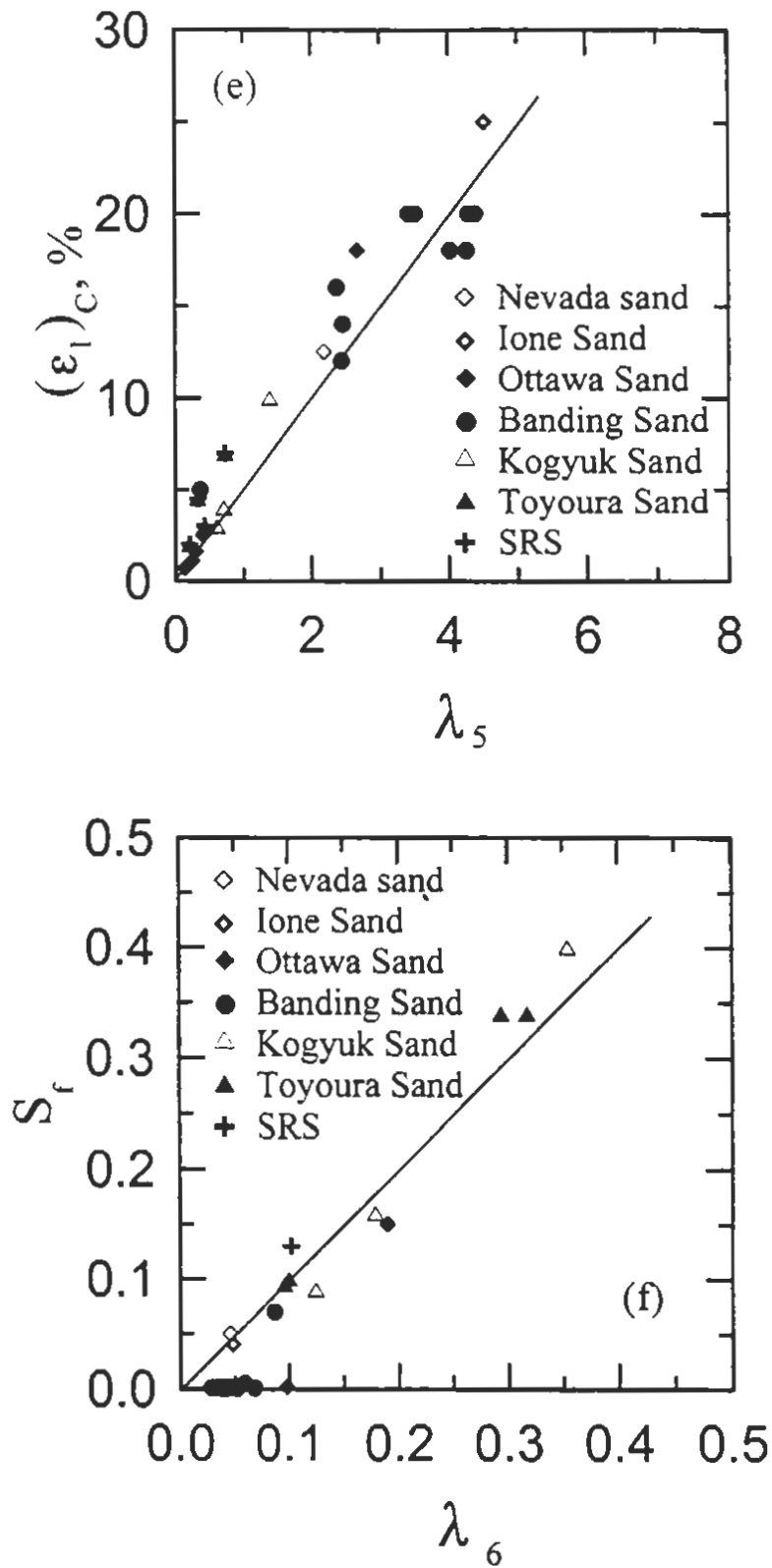


Fig. 4.5 Sand Properties vs. Axial and Volumetric Strains, and Slops at the Major Points on the Volumetric Strain Curve Due to Shear Stresses

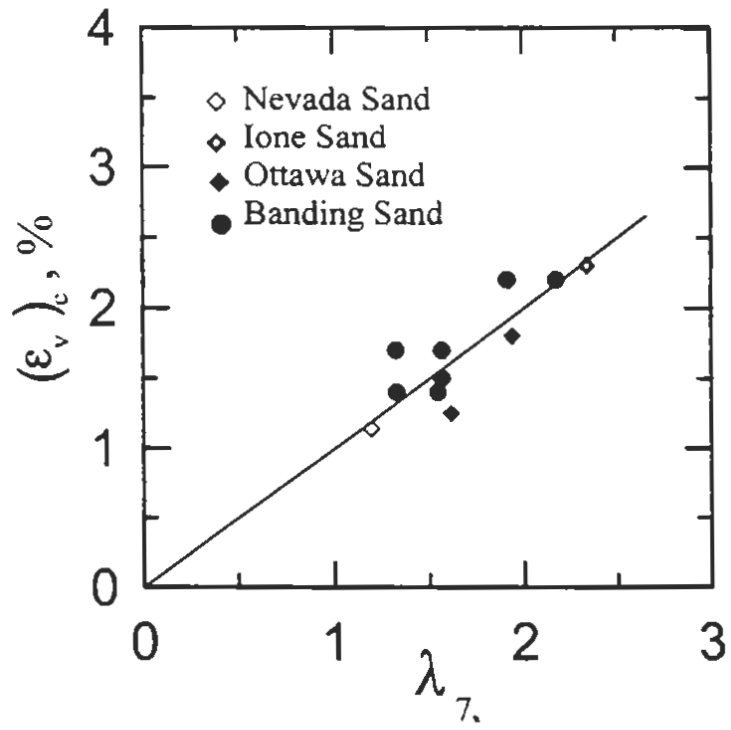


Fig. 4.6 Sand Properties vs. Isotropic Volumetric Strain at Consolidation Pressure

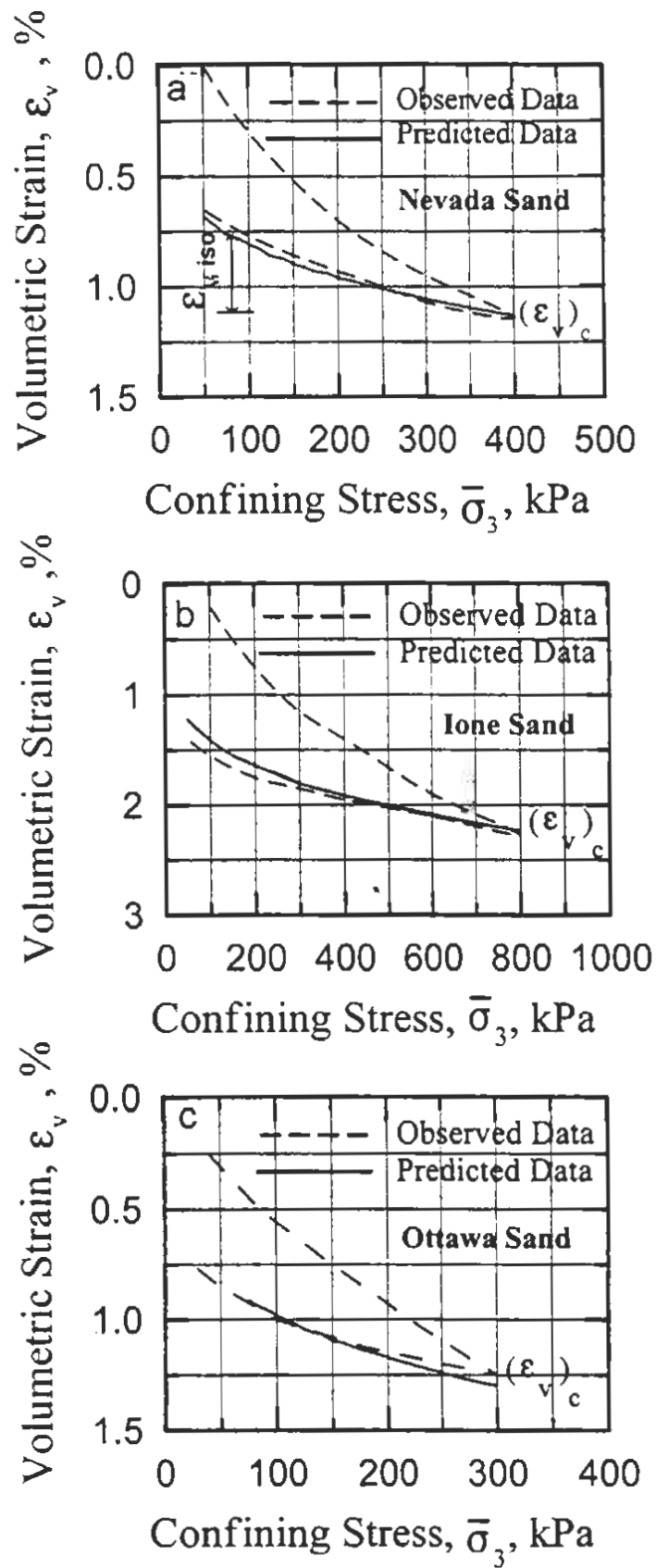


Fig. 4.7 Isotropic Consolidated-Rebounced Volumetric Change of Saturated Sands

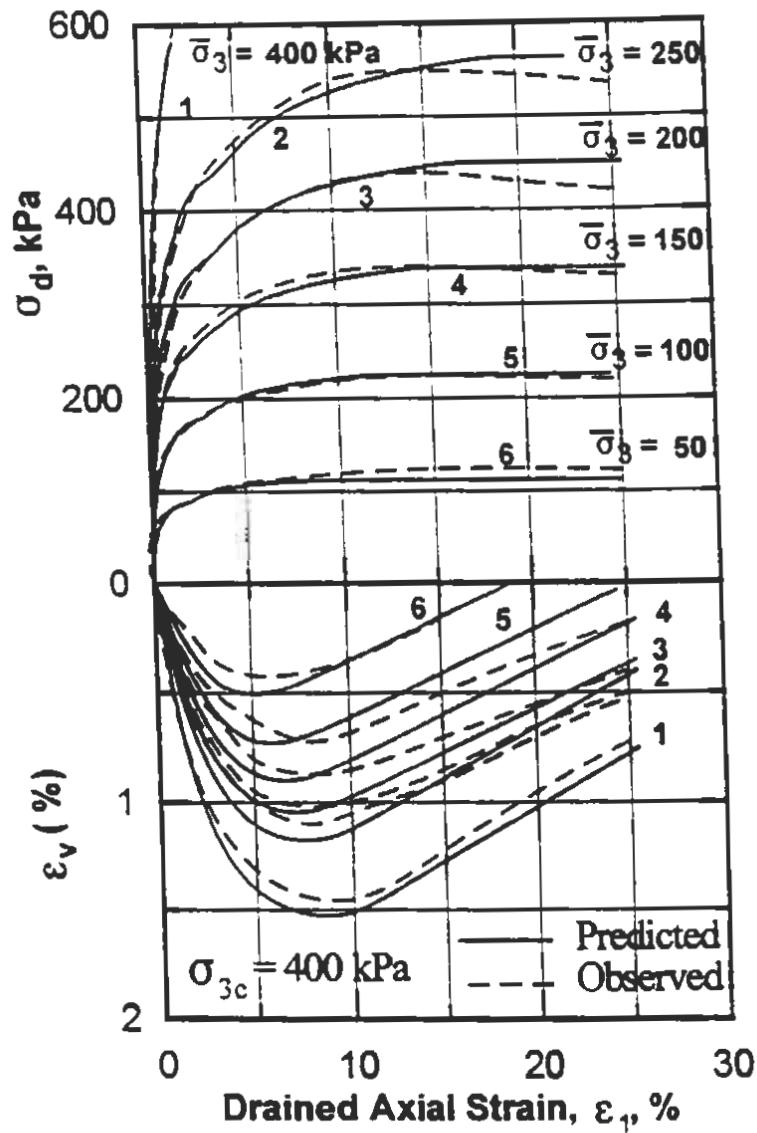


Fig. 4.8 Predicted and Observed Drained Response of Isotropically Consolidated and Overconsolidated Nevada Sand

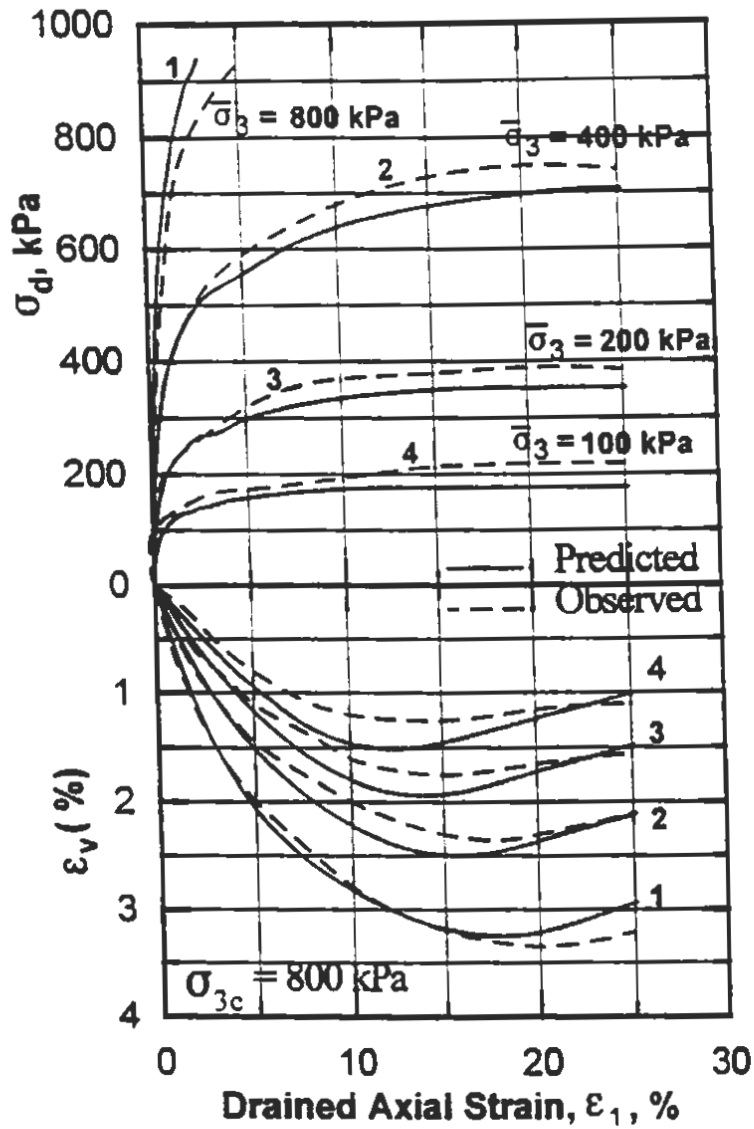


Fig. 4.9 Predicted and Observed Drained Response of Isotropically Consolidated and Overconsolidated Fine Sand

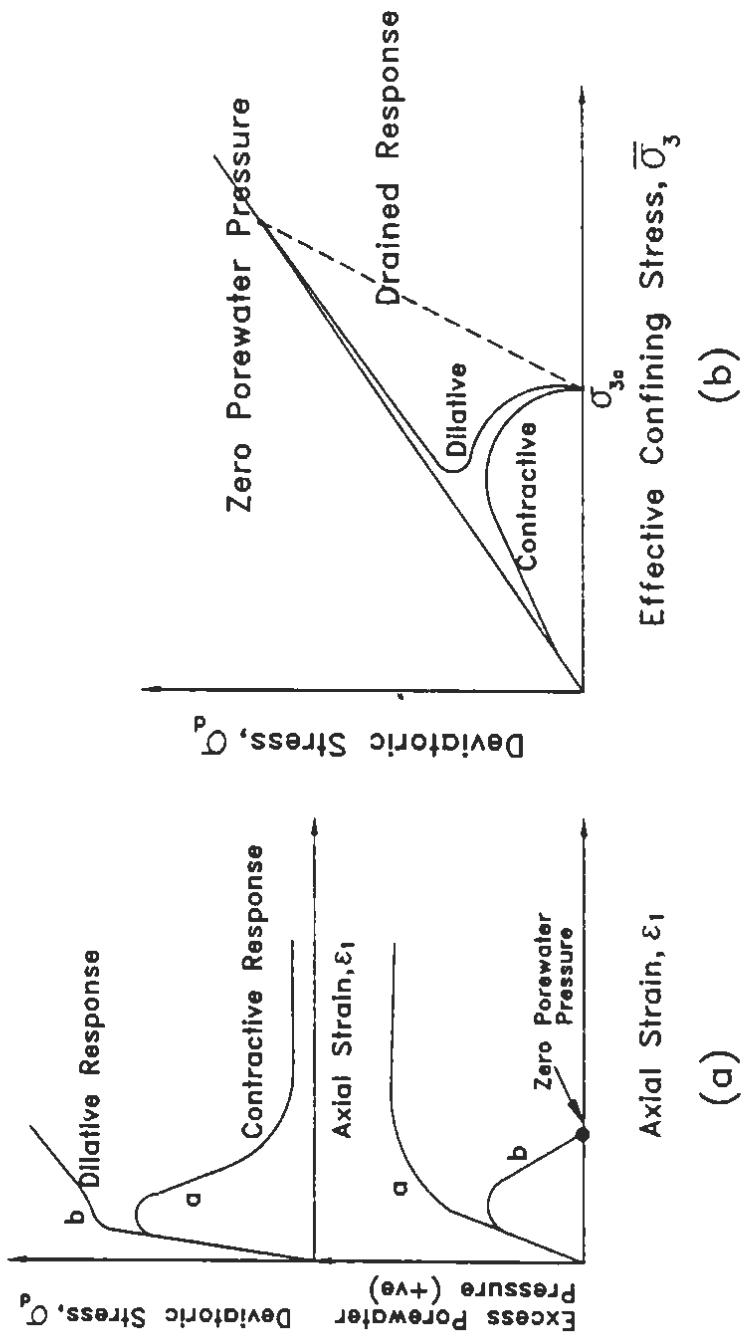


Fig. 4.10 The Excess Porewater Pressure with Undrained Response of Contractive and Dilative Sands

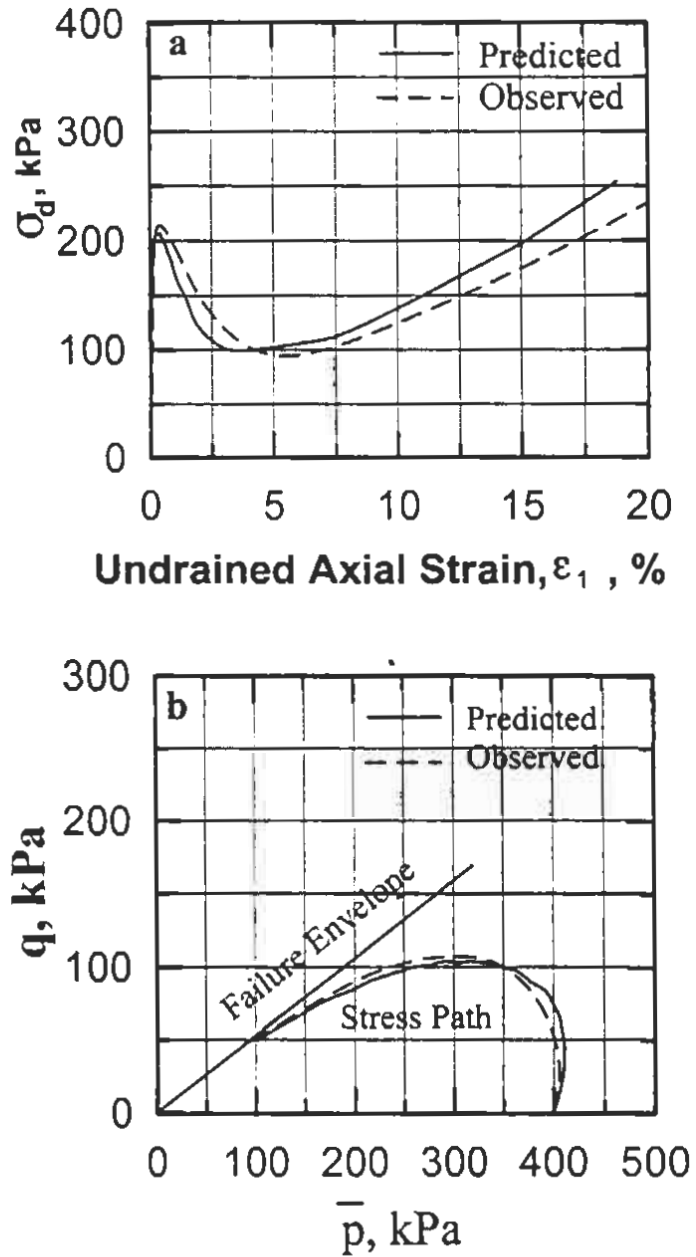


Fig. 4.11 Predicted and Observed Undrained Response of Nevada Sand

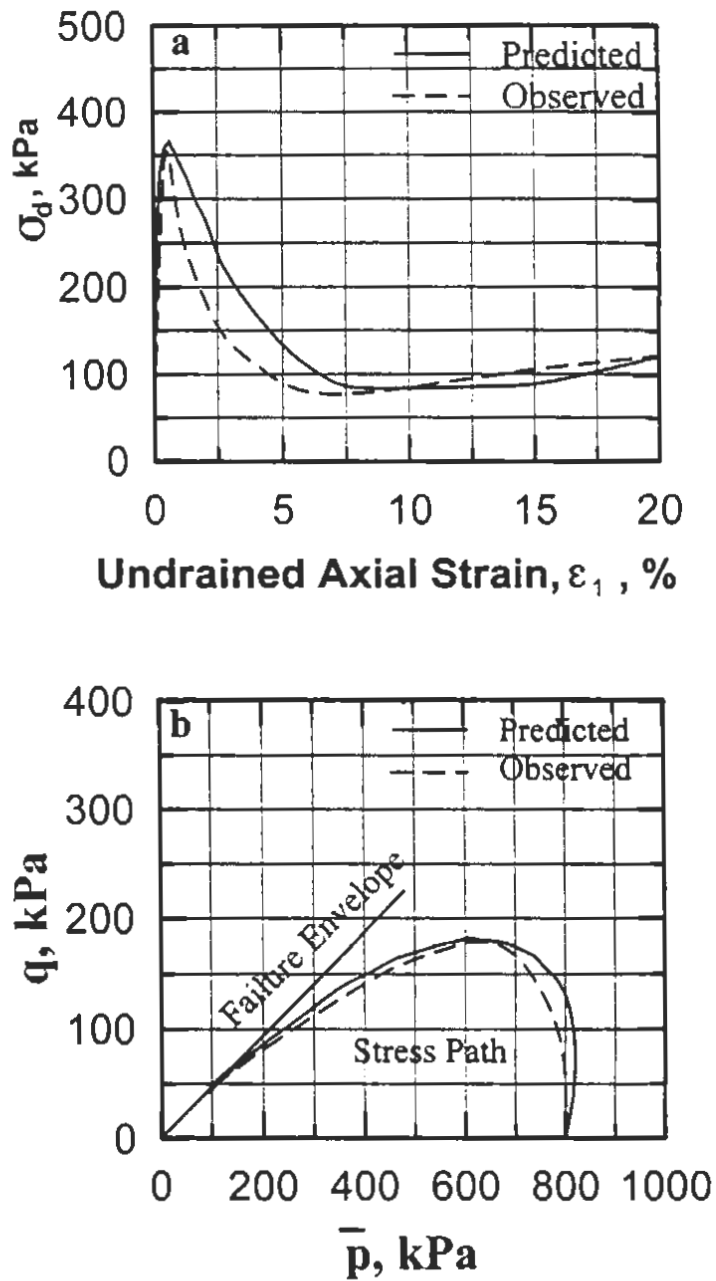


Fig. 4.12 Predicted and Observed Undrained Response of Ione Sand

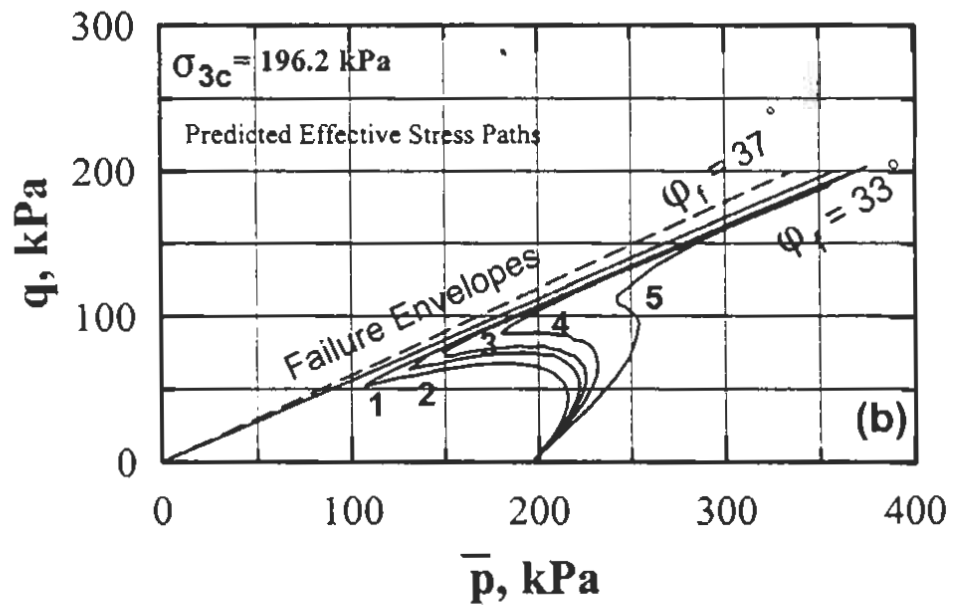
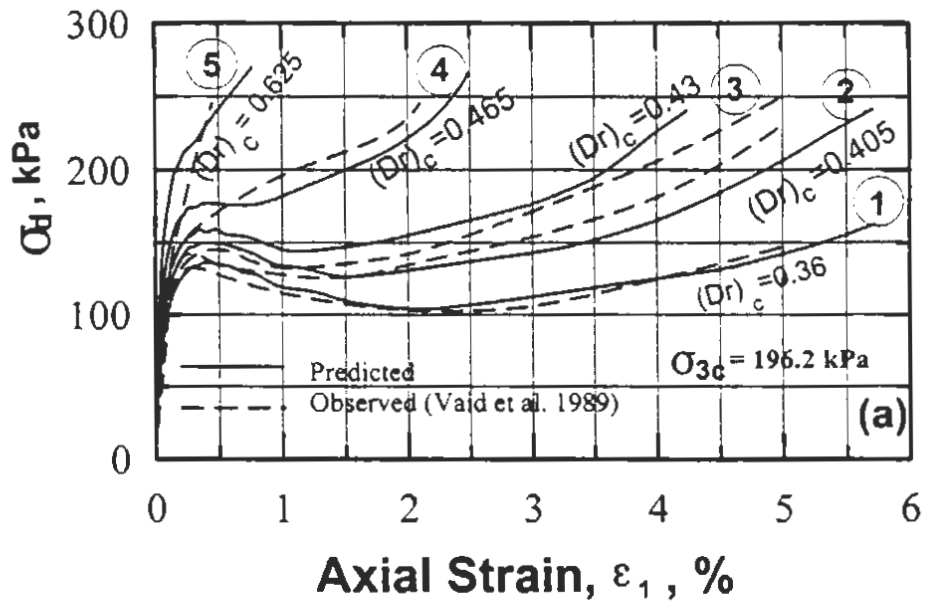


Fig. 4.13 Undrained Response of Ottawa Sand Under Monotonic Loading

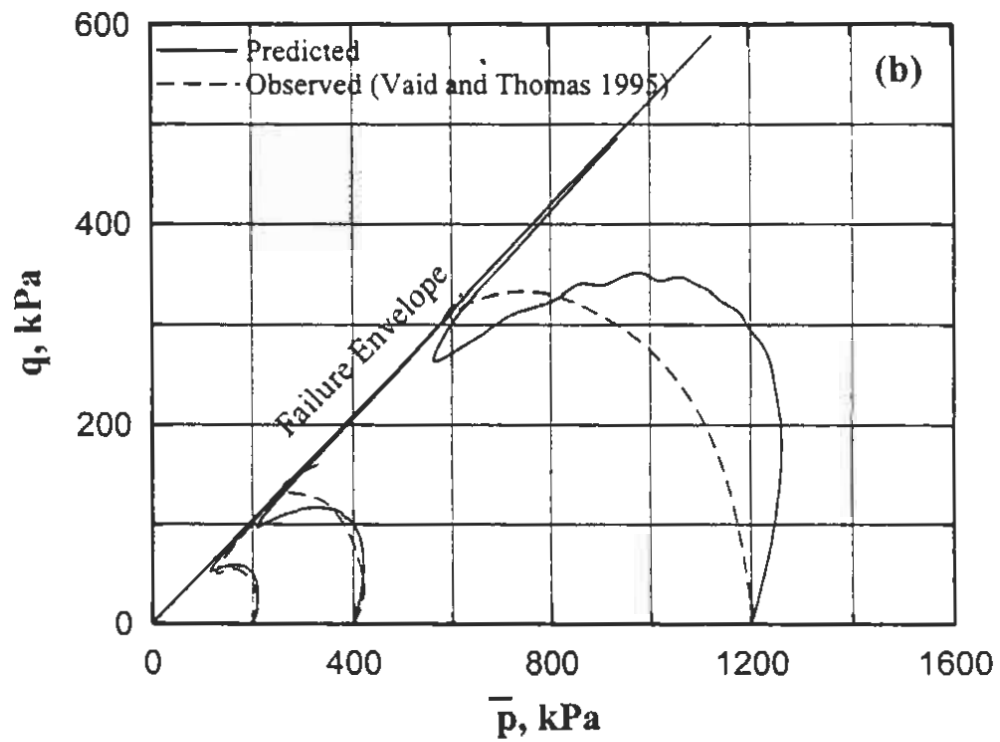
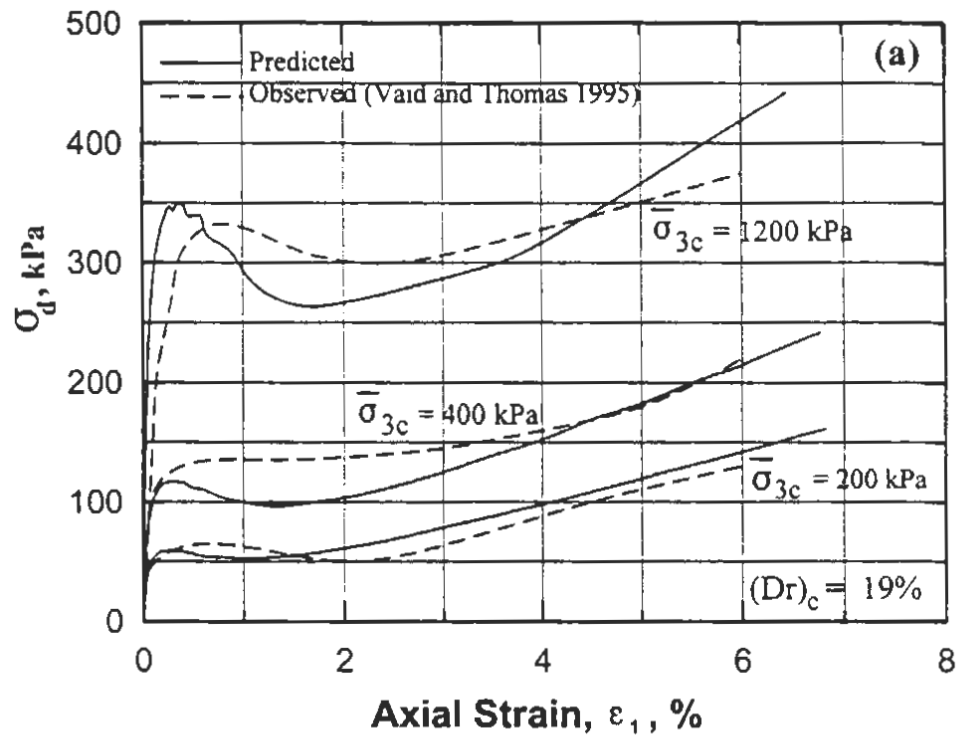


Fig. 4.14 Undrained Response of Ottawa Fraser River Sand Under Monotonic Loading (Vaid and Thomas 1995)

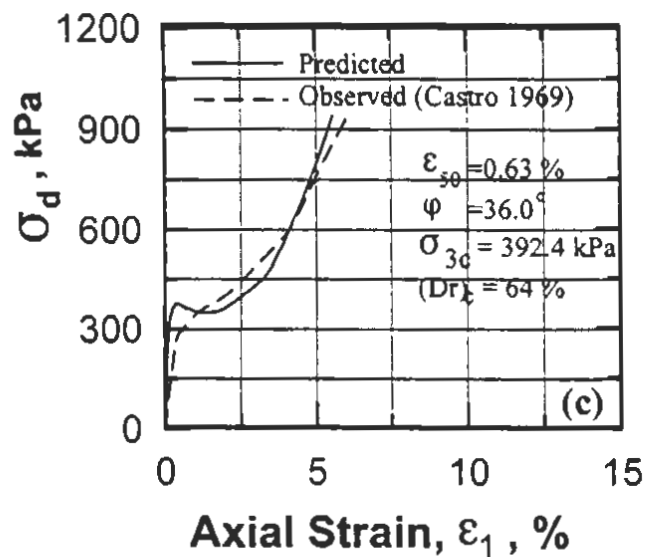
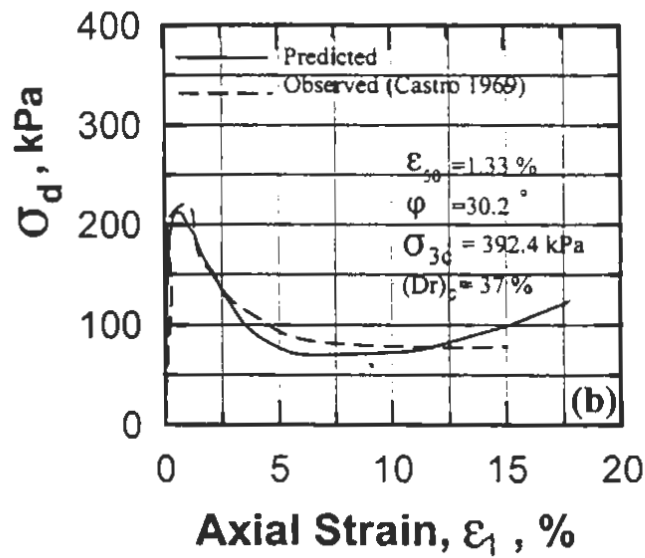
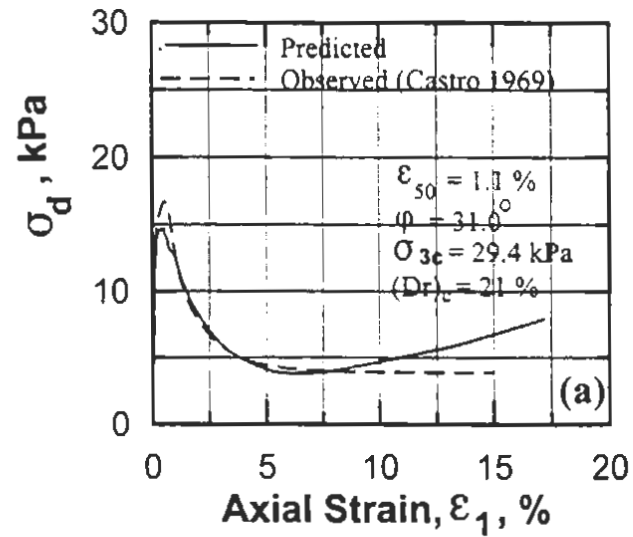


Fig. 4.15 Undrained Response of Banding Sand Under Monotonic Loading (Castro 1969)

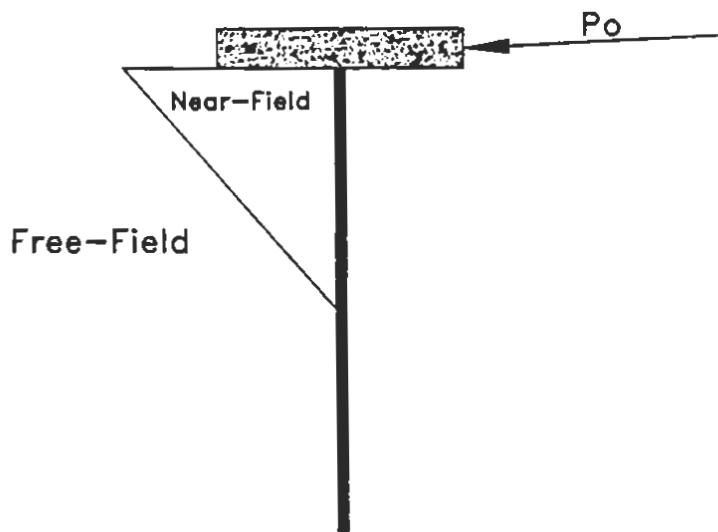


Fig. 5.1 Zones of Excess porewater pressures Around a laterally Loaded Pile

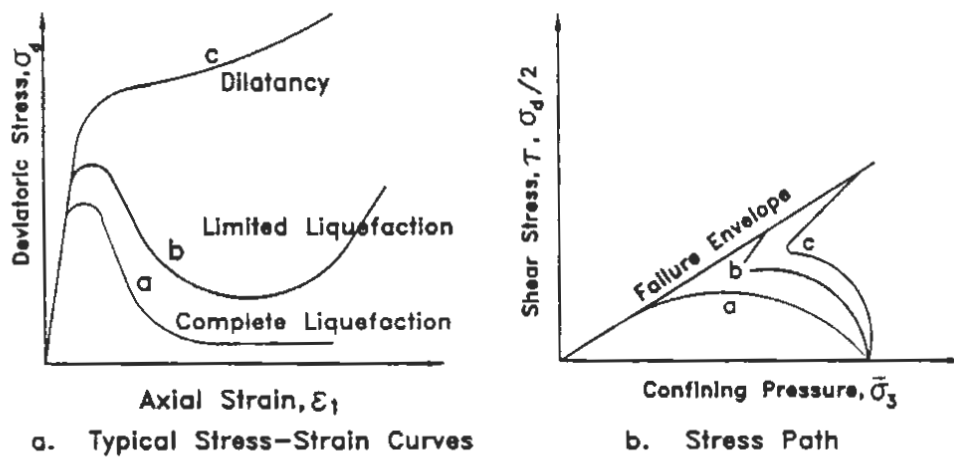


Fig. 5.2 Undrained Behavior of Saturated Sands Under Monotonic Loading

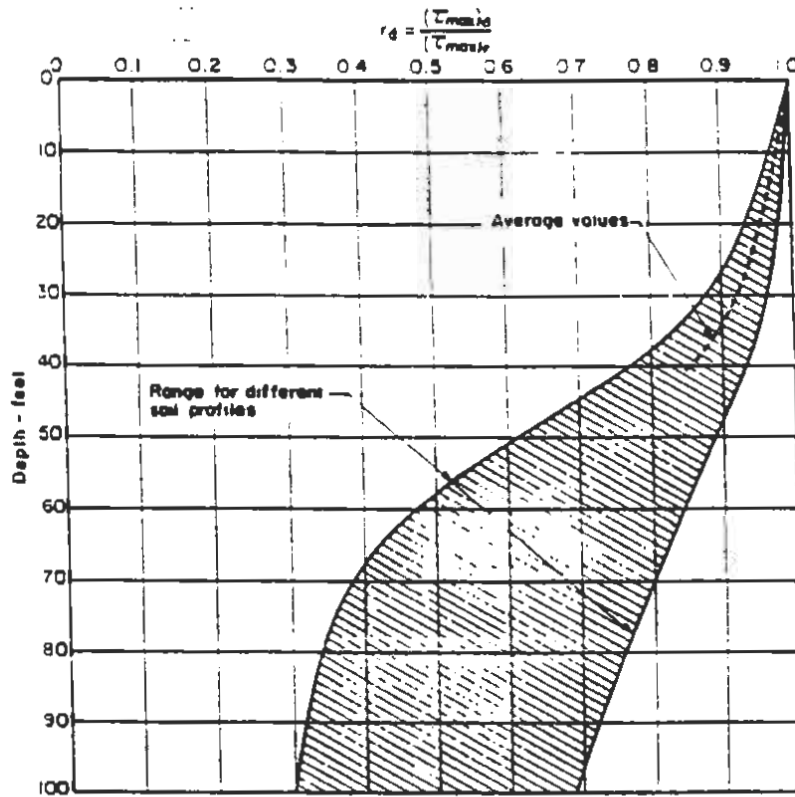


Fig. 5.3 Reduction factor (r_d) for Different Soil Profiles (Seed and Idriss 1971)

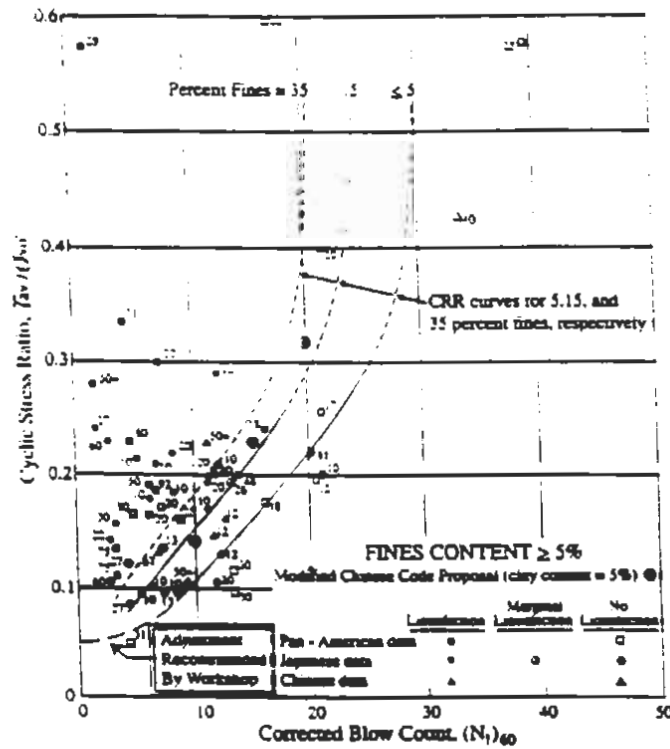


Fig. 5.4 Relationship Between Stress Ratio Causing liquefaction and $(N_1)_{60}$ Values for Silty Sands For $M = 7.5$ Earthquake (Modified from Seed et al. 1985 by Youd and Idriss 1997)

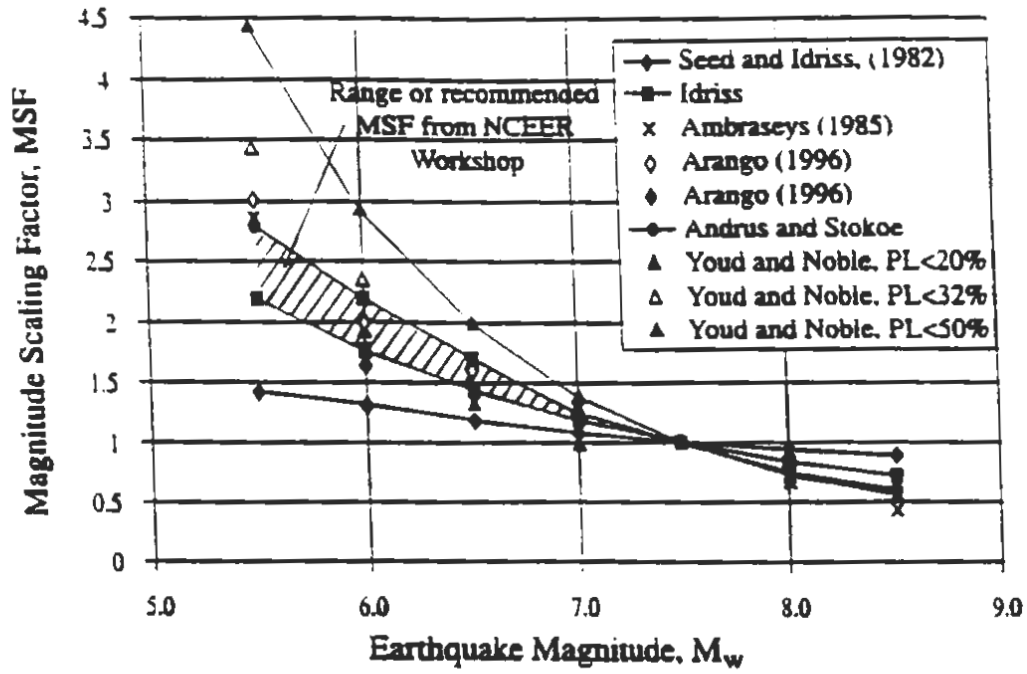


Fig. 5.5 Magnitude Scaling Factors Derived by Various Investigators (Youd and Idriss 1997)

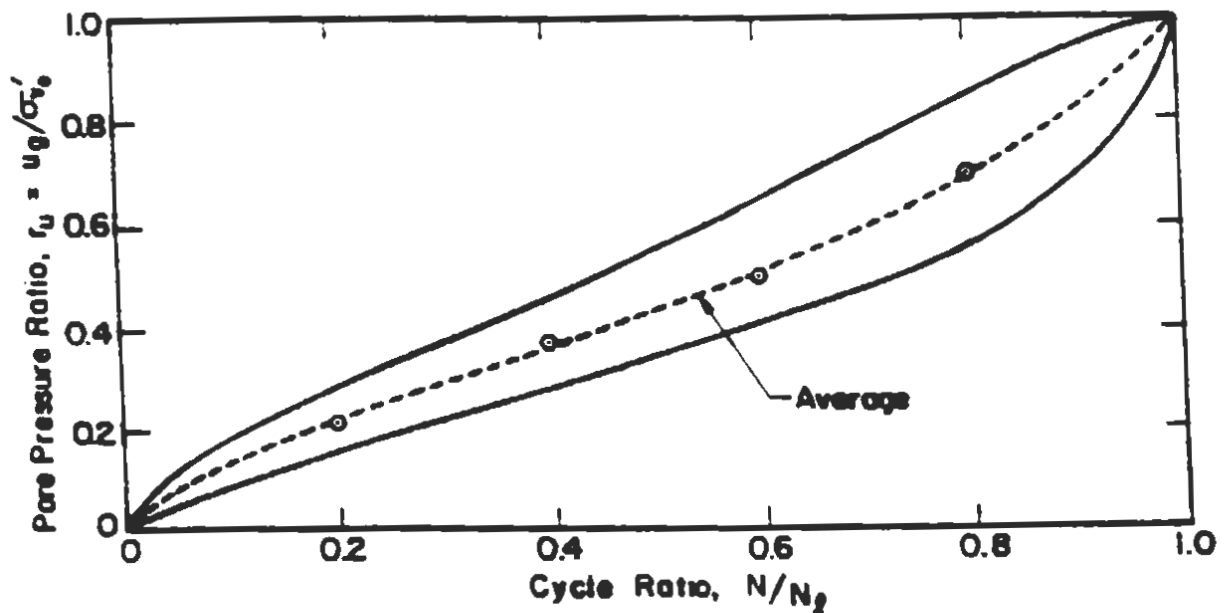


Fig. 5.6 Porewater Pressure Ratio due to Cyclic Simple Shear Tests (DeAlba et al. 1976)

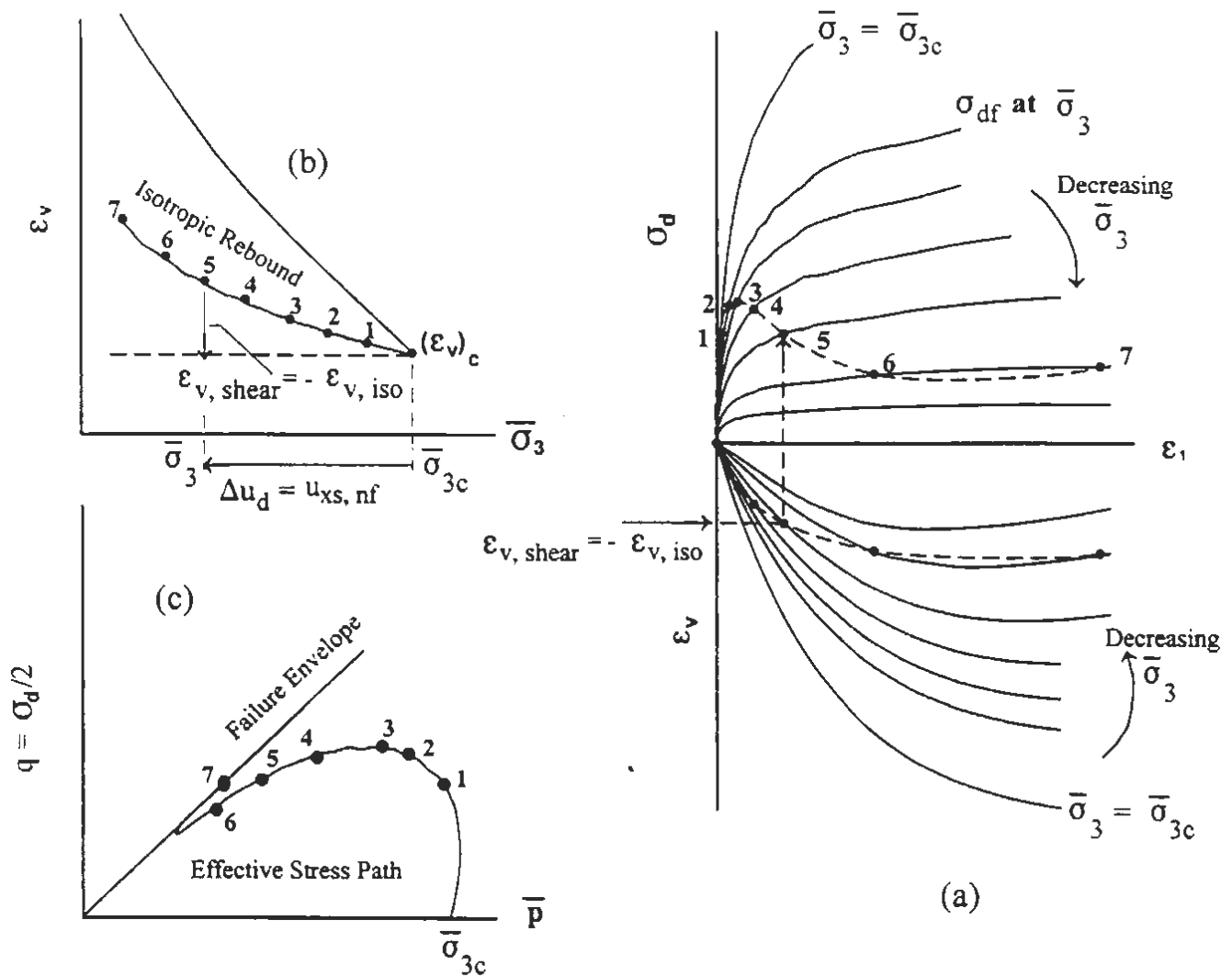
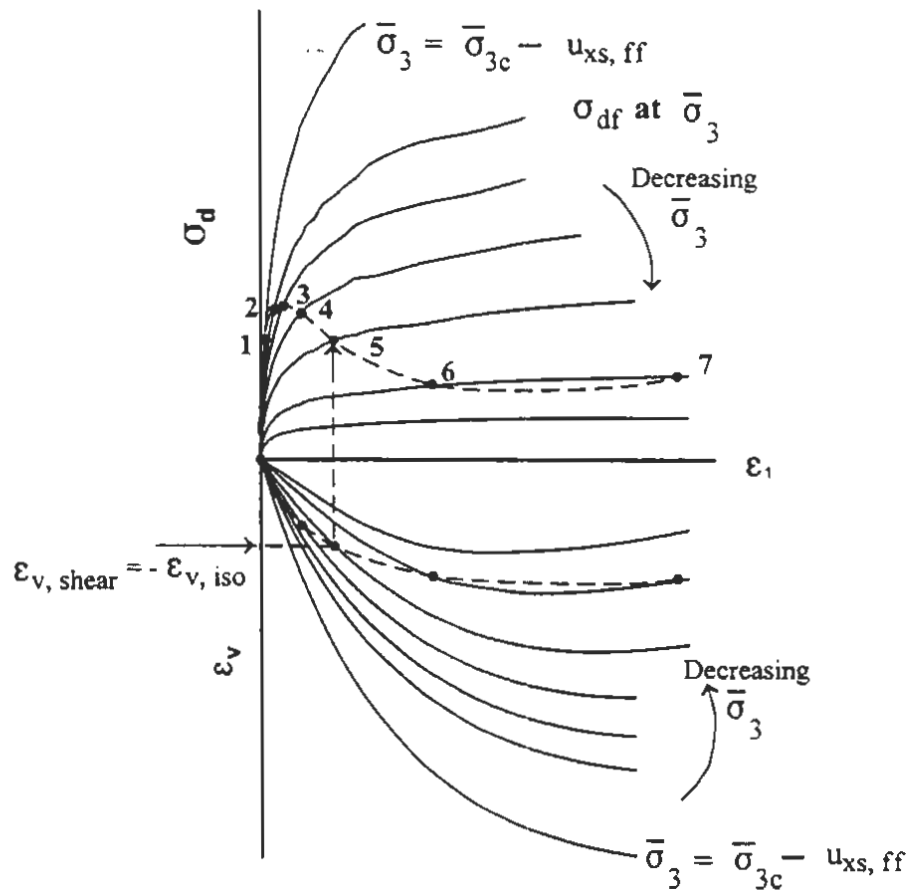


Fig.5. 7 Interrelationships Among (a) Drained and Undrained Stress-Strain Behavior (b) Isotropic Consolidation Rebound, and (c) Effective Stress Path (Norris et al. 1997)



(a)

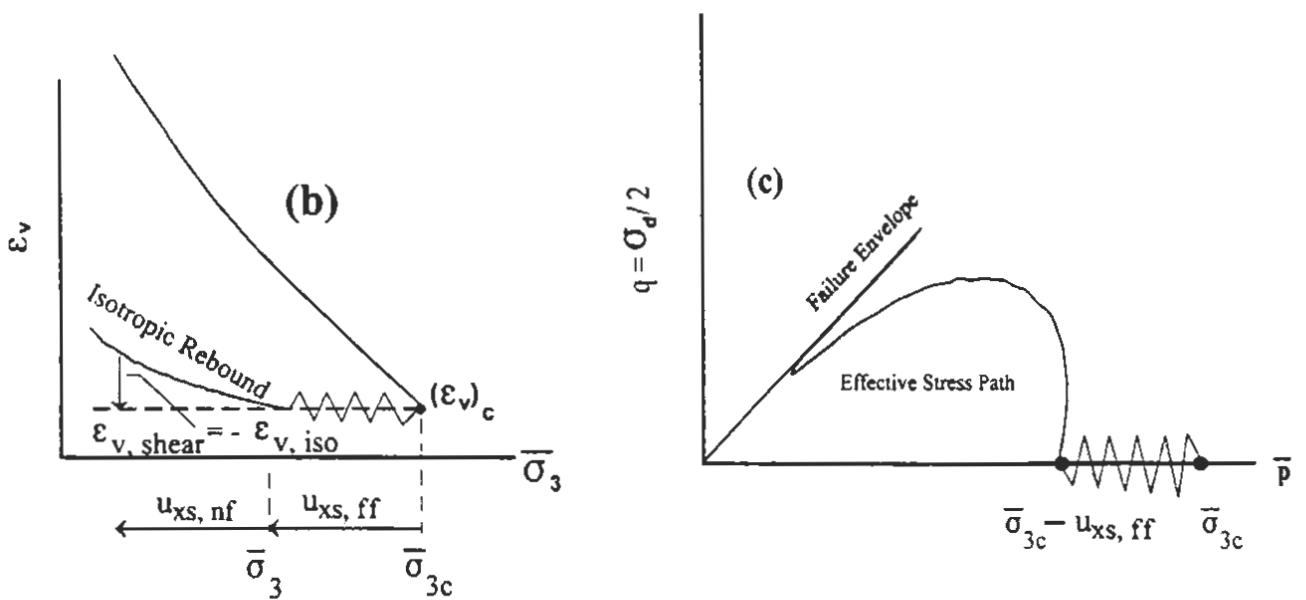


Fig. 5.8 Effect of Excess Porewater Pressure ($u_{xs, ff} + u_{xs, nf}$) on the Undrained Behavior
 (a) Isotropic Consolidation Rebound
 (b) Effective Stress Path

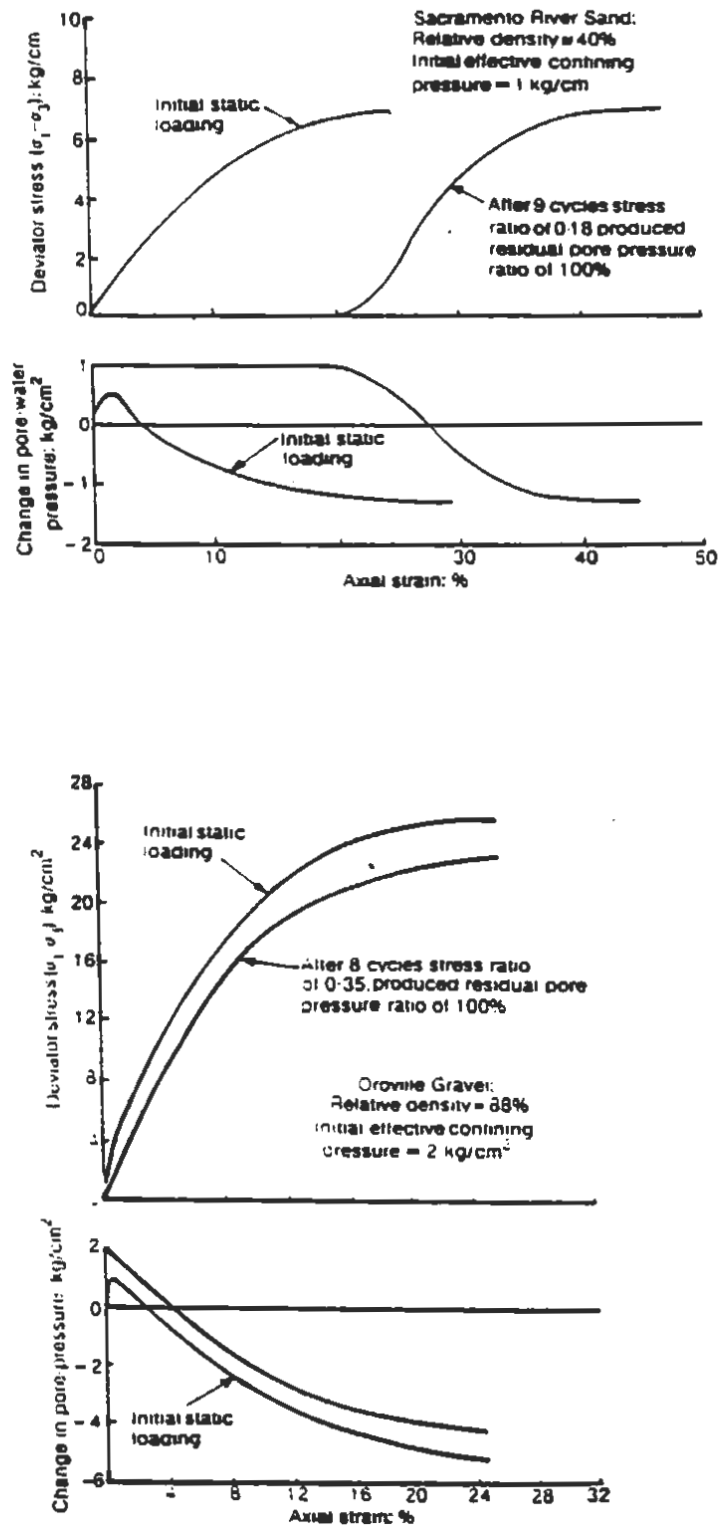


Fig. 5.9 Effect of Cyclic Loading on Undrained Stress-Strain Relationship for
 (a) Sacramento River Sand at Relative Density of 40%
 (b) Orville Gravel at Relative Density of 88% (Seed 1979)

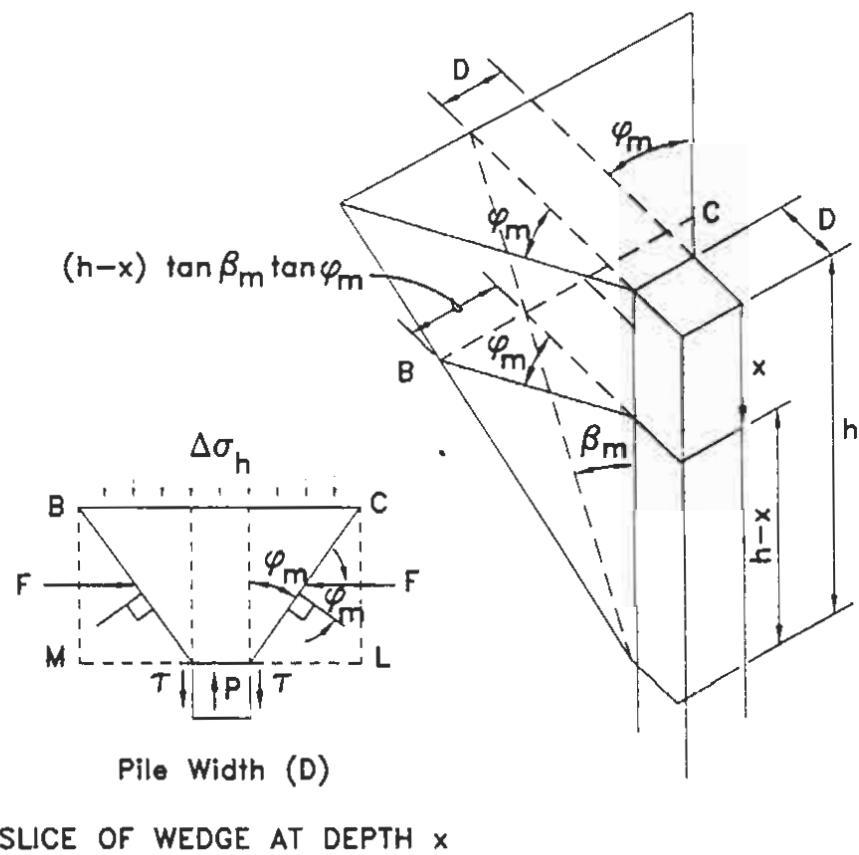


Fig. 5.10 The Basic Strain Wedge in Uniform Soil (Ashour et al. 1998)

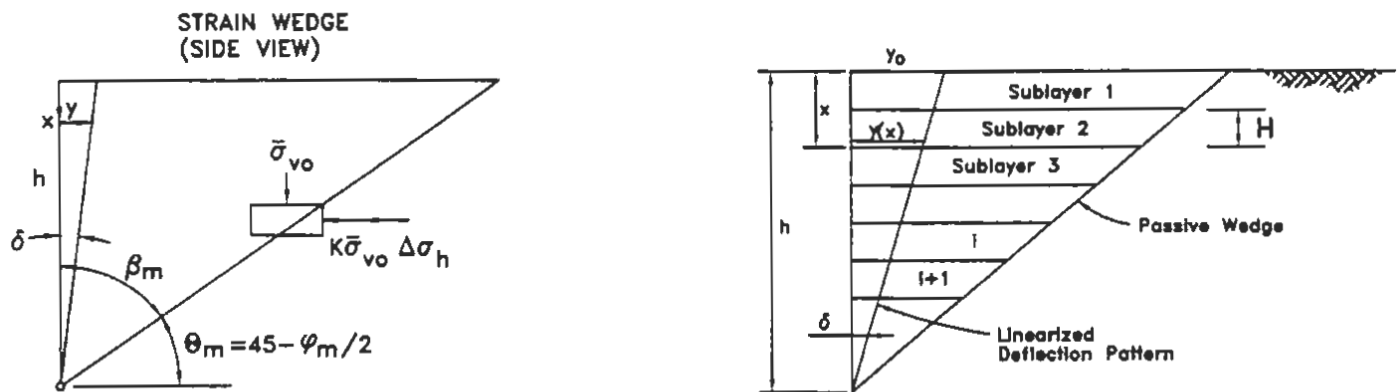


Fig. 5.11 Deflection Pattern and Soil Sublayers in the Strain Wedge Model

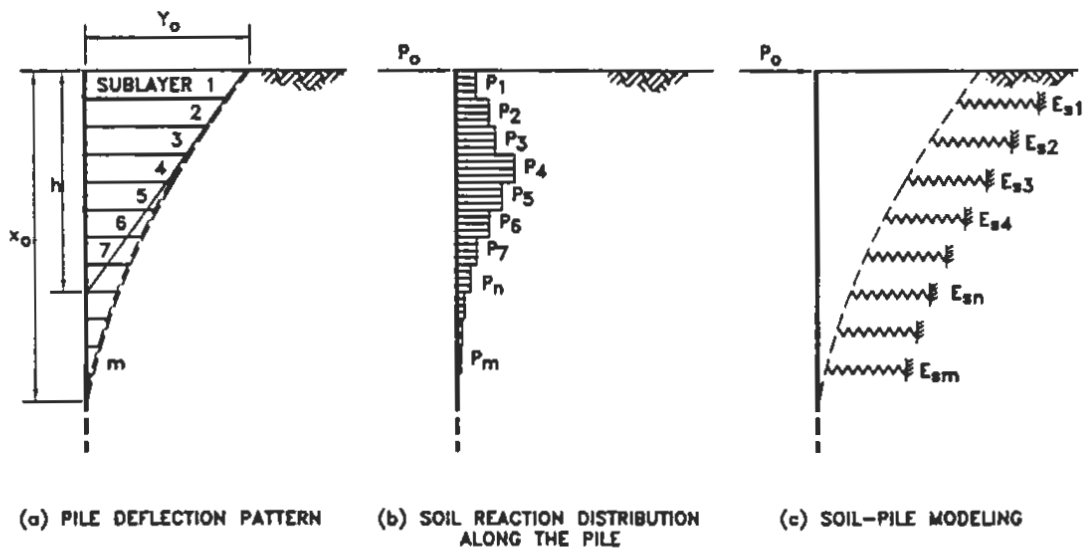


Fig. 5.12 A Laterally Loaded Pile Represented by a Beam on Elastic Foundation

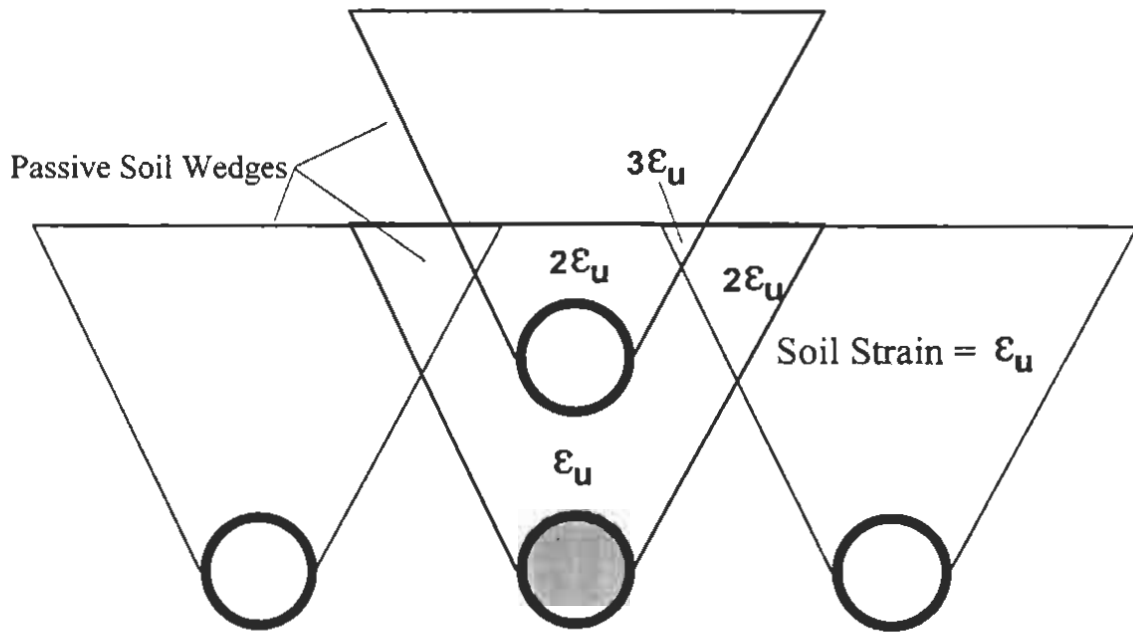


Fig. 5.13 Overlap Shear Zones in a Sand Sublayer Under Undrained Conditions Due to Pile Interference

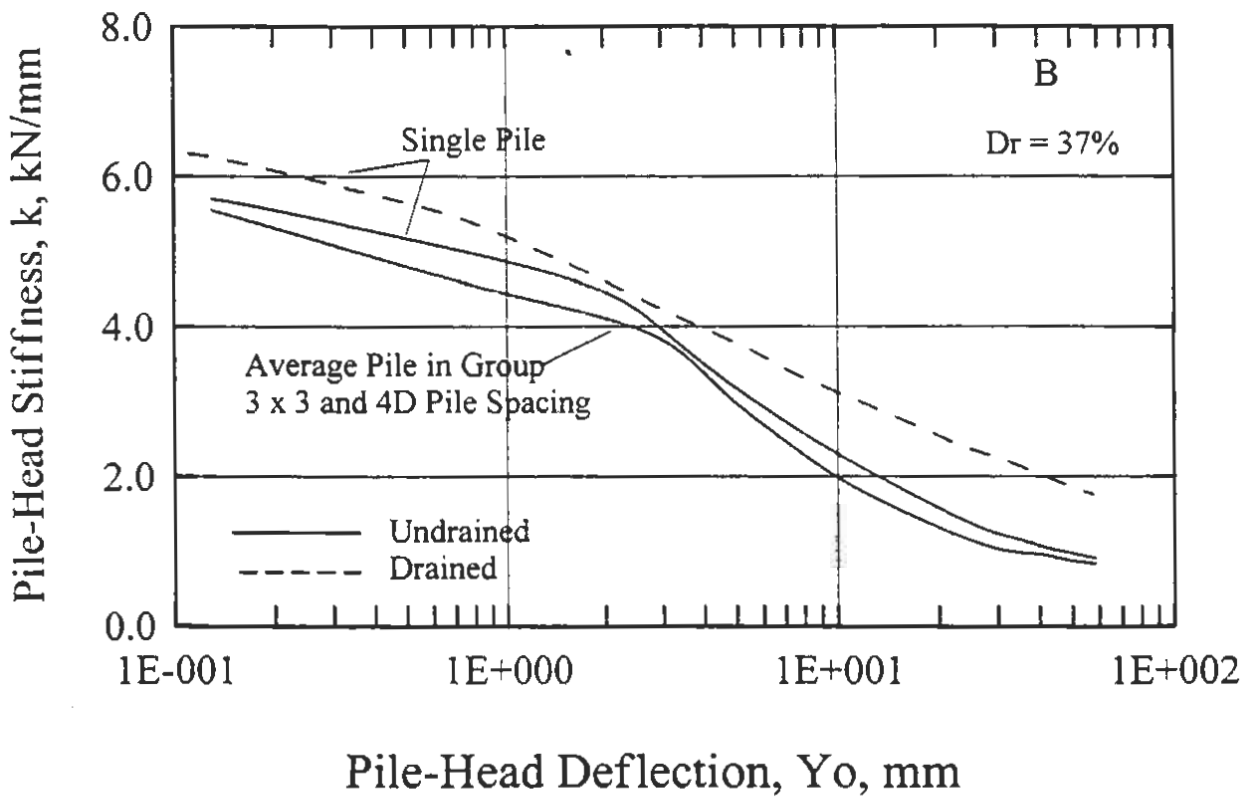
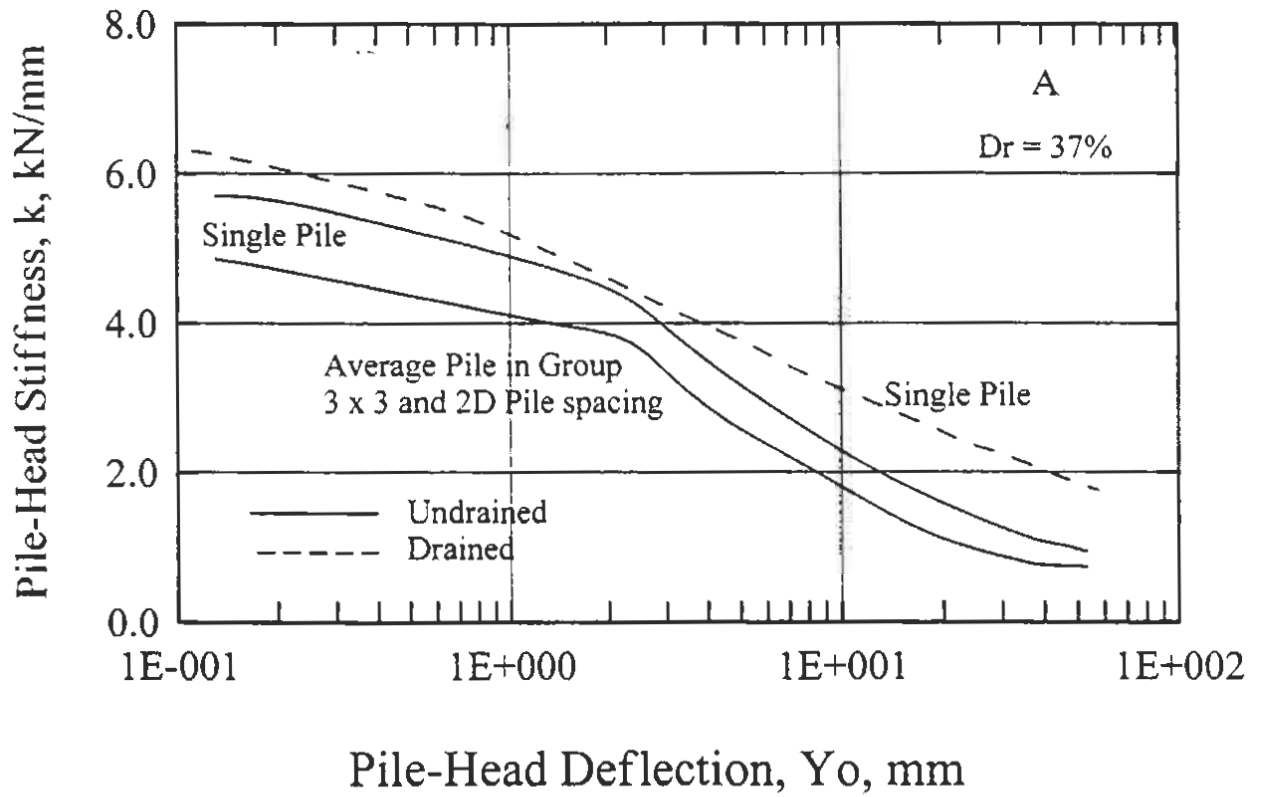


Fig. 5.14 Pile-Head Stiffness of a Single Pile and an Average Pile in a Group Driven in Loose Sand

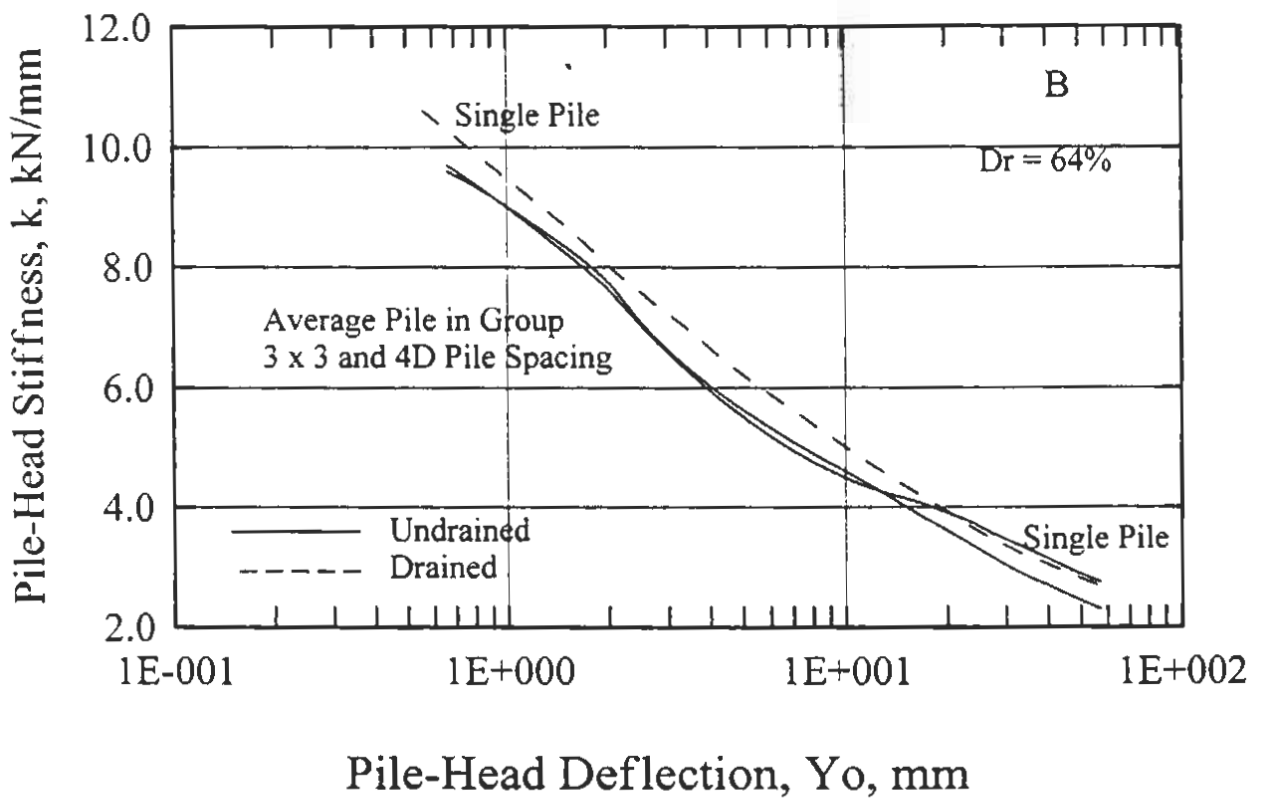
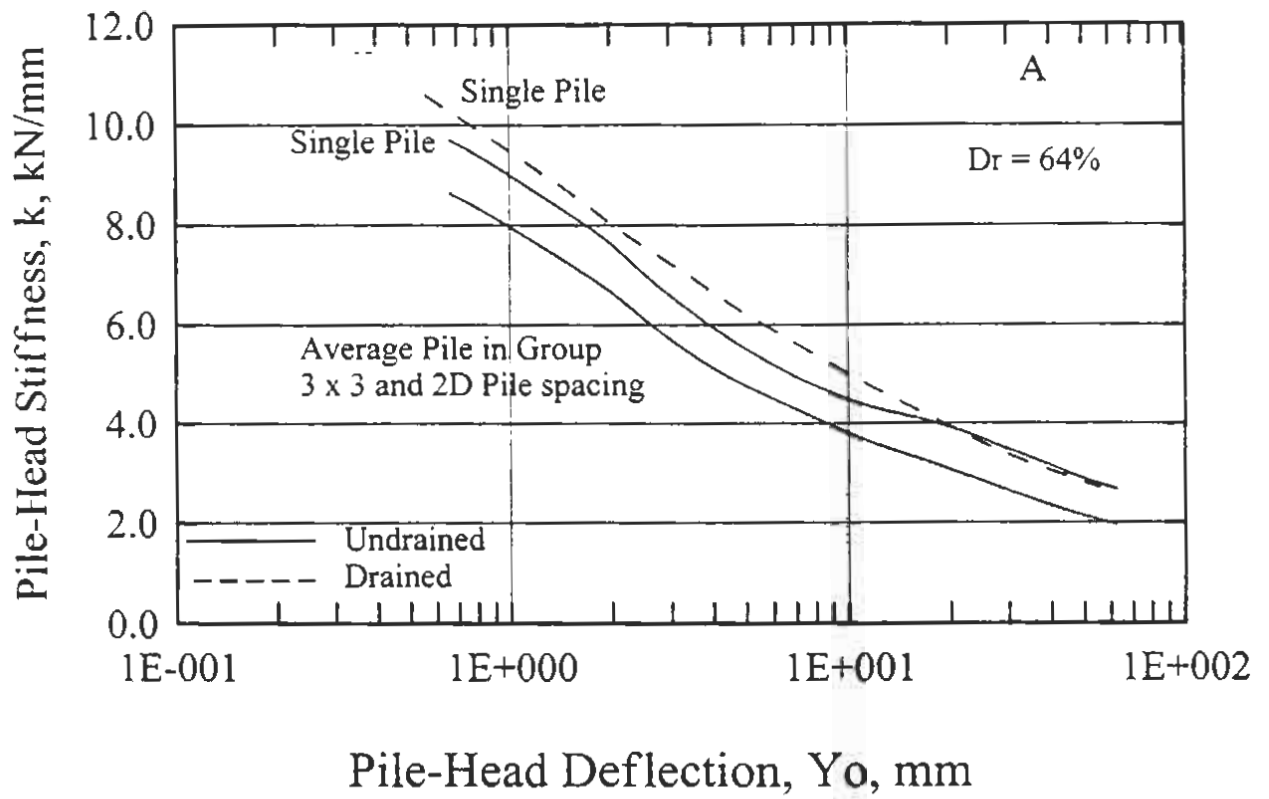


Fig. 5.15 Pile-Head Stiffness of a Single Pile and an Average Pile in a Group Driven in Medium Dense Sand

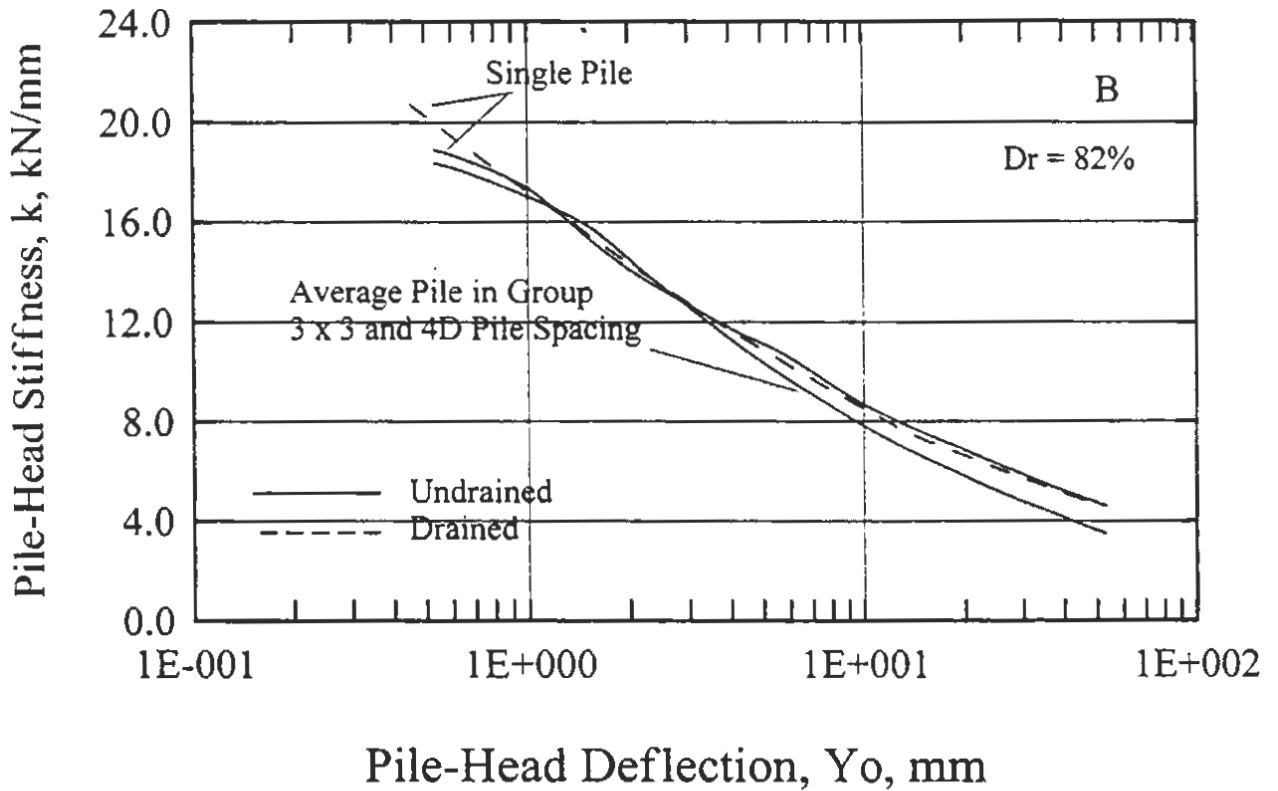
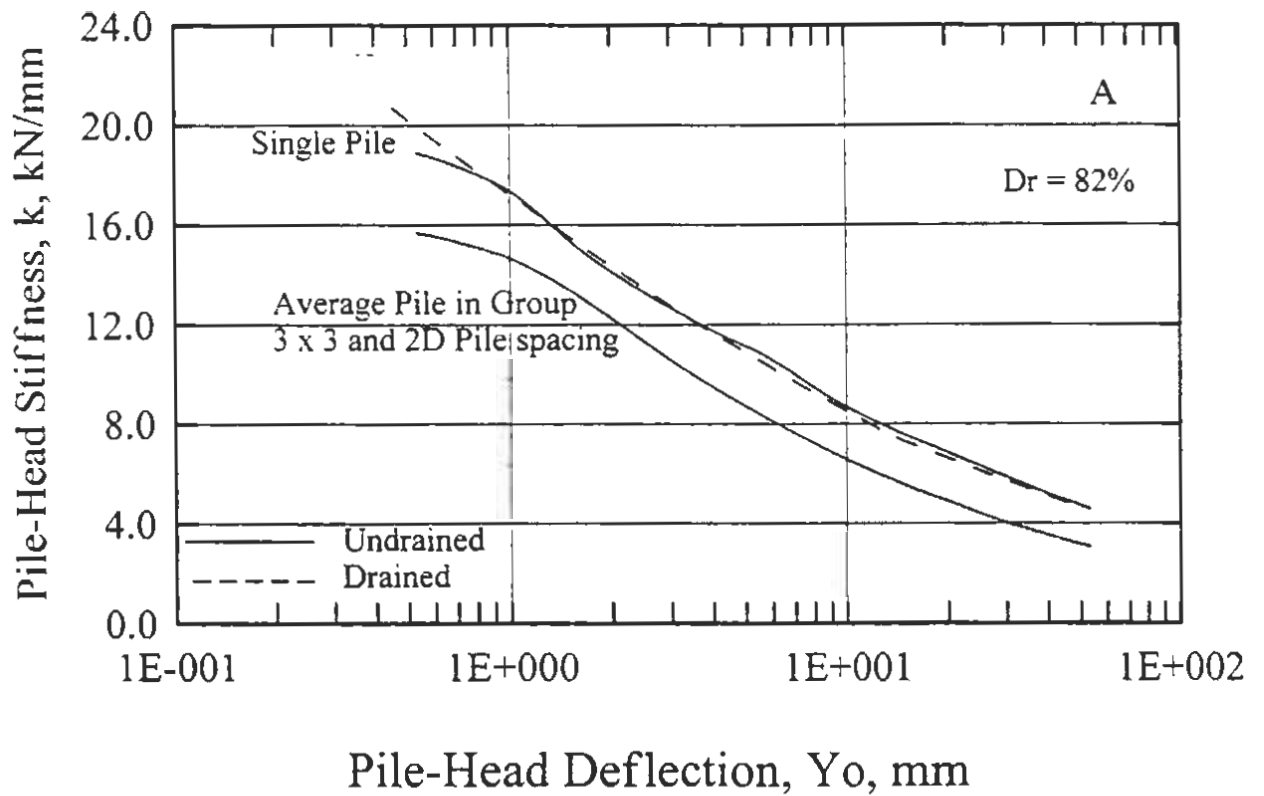


Fig. 5.16 Pile-Head Stiffness of a Single Pile and an Average Pile in a Group Driven in Dense Sand

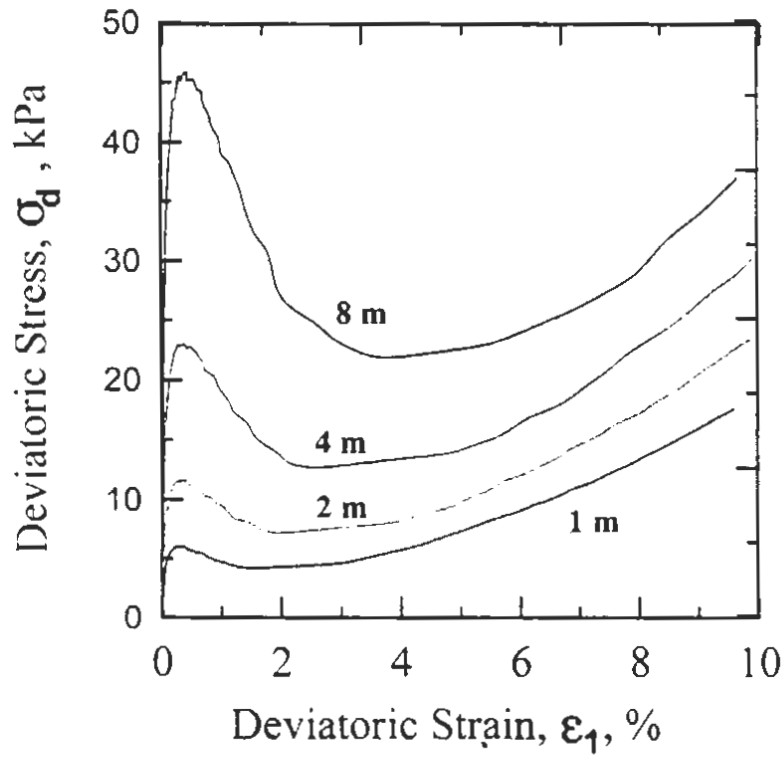


Fig. 6.1 Undrained Stress-Strain Behavior in Banding Sand at Different Depths

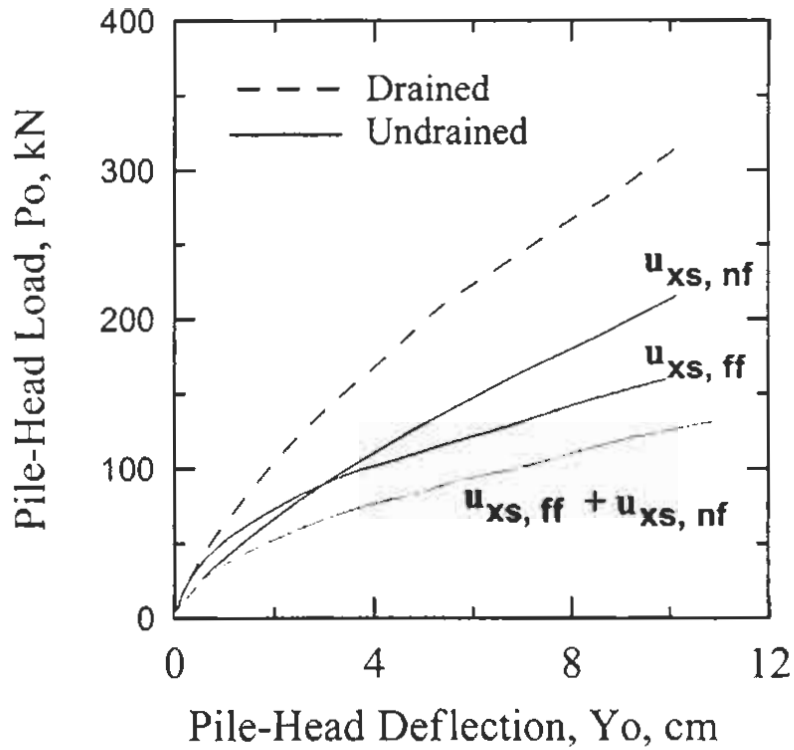


Fig. 6.2 Drained and Undrained Response of Pile Head

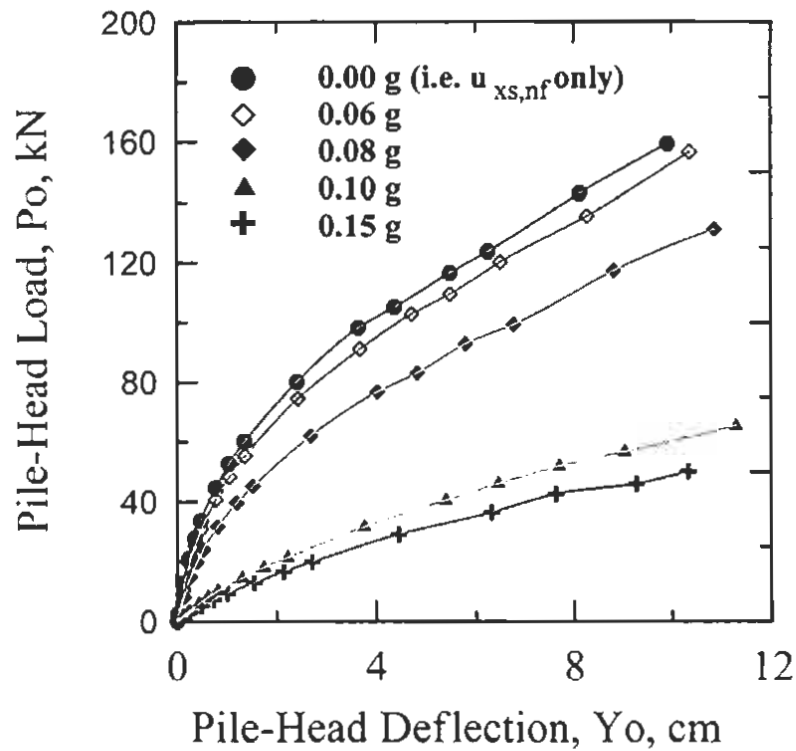


Fig. 6.3 Pile-Head Response in Baniding Sand Under Undrained Conditions ($u_{xs, nf} + u_{xs, ff}$)

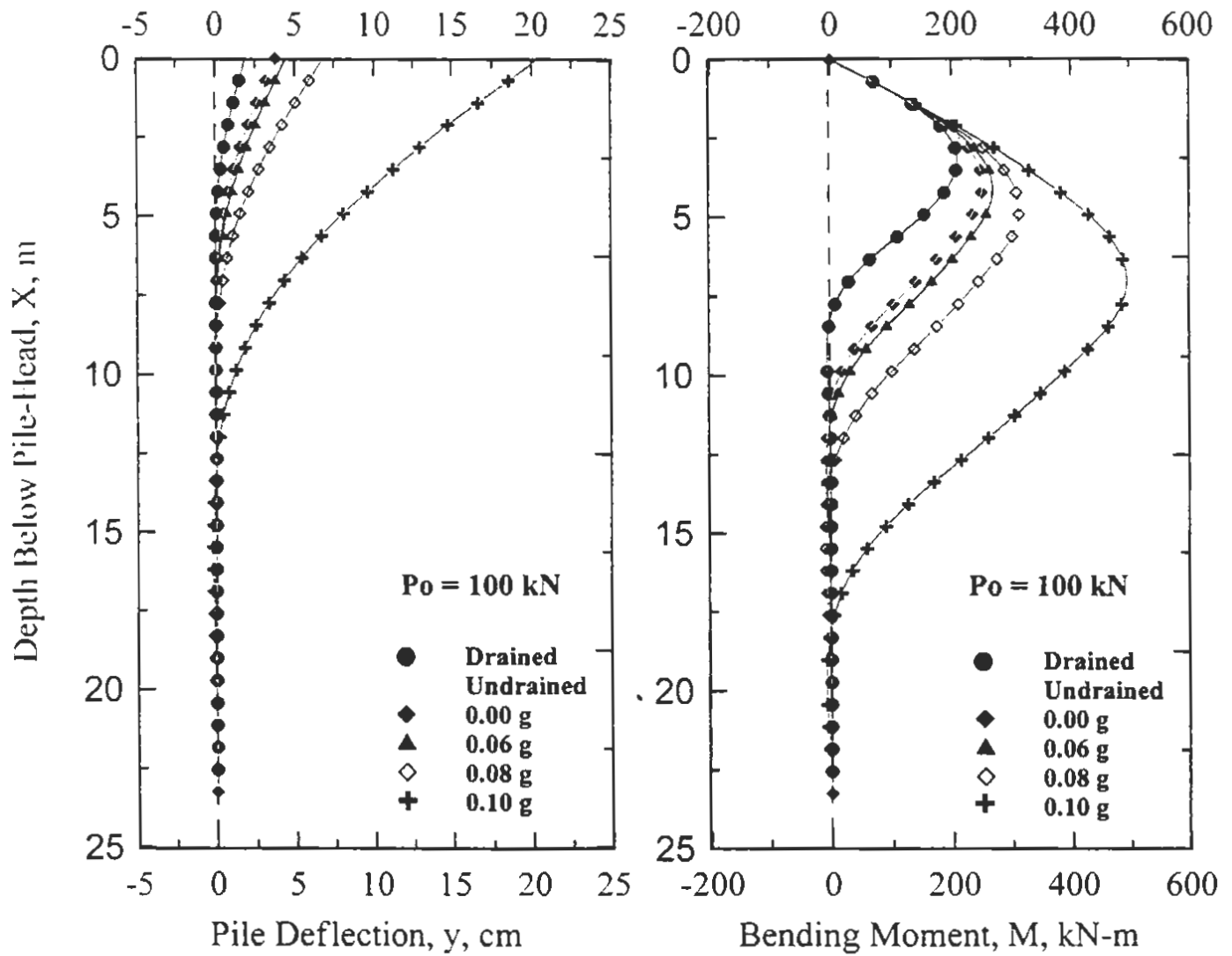


Fig. 6.4 Pile Response in Sand Under Drained and Undrained Conditions ($U_{hf} + U_{ff}$)

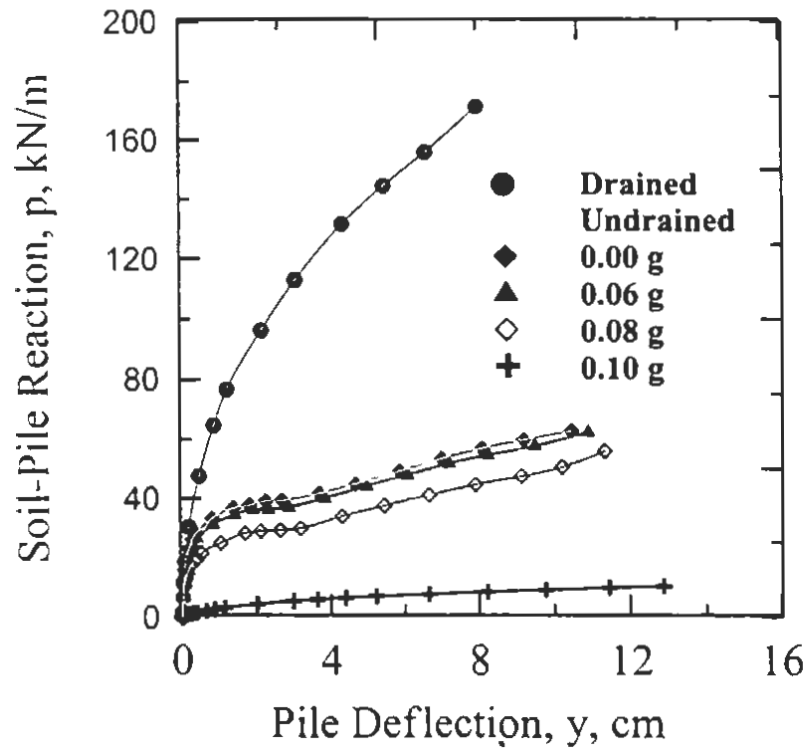


Fig. 6.5 Drained and Undrained p - y Curves at 3m Depth in Banding Sand

Brigham Young University 388 Clyde Building Provo, Utah 84604 Telephone: (801) 378-2811 Fax: (801) 378-4449		Boring No: BH-4 Logged By: JDL Date Started: 10/16/98 Date Finished: 10/16/98		Elevation (ft): D/H Contractor: Plicher Drilling Method: Rotary Wash		Sheet 1 of 2 Treasure Island San Francisco, California BYUUCSD - Research		OTHER DATA AND REMARKS	
Single Pile		Location		Sample Data		Atterberg Limits		Moisture Content %	
Material Description		Graphic Log		Blows/ft		Soil Classification		Dry Density (pcf)	
Brown, med, Fine-Grained Sand w/ Shells		Depth (ft)		Recovery (inches)		USCS		Liquid Limits	
Black, Saturated, Fine-Grained Silty Sand		Water Level		Type		AASHTO		Plastic Limits	
Dark Clay, Saturated Fine-Medium Sand w/ Some Sil		SPT		Number				Passing #200 Sieve (%)	
		SPT		Location					
		SPT		S-1					
		SPT		S-2					
		SPT		S-3					
		SPT		S-4					
		SPT		S-5					
		SPT		S-6					
		SPT		S-7					
		SPT		S-8					
		SPT		S-9					
		SPT		S-10					
		SPT		S-11					
		SPT		S-12					
		SPT		S-13					
		SPT		S-14					
		SPT		S-15					
		SPT		S-16					
		SPT		S-17					
		SPT		S-18					
		SPT		S-19					
		SPT		S-20					
		SPT		S-21					
		SPT		S-22					
		SPT		S-23					
		SPT		S-24					
		SPT		S-25					
		SPT		S-26					
		SPT		S-27					
		SPT		S-28					
		SPT		S-29					
		SPT		S-30					
		SPT		S-31					
		SPT		S-32					
		SPT		S-33					
		SPT		S-34					
		SPT		S-35					
		SPT		S-36					
		SPT		S-37					
		SPT		S-38					
		SPT		S-39					
		SPT		S-40					
		SPT		S-41					
		SPT		S-42					
		SPT		S-43					
		SPT		S-44					
		SPT		S-45					
		SPT		S-46					
		SPT		S-47					
		SPT		S-48					
		SPT		S-49					
		SPT		S-50					
		SPT		S-51					
		SPT		S-52					
		SPT		S-53					
		SPT		S-54					
		SPT		S-55					
		SPT		S-56					
		SPT		S-57					
		SPT		S-58					
		SPT		S-59					
		SPT		S-60					
		SPT		S-61					
		SPT		S-62					
		SPT		S-63					
		SPT		S-64					
		SPT		S-65					
		SPT		S-66					
		SPT		S-67					
		SPT		S-68					
		SPT		S-69					
		SPT		S-70					
		SPT		S-71					
		SPT		S-72					
		SPT		S-73					
		SPT		S-74					
		SPT		S-75					
		SPT		S-76					
		SPT		S-77					
		SPT		S-78					
		SPT		S-79					
		SPT		S-80					
		SPT		S-81					
		SPT		S-82					
		SPT		S-83					
		SPT		S-84					
		SPT		S-85					
		SPT		S-86					
		SPT		S-87					
		SPT		S-88					
		SPT		S-89					
		SPT		S-90					
		SPT		S-91					
		SPT		S-92					
		SPT		S-93					
		SPT		S-94					
		SPT		S-95					
		SPT		S-96					
		SPT		S-97					
		SPT		S-98					
		SPT		S-99					
		SPT		S-100					
		SPT		S-101					
		SPT		S-102					
		SPT		S-103					
		SPT		S-104					
		SPT		S-105					
		SPT		S-106					
		SPT		S-107					
		SPT		S-108					
		SPT		S-109					
		SPT		S-110					
		SPT		S-111					
		SPT		S-112					
		SPT		S-113					
		SPT		S-114					
		SPT		S-115					
		SPT		S-116					
		SPT		S-117					
		SPT		S-118					
		SPT		S-119					
		SPT		S-120					
		SPT		S-121					
		SPT		S-122					
		SPT		S-123					
		SPT		S-124					
		SPT		S-125					
		SPT		S-126					
		SPT		S-127					
		SPT		S-128					
		SPT		S-129					
		SPT		S-130					
		SPT		S-131					
		SPT		S-132					
		SPT		S-133					
		SPT		S-134					
		SPT		S-135					
		SPT		S-136					
		SPT		S-137					
		SPT		S-138					
		SPT		S-139					
		SPT		S-140					
		SPT		S-141					
		SPT		S-142					
		SPT		S-143					
		SPT		S-144					
		SPT		S-145					
		SPT		S-146					
		SPT		S-147					
		SPT		S-148					
		SPT		S-149					
		SPT		S-150					
		SPT		S-151					
		SPT		S-152					
		SPT		S-153					
		SPT		S-154					
		SPT		S-155					
		SPT		S-156					
		SPT		S-157					
		SPT		S-158					
		SPT		S-159					
		SPT		S-160					
		SPT		S-161					
		SPT		S-162					
		SPT		S-163					
		SPT		S-164					
		SPT		S-165					
		SPT		S-166					
		SPT		S-167					
		SPT		S-168					
		SPT		S-169					
		SPT		S-170					
		SPT		S-171					
		SPT		S-172					
		SPT		S-173					
		SPT		S-174					
		SPT		S-175					
		SPT		S-176					
		SPT		S-177					
		SPT		S-178					
		SPT		S-179					
		SPT		S-180					
		SPT		S-181					
		SPT		S-182					
		SPT		S-183					
		SPT		S-184					
		SPT		S-185					
		SPT		S-186					
		SPT		S-187					
		SPT		S-188					
		SPT		S-189					
		SPT		S-190					
		SPT		S-191					
		SPT		S-192					
		SPT		S-193					
		SPT		S-194					
		SPT		S-195					
		SPT		S-196					
		SPT		S-197					
		SPT		S-198					
		SPT		S-199					
		SPT		S-200					
		SPT		S-201					
		SPT		S-202					
		SPT		S-203					
		SPT		S-204					
		SPT		S-205					
		SPT		S-206					
		SPT		S-207					
		SPT		S-208					
		SPT		S-209					
		SPT		S-210					
		SPT		S-211					
		S							

Brigham Young University 368 Clyde Building Provo, Utah 84040 Telephone: (801) 378-2811 Fax: (801) 378-4449		Boring No: BH-4		Treasure Island		San Francisco, California		BYUUCSD - Research	
Single Pile		Logged By: JDL		Elevation (ft):		Soil Classification		Atterberg Limits	
Locallion		Date Started: 10/16/98		Drill Contractor: Pitcher		USCS		Liquid Limits	
Material Description		Date Finished: 10/16/98		Drilling Method: Rotary Wash		AASHTO		Plastic Limits	
Saturated, Gray Clay		Water Level		Blow Count		Soil Classification		Moisture Content %	
		Depth (ft)		Recovery (inches)		USCS		Dry Density (pcf)	
		Graphic Log		Type		USCS		Torque (ft-lb)	
		Location		Number		USCS		Pocket Penetrometer (tsf)	
		S-10		SPT		CL			
		S-11		SH		CL			
		S-12		SH		CL			
		S-13		SH		CL			
		S-14		SH		CL			
		S-15		SH		CL			
		S-16		SH		CL			
		35		18		CL			
		40		30		CL			
		45		30		CL			
		50		30		CL			
		55		30		CL			
		60		30		CL			
		65		30		CL			
		70		30		CL			
		75		30		CL			
		80		30		CL			
		85		30		CL			
		90		30		CL			
		95		30		CL			
		100		30		CL			
		105		30		CL			
		110		30		CL			
		115		30		CL			
		120		30		CL			
		125		30		CL			
		130		30		CL			
		135		30		CL			
		140		30		CL			
		145		30		CL			
		150		30		CL			
		155		30		CL			
		160		30		CL			
		165		30		CL			
		170		30		CL			
		175		30		CL			
		180		30		CL			
		185		30		CL			
		190		30		CL			
		195		30		CL			
		200		30		CL			
		205		30		CL			
		210		30		CL			
		215		30		CL			
		220		30		CL			
		225		30		CL			
		230		30		CL			
		235		30		CL			
		240		30		CL			
		245		30		CL			
		250		30		CL			
		255		30		CL			
		260		30		CL			
		265		30		CL			
		270		30		CL			
		275		30		CL			
		280		30		CL			
		285		30		CL			
		290		30		CL			
		295		30		CL			
		300		30		CL			
		305		30		CL			
		310		30		CL			
		315		30		CL			
		320		30		CL			
		325		30		CL			
		330		30		CL			
		335		30		CL			
		340		30		CL			
		345		30		CL			
		350		30		CL			
		355		30		CL			
		360		30		CL			
		365		30		CL			
		370		30		CL			
		375		30		CL			
		380		30		CL			
		385		30		CL			
		390		30		CL			
		395		30		CL			
		400		30		CL			
		405		30		CL			
		410		30		CL			
		415		30		CL			
		420		30		CL			
		425		30		CL			
		430		30		CL			
		435		30		CL			
		440		30		CL			
		445		30		CL			
		450		30		CL			
		455		30		CL			
		460		30		CL			
		465		30		CL			
		470		30		CL			
		475		30		CL			
		480		30		CL			
		485		30		CL			
		490		30		CL			
		495		30		CL			
		500		30		CL			
		505		30		CL			
		510		30		CL			
		515		30		CL			
		520		30		CL			
		525		30		CL			
		530		30		CL			
		535		30		CL			
		540		30		CL			
		545		30		CL			
		550		30		CL			
		555		30		CL			
		560		30		CL			
		565		30		CL			
		570		30		CL			
		575		30		CL			
		580		30		CL			
		585		30		CL			
		590		30		CL			
		595		30		CL			
		600		30		CL			
		605		30		CL			
		610		30		CL			
		615		30		CL			
		620		30		CL			
		625		30		CL			
		630		30		CL			
		635		30		CL			
		640		30		CL			
		645		30		CL			
		650		30		CL			
		655		30		CL			
		660		30		CL			
		665		30		CL			
		670		30		CL			
		675		30		CL			
		680		30		CL			
		685		30		CL			
		690		30		CL			
		695		30		CL			
		700		30		CL			
		705		30		CL			
		710		30		CL			
		715		30		CL			
		720		30		CL			
		725		30		CL			
		730		30		CL			
		735		30		CL			
		740		30		CL			
		745		30		CL			
		750		30		CL			
		755		30		CL			
		760		30		CL			
		765		30		CL			
		770		30		CL			
		775		30		CL			
		780		30		CL			
		785		30		CL			
		790		30		CL			
		795		30		CL			
		800		30		CL			
		805		30		CL			
		810		30		CL			
		815		30		CL			
		820		30		CL			
		825		30		CL			
		830		30		CL			
		835		30		CL			
		840		30		CL			
		845		30		CL			
		850		30		CL			
		855		30		CL			
		860		30		CL			
		865		30		CL			
		870		30		CL			
		875		30		CL			
		880		30		CL			
		885		30		CL			
		890		30		CL			
		895		30		CL			
		900		30		CL			
		905		30		CL			
		910		30		CL			
		915		30		CL			
		920		30		CL			
		925		30		CL			
		930		30		CL			
		935		30		CL			
		940		30		CL			
		945		30		CL			
		950		30		CL			
		955		30		CL			
		960		30		CL			
		965		30		CL			
		970		30		CL			
		975		30		CL			
		980		30		CL			
		985		30		CL			
		990		30		CL			
		995		30		CL			
		1000		30		CL			
		1005		30		CL			
		1010		30		CL			
		1015		30		CL			
		1020		30		CL			
		1025		30		CL			
		1030		30		CL			
		1035		30		CL			
		1040		30		CL			
		10							

R_u Dissipation @ 2.7 m Depth (E-W Alignment)

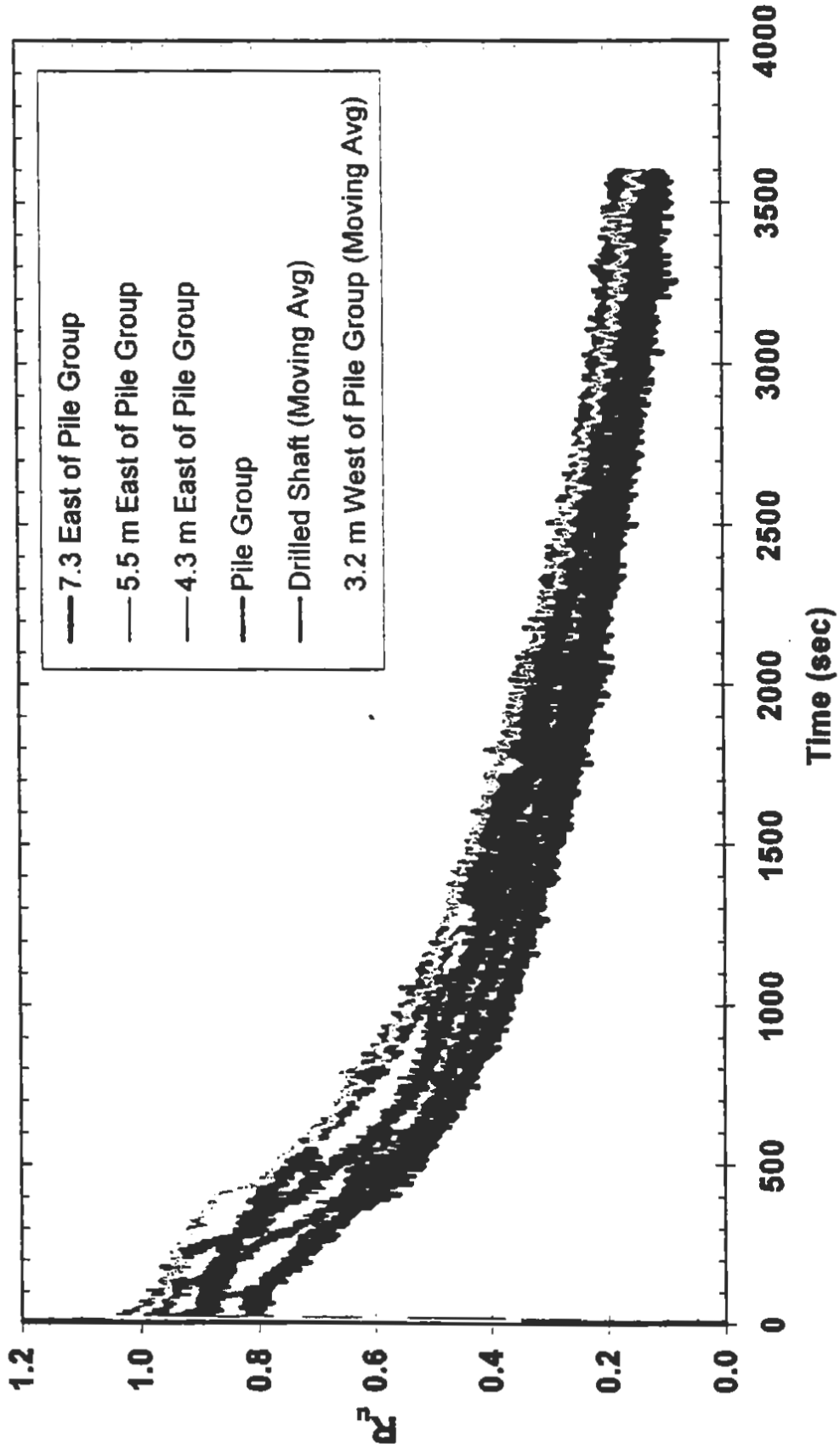


Fig. 6.8 Example of Porewater Pressure Data Collected During Liquefaction Study (Ashford and Rollins, 1999)

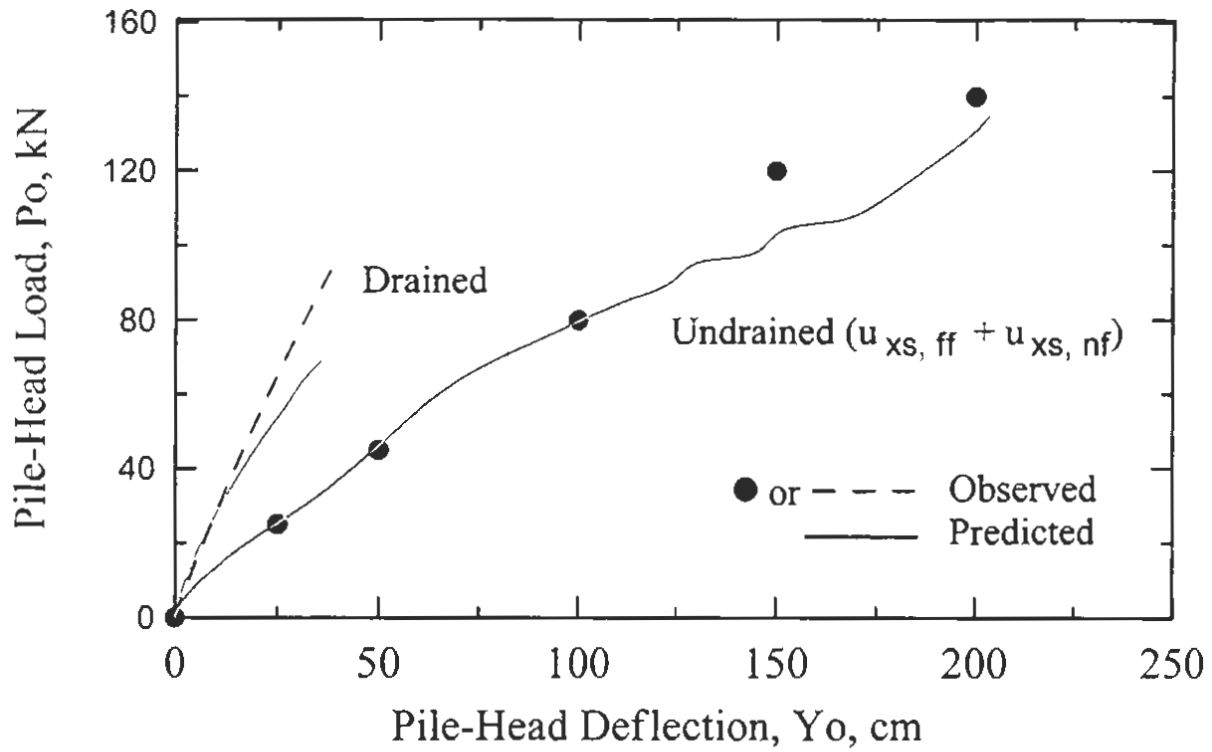


Fig. 6.9 Pile-Head Response at Treasure Island Test Site Under Undrained Conditions (Pipe Pile, 0.324 m Diameter)

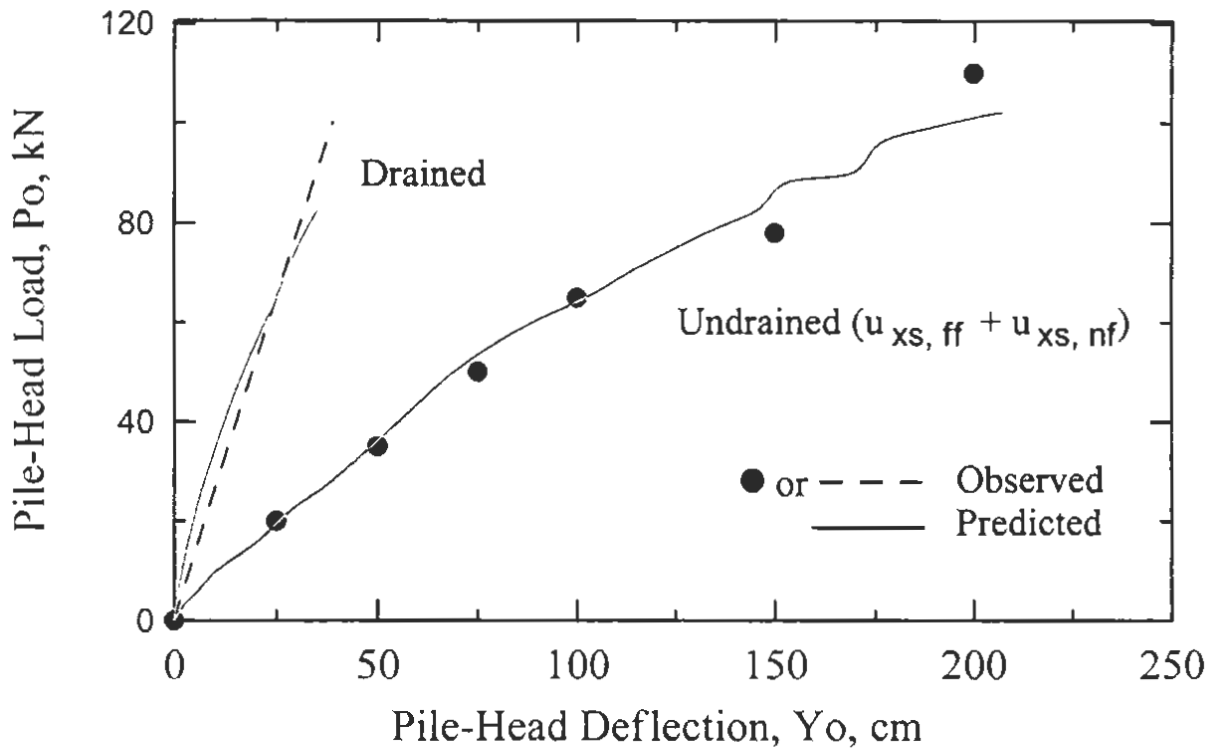


Fig. 6.10 Pile-Head Response at Treasure Island Test Site Under Undrained Conditions (H-Shape, 0.310 m Width)

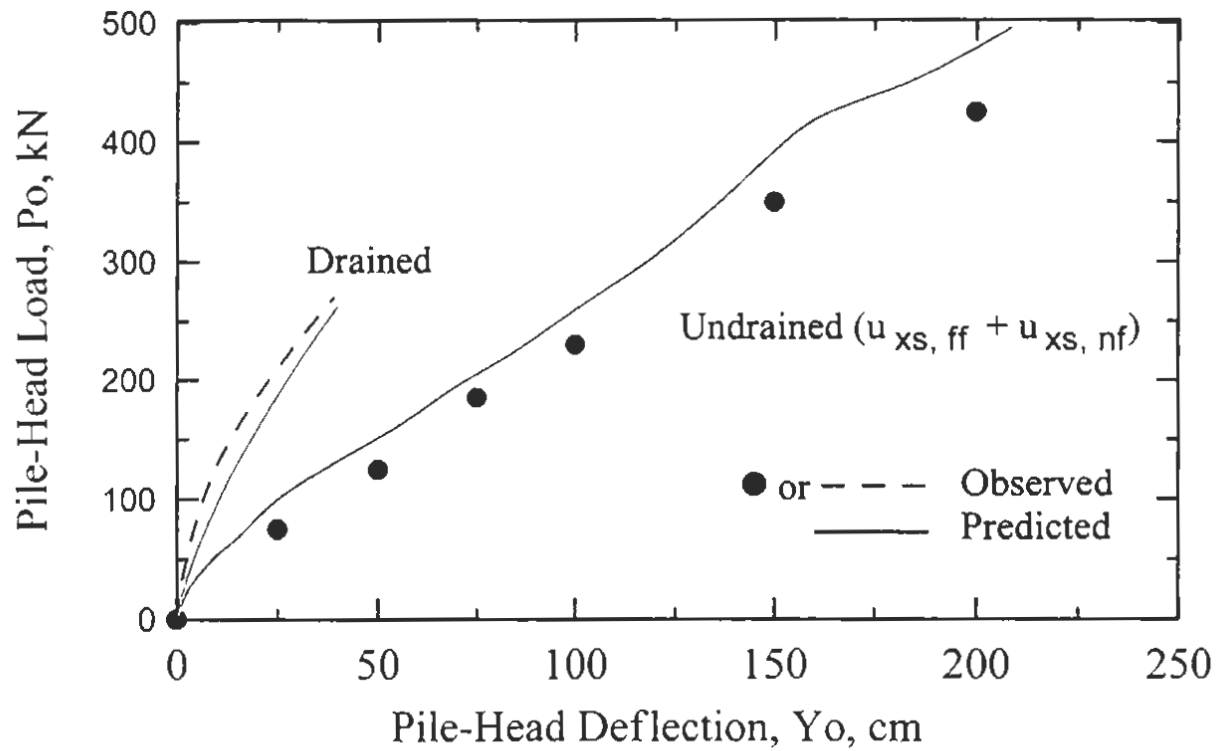


Fig. 6.11 Pile-Head Response at Treasure Island Test Site Under Undrained Conditions (CISS, 0.61 m Diameter)

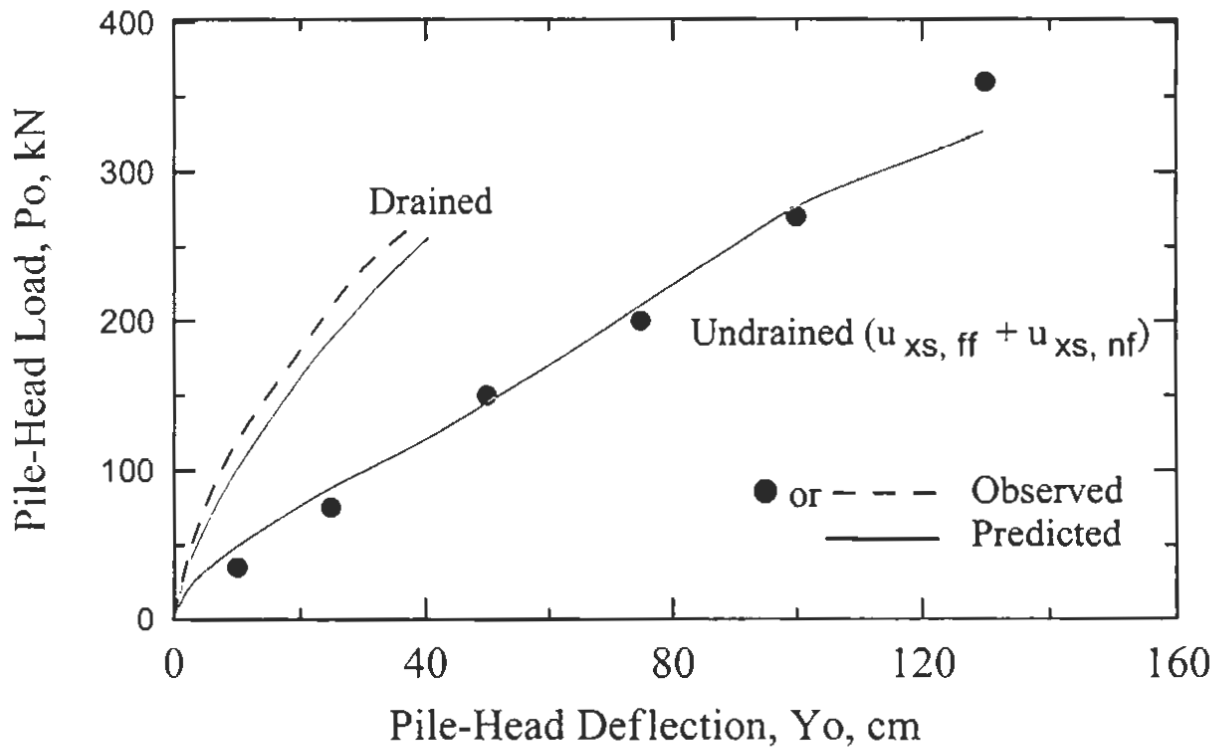


Fig. 6.12 (2 x 2) Pile Group Response at Treasure Island Test Site Under Undrained Conditions (0.324 m Diameter)

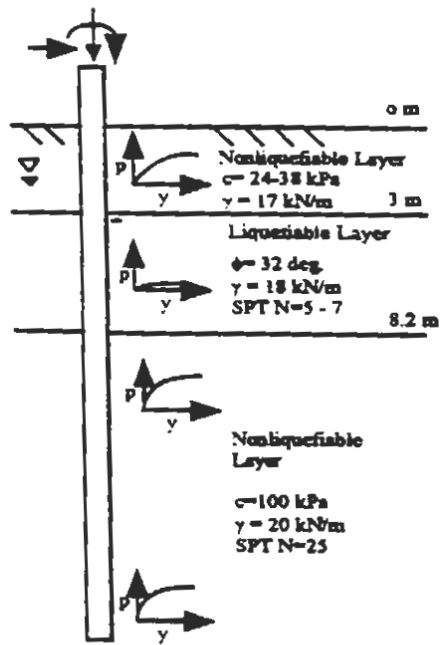


Fig. 6.13 Soil Profile for Various Soil Layer (Wang and Reese 1998)

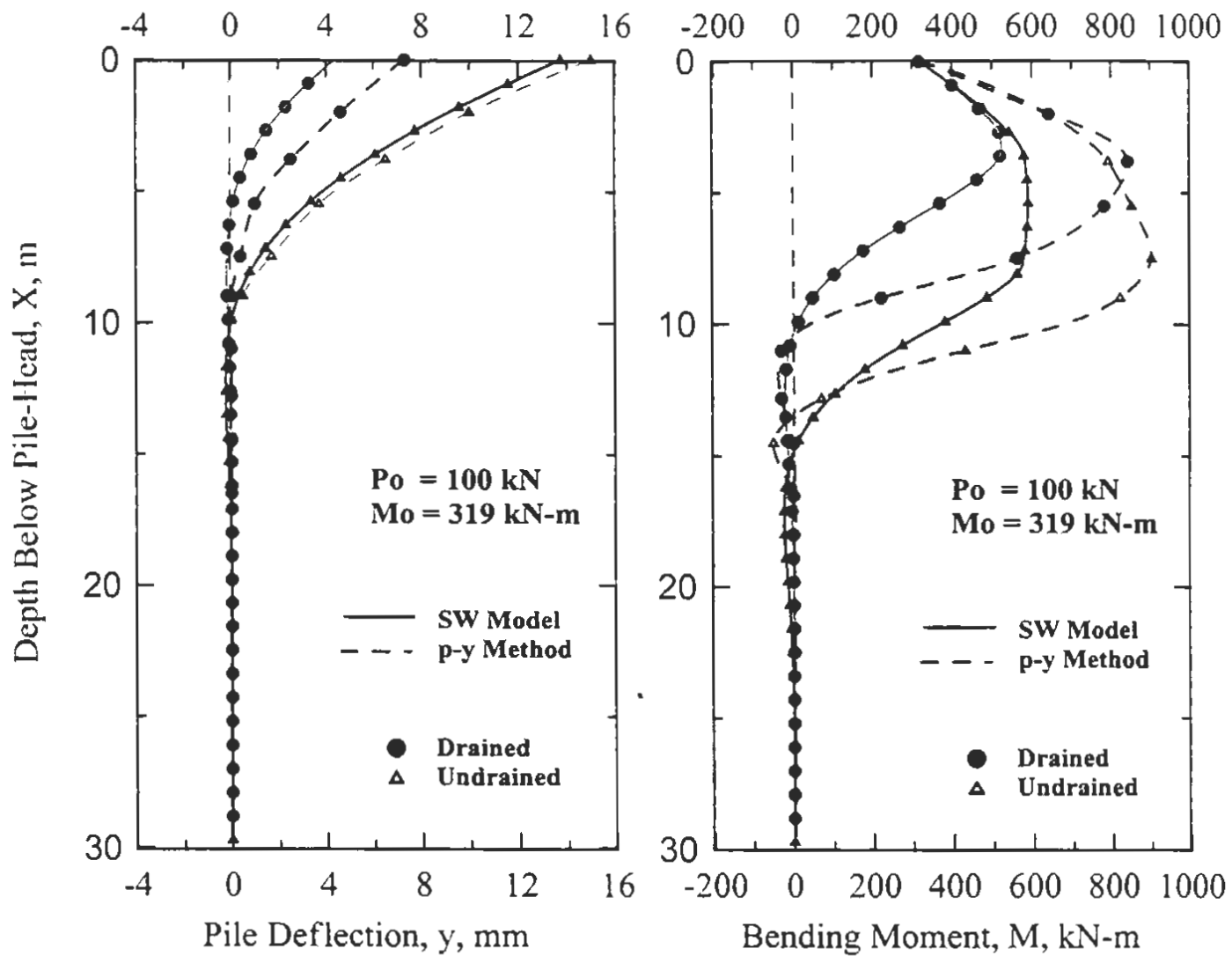


Fig. 6.14 Pile Response Under Drained and Undrained Conditions